

Electronic Theses and Dissertations, 2004-2019

2009

Structural Health Monitoring With Emphasis On Computer Vision, Damage Indices, And Statistical Analysis

Ricardo Zaurin
University of Central Florida

 Part of the [Civil Engineering Commons](#)
Find similar works at: <https://stars.library.ucf.edu/etd>
University of Central Florida Libraries <http://library.ucf.edu>

This Doctoral Dissertation (Open Access) is brought to you for free and open access by STARS. It has been accepted for inclusion in Electronic Theses and Dissertations, 2004-2019 by an authorized administrator of STARS. For more information, please contact STARS@ucf.edu.

STARS Citation

Zaurin, Ricardo, "Structural Health Monitoring With Emphasis On Computer Vision, Damage Indices, And Statistical Analysis" (2009). *Electronic Theses and Dissertations, 2004-2019*. 3853.
<https://stars.library.ucf.edu/etd/3853>

STRUCTURAL HEALTH MONITORING WITH EMPHASIS ON COMPUTER
VISION, DAMAGE INDICES AND STATISTICAL ANALYSIS

by

RICARDO ZAURIN
B.S. Universidad de Oriente, 1985
M.Sc. Universidad de Oriente, 1994
M.Sc. University of Central Florida, 2008

A dissertation submitted in partial fulfillment of the requirements
for the degree of Doctor of Philosophy
in the Department of Civil, Environmental and Construction Engineering
in the College of Engineering and Computer Science
at the University of Central Florida
Orlando, Florida

Fall Term
2009

Major Professor: F. Necati Çatbaş

© 2009 Ricardo Zaurín

ABSTRACT

Structural Health Monitoring (SHM) is the sensing and analysis of a structure to detect abnormal behavior, damage and deterioration during regular operations as well as under extreme loadings. SHM is designed to provide objective information for decision-making on safety and serviceability. This research focuses on the SHM of bridges by developing and integrating novel methods and techniques using sensor networks, computer vision, modeling for damage indices and statistical approaches. Effective use of traffic video synchronized with sensor measurements for decision-making is demonstrated. First, some of the computer vision methods and how they can be used for bridge monitoring are presented along with the most common issues and some practical solutions. Second, a conceptual damage index (Unit Influence Line) is formulated using synchronized computer images and sensor data for tracking the structural response under various load conditions. Third, a new index, N_d , is formulated and demonstrated to more effectively identify, localize and quantify damage. Commonly observed damage conditions on real bridges are simulated on a laboratory model for the demonstration of the computer vision method, UIL and the new index. This new method and the index, which are based on outlier detection from the UIL population, can very effectively handle large sets of monitoring data. The methods and techniques are demonstrated on the laboratory model for damage detection and all damage scenarios are identified successfully. Finally, the application of the proposed methods on a real life structure, which has a monitoring system, is presented. It is shown that these methods can be used efficiently for applications such as damage detection and load rating for decision-making. The results from this monitoring project on a movable bridge are demonstrated and presented along with the conclusions and recommendations for future work.

DEDICATION

- To my parents; for teaching me to never quit.

 - To my wife Diana; for her continuous support and help. I could never do it without you.

 - To Stephanie, Victor and Ricardo; for your understanding on those moments when I was not there. I will try to repay all the time stolen from you.
- May this new step I have achieved serve to you as motivation and example for your life.

I love you all.

ACKNOWLEDGMENTS

First, I would like to express my sincere appreciation and gratitude to Dr. F. Necati Çatbaş for his guidance and support throughout my PhD studies. I also thank Dr. Lakshmi Reddi, Dr. Manoj Chopra, Dr. Kevin Mackie, and Dr. Mubarak Shah for accepting to be members of my dissertation committee as well as for their time and feedback.

I would like to also thank to the current and former members of our research team, Dr. Mustafa Gul, Hasan Burak Gokce, Taha Dumlupinar, Ozerk Sazak, Danny Maier, Tom Terrell, Marcus Lisicki, Nick Nolin, and Melih Susoy for their collaboration and help.

Thanks to you all.

TABLE OF CONTENTS

LIST OF FIGURES.....	IX
1. CHAPTER ONE: INTRODUCTION.....	1
1.1. WHAT IS STRUCTURAL HEALTH MONITORING?.....	1
1.2. OBJECTIVE AND SCOPE	2
1.3. ORGANIZATION OF THE DISSERTATION	5
2. CHAPTER TWO: STRUCTURAL HEALTH MONITORING APPLICATIONS AND NEEDS.....	8
2.1. RELATED WORK.....	8
2.1.1 Visual Inspections	8
2.1.2 Use of SHM and Sensing Technology for Damage Detection.....	9
2.1.3 Incorporation of Imaging Technology with Sensors	12
2.2. AN SHM FRAMEWORK USING COMPUTER VISION.....	16
2.3. SUMMARY	18
3. CHAPTER THREE: INTEGRATION OF VIDEO IMAGING AND SENSOR DATA FOR STRUCTURAL HEALTH MONITORING OF BRIDGES.....	19
3.1. COMPUTER VISION TECHNIQUES USED FOR STRUCTURAL HEALTH MONITORING (SHM).....	19
3.1.1 Detection Approach with an Example from a Real Life Bridge	19
3.1.2 Tracking Approach with an Example from a Real Life Bridge.....	26
3.1.3 Classification Approach	30
3.2. DEVELOPMENT AND SYNCHRONIZATION OF DAMAGE INDICES WITH IMAGE DATA	31
3.2.1 Description of Unit Influence Line (UIL) as a Damage Index.....	32
3.2.2 Limitations and Uncertainties	35
3.3. LABORATORY DEMONSTRATION.....	36
3.3.1 Structure Description and Instrumentation (UCF 4-Span Bridge).....	36
3.3.2 Data Filtering	39

3.4.	INTEGRATION AND IMPLEMENTATION OF COMPUTER VISION AND CONDITION INDEX IN THE	
	LABORATORY	42
3.4.1	Detection of the Vehicles	42
3.4.2	Classification of the Two Trucks Used in the Laboratory.....	43
3.4.3	Tracking of the Moving Vehicles on the Laboratory Bridge	45
3.5.	LOAD LOCATION AND RESPONSE SYNCHRONIZATION	47
3.6.	IDENTIFYING UNIT INFLUENCE LINES FROM THE MONITORING DATA IN THE LABORATORY	48
3.7.	SUMMARY	53
4.	CHAPTER FOUR: COMPUTER VISION AND SENSOR DATA ANALYSIS FOR DAMAGE	
	DETECTION.....	54
4.1.	STATISTICAL ANALYSIS - OUTLIERS DETECTION.	54
4.2.	DESCRIPTION OF THE EXPERIMENTS.....	55
4.2.1	Damage Scenarios.....	56
4.3.	DAMAGE DETECTION USING A STATISTICAL DISTRIBUTION OF UIL VECTORS AS DAMAGE	
	FEATURE	58
4.3.1	Unit Influence Lines Extraction	58
4.3.2	Overview of Outlier Detection from UIL Population for Damage Detection	59
4.4.	OUTLIERS DETECTION-CLUSTERING	61
4.5.	A NEW METHOD FOR IDENTIFICATION OF DAMAGE.....	69
4.6.	SUMMARY	77
5.	CHAPTER FIVE: REAL LIFE APPLICATIONS	79
5.1.	A REVIEW OF THE STRUCTURAL HEALTH MONITORING SYSTEM OF A MOVABLE BRIDGE	80
5.1.1	Description of the Structure	82
5.1.2	Design of the Sensor Network	84
5.1.3	Instrumentation and Data Collection.....	88
5.1.4	Data Acquisition System Configuration.....	89
5.1.5	Field Installation	89

5.1.6	Data Transmission and Synchronization	90
5.2.	DATA ANALYSIS FROM OPERATIONAL TRAFFIC FOR LOAD RATING	92
5.2.1	Detection	94
5.3.	CLASSIFICATION	95
5.4.	TRACKING	96
5.4.1	Load Location and Response Synchronization	97
5.4.2	Unit Influence Lines Extraction	98
5.4.3	Rating Truck Response Prediction	99
5.4.4	Load Rating Results	101
5.5.	DAMAGE DETECTION ON A MOVABLE BRIDGE	104
5.5.1	Live Load Shoes	105
5.5.2	Span Locks	106
5.6.	DAMAGE SCENARIOS	108
5.7.	EXTRACTION OF THE UNIT INFLUENCE LINE FOR DAMAGE CONDITIONS	111
5.8.	DAMAGE IDENTIFICATION	118
5.9.	SUMMARY	120
6.	CHAPTER SIX: SUMMARY, CONCLUSIONS AND RECOMMENDATIONS	122
6.1.	STRUCTURAL HEALTH MONITORING APPLICATIONS AND NEEDS	122
6.2.	IMPLEMENTATION OF COMPUTER VISION FOR STRUCTURAL HEALTH MONITORING	123
6.3.	COMPUTATION OF UNIT INFLUENCE LINE USING VIDEO STREAM AND SENSOR DATA	124
6.4.	DATA ANALYSIS FOR DAMAGE DETECTION	125
6.5.	FIELD DEMONSTRATION ON A MOVABLE BRIDGE	126
	LIST OF REFERENCES	130

LIST OF FIGURES

Figure 1. A Monitoring with Cameras and Sensor Networks along with Novel Data Analysis.....	4
Figure 2. The Components of a Monitoring Framework with Computer Vision	17
Figure 3. General Background Subtraction Method.....	20
Figure 4. Image Mean for a Bridge in Florida.....	22
Figure 5. Image Standard Deviation.....	22
Figure 6. Background Subtraction Results for Different Threshold Values.....	24
Figure 7. Background Results for the Same Threshold under Different Illumination Conditions.....	25
Figure 8. Geometry of the camera location and test set-up	28
Figure 9. Results of Proposed Tracking Algorithm.....	30
Figure 10. Classification of Vehicles.....	31
Figure 11. Example of UIL for the Reaction at the Pin Support of a Statically Determined Beam.....	32
Figure 12. Example of UIL extraction for Moment Response (Adapted from [48]).....	33
Figure 13. Experimental Setup, Finite Element Model and Boundary Conditions	37
Figure 14. Sensor array	38
Figure 15. Data Collection.....	39

Figure 16. Conversion of Responses to Frequency Domain.....	40
Figure 17.Raw & Filtered Data for 2-Axle-Vehicle (Lane 1-SG2).....	41
Figure 18. Strain Data for 2-Axle Vehicle (Filtered).....	41
Figure 19. Vehicle Detection Results	43
Figure 20. Characteristics of 2-Axle Vehicle Determined using Computer Vision.	44
Figure 21.Characteristics of 5-Axle Vehicle Determined using Computer Vision.	45
Figure 22. Tracking of the 2-Axle Vehicle.....	46
Figure 23. Calculated Instantaneous Speed for the Test Vehicles.....	46
Figure 24. Video Image Frame Sequence with Time Stamp.....	47
Figure 25. Strain vs. Distance for L1-SG2 (Both Vehicles with Minimum Load Capacity).....	48
Figure 26. Unit Influence Line sensor L1-SG2 for 2-Wheel -Axle Vehicle. Manual Procedure	49
Figure 27. Unit Influence Line sensor L1-SG2 for 5-Wheel -Axle Vehicle. Manual Procedure	50
Figure 28.Unit Influence Line sensor L1-SG2 for 2-Wheel -Axle Vehicle. Automated Computer Vision Method	51
Figure 29.Unit Influence Line sensor L1-SG2 for 5-Wheel -Axle Vehicle. Automated Computer Vision Method	51
Figure 30. UIL Results for all Studied Cases	52

Figure 31. Loading Scenarios	55
Figure 32. Studied Damage Cases	57
Figure 33. Simulated Damage Cases	57
Figure 34. Procedure for Unit Influence Line Extraction	59
Figure 35. Overview of the Methodology.....	60
Figure 36. Damage Case 1: Rusted Rollers (First Support).....	62
Figure 37. Damage Case 2: Rusted Rollers (First and Second Support).....	63
Figure 38. Damage Case 3: Rusted Rollers (Second Support).....	64
Figure 39. Damage Case 4: Missing Bolts (One Location).....	65
Figure 40. Damage Case 5: Missing Bolts (Two Locations).....	66
Figure 41. Damage Case 6: Worn or not Fully Settled Pads (Elastomeric Pads).....	68
Figure 42. Distance Between two UIL Sets.....	70
Figure 43. Damage Identification for Case 1 (Rusted Rollers on Left Support).....	71
Figure 44. UIL for Tiltmeters 1 and 2 (Undamaged Case and Case 1).....	72
Figure 45. Damage Identification for Case 2 (Rusted Rollers on Left and Central).....	73
Figure 46. Damage Identification for Case3 (Rusted Rollers Central Support).....	74
Figure 47. Damage Identification for Case 4 (4-Missing Bolts).....	75
Figure 48. Damage Identification for Case 5 (8-Missing Bolts).....	75
Figure 49. Damage Identification for Case 6 (Worn/Not Fully Settled Pads).....	76

Figure 50. Sunrise Bridge	83
Figure 51. Location for Some of the Strain Gages	86
Figure 52. Monitoring System	87
Figure 53. Finite Element Model	87
Figure 54. Strain Gage Location and Video Camera	88
Figure 55: Sensor Installation on Girders	90
Figure 56: Scheme for Data Transmission.....	91
Figure 57. Background Subtraction and Filtering.....	95
Figure 58. Classification of Vehicles.....	96
Figure 59. Results from the Tracking Algorithm.....	97
Figure 60. Measured Responses and FEM Simulation.....	98
Figure 61. Unit Influence Lines for Bus (Assuming Empty and Fully Loaded Bus)	99
Figure 62. Predicted Responses for HL-93 by using UILs Obtained with the Operational Traffic	100
Figure 63. Studied Location and Section Properties.....	102
Figure 64. Load Rating Capacity for Section FB-A with respect to Truck Location.....	104
Figure 65. Live load shoe (LLS).....	106
Figure 66. Span Lock Compartment.....	107
Figure 67. Typical Span Lock.....	107

Figure 68. Induced Damage in LLS.....	109
Figure 69. FDOT Contractor Removing Some of the Shims.....	109
Figure 70. FDOT Contractors Removing Some of the Shims from the SL Receiver	110
Figure 71. Raw (Dynamic) and Filtered (Static) Response for ES3-SG1 under Fire Truck	111
Figure 72. Responses vs. Location of the Front Axis (ES3-SG1)	112
Figure 73. Unit Influence Lines for Fire Truck and RTA Passenger Bus	113
Figure 74. UILs for WS3-DSG2 (before and after damage)	114
Figure 75. UILs for WN3-DSG2 (before and after damage).....	114
Figure 76. UILs for ES3-DSG2 (before and after damage).....	116
Figure 77. UILs for EN3-DSG2 (before and after damage).....	116
Figure 78. UILs for ES1-DSG1 (before and after damage).....	117
Figure 79. Damage Index for Case 1 with 1/8"-3/16" Gap created between LLS and Support.....	118
Figure 80. Damage Index for Case 2 with Gap Created between LLS and Support plus Some Shims Removed from SL Receiver	119

1. CHAPTER ONE: INTRODUCTION

1.1. What is Structural Health Monitoring?

Structures are complex engineered systems that are critical for a society's prosperity and quality of life in general. To design structures that are operational and safe, standard building codes and design methodologies have been developed. In addition to routine daily loading, structures are often subjected to unexpected loading and severe environmental conditions that might result in long-term structural damage and deterioration[1, 2]. To assess the existing condition, to detect damage and to design safer and more durable structures, novel sensing technologies and data analysis methods have been explored for existing structures as well as for next generation "smart structures". A new paradigm, Structural Health Monitoring, is an enabling approach for smart structures than can sense and even see [1, 2].

Structural Health Monitoring (SHM) is the sensing and analysis of a structure to detect abnormal behavior, damage and deterioration during regular operations as well as under extreme loadings. There are different definitions for SHM in the engineering literature. One that will be presented here defines SHM as the measurement of the operating and loading environment as well as the critical responses of a structure to track and evaluate the symptoms of incidents, anomalies, damage and/or deterioration that may affect operation, serviceability, or safety and reliability [3]. SHM is designed to provide objective information for decision-making on safety and serviceability, and can be implemented to different types of aerospace, mechanical and civil structures to monitor their behavior by means of the information extracted from the sensor data. Monitoring

has long been implemented to evaluate the condition and performance by using different methods. For example, the railroad workers used the sound of a hammer strike on the train wheel to evaluate if damage was present since the beginning of the 19th century as a routine inspection process. The modern SHM applications started within the aerospace community studying the use of vibration-based damage identification during the late 1970s and the early 1980s in conjunction with the development of the space shuttle. The civil engineering community has focused on vibration-based damage assessment of bridge structures and buildings since the early 1980s [4].

In the last ten to fifteen years, new SHM technologies have emerged, taking this field to the intersection of various engineering disciplines, making it a more multidisciplinary area. In addition to multidisciplinary engineering aspects of SHM, other factors such as the socio-organizational and non-technical challenges are to be considered as an integral part of complete and successful SHM applications especially in real life. Therefore, fundamental engineering, technology and socio-organizational challenges for routine health monitoring applications have to be carefully addressed [5]. In this study, the problem formulation addresses the fundamental aspects along with the technologies employed to fulfill the monitoring needs. The design and execution of the field monitoring presented at the end of the dissertation have been completed by also considering the non-technical and organizational challenges.

1.2. Objective and Scope

As previously stated, SHM is a new paradigm which, if implemented effectively, is expected to improve effective management of civil infrastructure systems (CIS). There

is a growing need and an interest for developing new technologies and methods for CIS to not only collect and analyze data but also to manage civil infrastructures with proactive and effective decision-making for improved safety and serviceability.

Integration of image and computer vision technologies with traditional sensing data has not been fully explored by the SHM researchers. The literature review of different studies illustrate that there is still a need for structural condition assessment and damage detection with conceptual damage indices that integrates sensor networks, computer vision, modeling for damage indices, and statistical approaches.

The research conducted for this dissertation describes a methodology that uses both images and sensor data in conjunction with outlier detection methods to determine the changes in structural behavior and damage, especially for bridge type structures. The approach in this study is as follows. First, some of the most common computer vision applications used for SHM are discussed, and related issues in using these technologies as well as practical solutions for SHM of bridges are presented. Second, a conceptual damage index (Unit Influence Line, UIL) is formulated using synchronized computer images and sensor data for tracking the structural response under various load conditions. Third, a new index, N_d , is formulated and demonstrated to more effectively identify, localize and quantify damage in the case of large data sets. This approach combines the UILs feature vectors and utilizes a Mahalanobis distance-based outlier detection algorithm as summarized in Figure 1. Results of these experiments conducted on a large-scale experimental setup (the UCF 4-span bridge), which was designed and built for this study are also presented and discussed. Finally, a movable bridge in Fort Lauderdale,

Florida is used to demonstrate these methods and technologies on a real life structure.

It is shown that these methods can be used efficiently for applications such as damage detection and load rating for decision making. The movable bridge was subjected to various damage scenarios where the structural configurations were slightly altered while the bridge was being monitored. The data is analyzed and presented for these scenarios. In addition, UILs extracted under the operational traffic by means of sensors and images are used to predict the bridge response and calculate the load rating that is commonly used by bridge engineers for decision-making. The results are also compared with Finite Element Model (FEM) of the bridge for verification purposes. Finally, the results are discussed along with the general conclusions and future work.

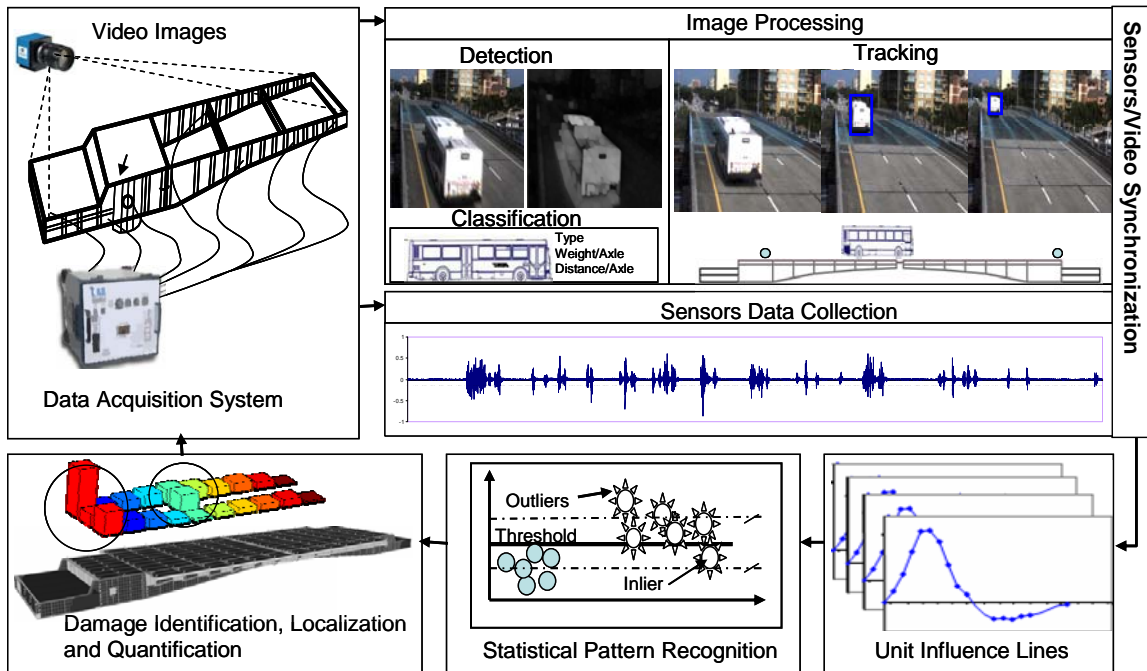


Figure 1. A Monitoring with Cameras and Sensor Networks along with Novel Data Analysis

1.3. Organization of the Dissertation

This dissertation is organized as follows.

Chapter 2 presents a review of some of the methods and procedures currently used for damage detection on structures. First visual inspections are briefly discussed. Then, methods and sensing technology for damage detection are presented with emphasis on previous experiments exploring the use of images, computer vision technologies and sensor data. Finally, a vision based structural health monitoring framework is proposed and described for the research conducted in this dissertation .

Chapter 3 includes the computer vision techniques employed in this research for SHM of bridges. Also, some of the most common issues of using images and some possible practical solutions for bridge applications are discussed. It is also shown how the structure response under various load conditions can be tracked by using a conceptual damage index called Unit Influence Line (UIL). An experimental laboratory bridge model, the UCF 4-span bridge, built specifically for this research, is described and utilized to demonstrate the methods. Two different types of vehicles with various loading are driven over the UCF-4 span bridge while video images and computer vision techniques are utilized to detect, classify, and track the vehicles as sensors measure the corresponding responses. Synchronization of the vehicles images and the sensor responses is achieved to extract the UILs for damage detection.

In *Chapter 4*, first a Mahalanobis distance based outlier detection algorithm is used to show the presence of damage. Then, a new index, N_d , is formulated and

demonstrated to more effectively identify, localize and quantify damage. Commonly observed damage conditions on real bridges are simulated on the UCF-4 span bridge for the demonstration of the computer vision method, UIL and the new index. This new method and the index, which are based on outlier detection from the UIL population, can very effectively handle large sets of monitoring data. The methods and techniques are demonstrated on the laboratory model for damage detection and all damage scenarios are identified successfully

Chapter 5 is mainly dedicated to the validation of extracting UIL feature vectors for real life data. This UIL vectors obtained directly from operational traffic video and sensor data are used for damage detection and bridge load rating. The real life studies were conducted on a movable bridge in Ft. Lauderdale, Florida where the bridge was monitored under regular traffic load and also with slight structural alterations that represent the most common maintenance problems. The UILs are extracted as discussed in the previous chapters for the undamaged and damaged condition of the bridge. The results are presented in a comparative fashion. The UILs are also employed to calculate the load rating of the bridge. One of the novel aspects of the study is that a load test can be conducted with the traffic on the bridge, without any lane closure or special vehicles as well as any Weigh-in-motion device. Any heavy vehicle crossing the bridge can be employed for load testing as they are detected using the cameras, tracked over the bridge while synchronized sensor data collection provides the bridge response at the measurement locations. The classification of the vehicle gives information in terms of axle spacing and empty and fully loaded weight of the vehicle, which are used to obtain upper and lower bound normalized UIL responses. These UILs can be employed to

determine the load rating under commonly used American Association of State Highway Transportation Officials (AASHTO) HL93 truck as well as any other given vehicle. In this dissertation, the load rating for HL93 truck is presented along with the corresponding Finite Element Model (FEM) simulations, which are conducted for verification purposes.

Finally, *Chapter 6* contains the summary and the conclusions on developing and integrating novel methods and techniques using sensor networks, computer vision, modeling for damage indices and statistical approaches. The results from laboratory and field studies are also summarized along with the conclusions and recommendations for future research work.

2. CHAPTER TWO: STRUCTURAL HEALTH MONITORING APPLICATIONS AND NEEDS

2.1. Related Work

The ability to identify the condition of a structure and to detect damage or changes in condition at early stages is important to ensure safety and to maintain efficiently . Several approaches can be used within this realm: visual inspections, use of traditional sensors and statistical techniques for damage detection, and very recently incorporating and analyzing video images combined with the sensor data are some of them.

2.1.1 Visual Inspections

Traditionally, visual inspections have been used for inspecting structures and identify damage and deterioration. In the case of bridges, inspectors go to the structures according a scheduled inspection plan, at least every two years in most of the cases, to identify if there is a need for maintenance, minor or major repair work, load posting or replacement. This method has some inherent drawbacks. One big problem with this approach is that if damage occurs gradually, it may not be observed by inspectors. The damage must have progressed far enough to be visually observable and in many cases accessible by inspectors. Also, the extent of damage is assessed based on subjective criteria. Visual inspection may not be very reliable when there is limited access to some elements or parts of a bridge, and observations are carried out from a distance. Shortcomings of visual inspections are well-documented in a study by FHWA in [6].

Unless a major damage is present, the next inspection will be scheduled according to the inspection plan irrespective of the bridge condition until the next visit. Even if the damage is successfully identified, the final problem facing the engineer is accurately assessing its effect on the overall health of the structure [7]. Structural Health Monitoring (SHM) is expected to provide complementary information to visual inspections, helping to objectively detect damage and assess the condition.

2.1.2 Use of SHM and Sensing Technology for Damage Detection

A number of different methodologies have been introduced for damage detection by using the SHM approach. The theory behind monitoring structural dynamic properties is that if damage is present, then the physical properties of the structure will change and these changes will modify the dynamic response. Modes of vibration and natural frequencies are studied and compared with the ideal undamaged structure responses. Recently, there have been rapid advances in the development of technologies for the evaluation of bridges. Monitoring approaches such as non-intrusive damage detection techniques, by means of dynamic properties, can be integrated into a structure to monitor the complete bridge or individual bridge members. If properly implemented, it is believed that these technologies extend the useful life of bridges by allowing deterioration/damage to be identified earlier and thereby allowing relatively minor corrective actions to be taken before the deterioration/damage grows to a state where major actions are required. In addition, SHM systems allow designers to learn from previous designs to improve the performance of future bridges [6]. It is also possible to permanently install the sensors on the bridge to reduce the amount of time required for testing and also to minimize the

impact on traffic, in particular associated with sensor installation [8].

Damage detection has been carried out based on modal parameters such as natural frequencies, mode shapes, and damping ratios from the recorded data. Other physical properties as system stiffness matrices were obtained and used with the other mentioned parameters as damage indicators [9-11]. One important drawback for those methods is that often, damage has to be large enough to induce significant changes in mode shapes and a large spatial resolution for the experimental setup is needed. For large structures, excitations caused by ambient vibrations or traffic may not be sufficient to reveal changes due to local damage.

Modal analysis techniques have been extensively investigated by laboratory tests. In the following, some of them are presented. Two models were created at the University of Cincinnati and Drexel University to study the barriers for successful SHM applications. One of the main thrusts behind the research on these models is to quantify the effects and mechanisms of uncertainty [12]. The models were developed as adaptable structures that can be configured to simulate various damage scenarios, and study advanced health monitoring instrumentation technologies and algorithms [8, 13].

These plane grid models also represent the early generations of the more complicated grid developed at UCF [14] which also serves as a benchmark model for an international study [15-17]. This grid structure has two clear spans with continuous beams across the middle supports. These supports may easily be removed to obtain a single span grid. The model is 18' by 6' and transverse bracing at 3 ft intervals from end to end of the grid is placed for lateral stability. Additionally, the structure is doubly

symmetric with typical parts that are interchangeable. Columns and beams are composed of W12x26 and S3x5.7 sections respectively, providing the responses in terms of modal frequencies, deflections, rotations, stresses, and strains that are representative for typical short to medium span highway bridges. A very significant characteristic of this steel grid is that it can be easily modified for different test setups. As mentioned before, for example, the two middle supports can easily be removed to analyze a simply supported structure. Furthermore, with specially designed connections, various boundary conditions can be obtained. These boundary conditions may include pin supports, rollers, fixed support, semi-fixed support, and any type of elastic material like neoprene pads. The adjustability of the structure allows a number of damage cases to be simulated including scour, boundary support change and reduced connection stiffness. A recent dissertation provides the experimental and analytical studies from this grid especially with emphasis on a novel time series analysis method to detect, locate and quantify damage from sensor clusters [18].

A benchmark study has been developed on a four story steel frame model on which several SHM tests were and are being performed with the major aim of damage detection for different damage case scenarios. Excitation to the structure was provided by an electro-dynamic shaker. The study sought the most dependant algorithm for different types of structures [19]. This study was followed by a two-phase benchmark problem on a cable-stayed bridge (Bill Emerson Memorial Bridge) as a test-bed for application of response control algorithms. The latter phase included consideration of more complex behavior [20, 21].

2.1.3 Incorporation of Imaging Technology with Sensors

Very recently, some investigators have explored the possibility of incorporating imaging and optical devices and combining them with sensing technology. It should be noticed that there are only a few and limited attempts of real life testing and implementations of these ideas.

One technique, applied by Wahbeh et al., consists of using a high fidelity video camera to track the position of two high-resolution low-power light-emitting-diodes (LED). This study was implemented on the “Vincent Thomas Bridge”, San Pedro California, and the results were compared with experimental ambient data obtained previously by other studies. The results indicate that the first and second modes match reasonably well [22].

In another similar study, Lee and Shinozuka, implemented a real-time displacement measurement of bridges by means of digital image processing techniques. First, the measurement point is marked with a target panel of known geometry. Then, the video camera takes a motion picture of the target. Meanwhile, the motion of the target is calculated using image processing techniques. The test results gave sufficient dynamic resolution in amplitude as well as the frequency. No direct input-output relationship can be established [23].

Another experiment was conducted by Lin et al., and photogrammetric techniques were used to measure displacements in an experimental setup composed of a masonry wall. A digital camera was placed perpendicular to the wall and several pictures were taken while static horizontal-in-plane loads were applied. Those images were post

processed and displacements were calculated. In this study, only in-plane static loads were considered and 2-D displacements were determined by post-processing the data [24].

Hanji et al. presented a work using two digital images and stereography methods for corrosion measuring. Results of measurements were compared with those from the laser displacement meter and matched for small distances between the lens and the specimen [25].

Yoshida et al., constructed a measurement system for quantifying membrane displacements using three synchronized Charge-Couple Device (CCD) video cameras and stereo vision algorithms. Results were matched with Laser Displacement Meter showing good correlation with the real behavior of the membrane and the time-history response [26].

Kanda and Miyamoto applied optical motion tracking technologies to measure earthquake induced motion with surveillance cameras. Test was conducted in a two-story model subjected to uni-axial seismic motion. Ten spherical 2.5 mm. markers wrapped in reflective tape were tracked by two digital video cameras. Also conventional sensors were installed. According the investigators, results showed good correlation between sensors displacements and video cameras readings [27].

Basharat et al., proposed a framework for intelligent sensor network with video camera for structural health monitoring of bridges. They suggested the use of mote sensor networks to monitor a structure. The use of video cameras was prescribed to monitor traffic and other activities on the bridge. Video cameras can also be triggered when the

activity metric is higher than some threshold, indicating that there is significant vibration in that particular section [28].

Javed et al., successfully developed a real time surveillance system for multiple overlapping and non-overlapping cameras called “KNIGHT^M” The system uses a client-server architecture and runs at 10 Hz with three cameras [29].

A framework was proposed by Elgamal et al., combining a network sensors array, a database for storage and archival, computer vision applications for detection and classification of traffic, probabilistic modeling structural reliability and risk analysis and damage detection [30].

Achler and Trivedi presented a vehicle detector algorithm. The vehicle detector finds wheels and infers vehicle location from background segmentation and wheel detection. Some results were presented mainly showing a big proportion of false positives and a successful ratio of detection around 60% [31].

Chang, Tarak and Trivedi suggested the use of multiple sensor modalities in order to perform traffic analysis for health monitoring of transportation infrastructure. Computer vision algorithms are used to detect and track vehicles and extract their properties. Information is combined with data from seismic sensors for classification of vehicles [32].

Fraser presented his doctoral dissertation, based his work as an extension of a large team NSF ITR effort. Fraser shows a comprehensive study where one of the main objectives is the use of video analysis of pre-recorded data, computer vision algorithms, and artificial intelligence as a mean to classify and keep records of traffic (type, number

of vehicles, velocity, peak strain readings) over a fiber reinforced composite deck used as test bed. Fraser also worked on damage detection, using a one dimensional finite element model and simulating two scenarios for a damage and undamaged structure with the vehicular loads coming from the video. Then by examining changes in the computed peak strains for both cases, it was possible to locate damage and to predict the level of the reduction in stiffness [33]. In another related publication, accelerometer data was used to correlate with traffic images [34].

Zhang et al., presented a video-based vehicle detection and classification system for truck data collection using wide-ranging available surveillance cameras. Several computer-vision based algorithms were developed or applied to extract background image from a video sequence, detect presence of vehicles, identify and remove shadows, and calculate pixel-based vehicle lengths for classification [35].

Malinovskiy et al. presented, implemented, and tested a computer-vision based algorithm for vehicle detection. The approach uses spatio-temporal slices that combine to create diagonal strands for every passing vehicle. The strands are then analyzed using the Hough transform to obtain groups of lines. A connected graph of the line objects is constructed for a connected-component analysis. Each connected line group represents one vehicle. Line group data can also be used to reconstruct vehicle trajectories and therefore track vehicles. Vehicle count errors ranged from 8% to 19% in the tests, with an overall average detection accuracy of 86.6% [36].

Another framework for structural health monitoring of bridges by combining computer vision and a distributed sensor network that allows not only recording the

events but identifying the change in performance possibly due to damage by using a damage index was proposed [2] and demonstrated [37].

In this framework, video stream is used in conjunction with computer vision techniques to determine the class and the location of the vehicles moving over a bridge as well as to have security surveillance on the bridge. By knowing the position and magnitude of moving loads; sensors data and video are synchronized and the structure is monitored at every instant by using operational traffic.

This review shows that the implementation of computer vision based methods presents limited results for condition assessment of structures with conceptual damage indices. As a result, an SHM framework that also incorporates computer vision components is presented and discussed.

2.2. *An SHM Framework Using Computer Vision*

Computer-vision is the processing of acquired images in order to detect and track certain features. Recently, computer vision applications have gained attention for SHM. This approach has been implemented and tested at the UCF Structures and Systems Research Laboratory [37-39]. Also a novel framework for real-life structures has been developed and it is currently operating on a movable bridge in Fort Lauderdale, Florida [40].

Most of the previous work presented in the literature search was based on studies using mainly ambient vibration data and could not differentiate ambient from traffic readings, unless testing was scheduled by closing the bridge. An effective system should include the following closely interrelated components: the vision module, the distributed

sensors network array, the analytical model, the database, and the diagnostic module as shown in Figure 2.

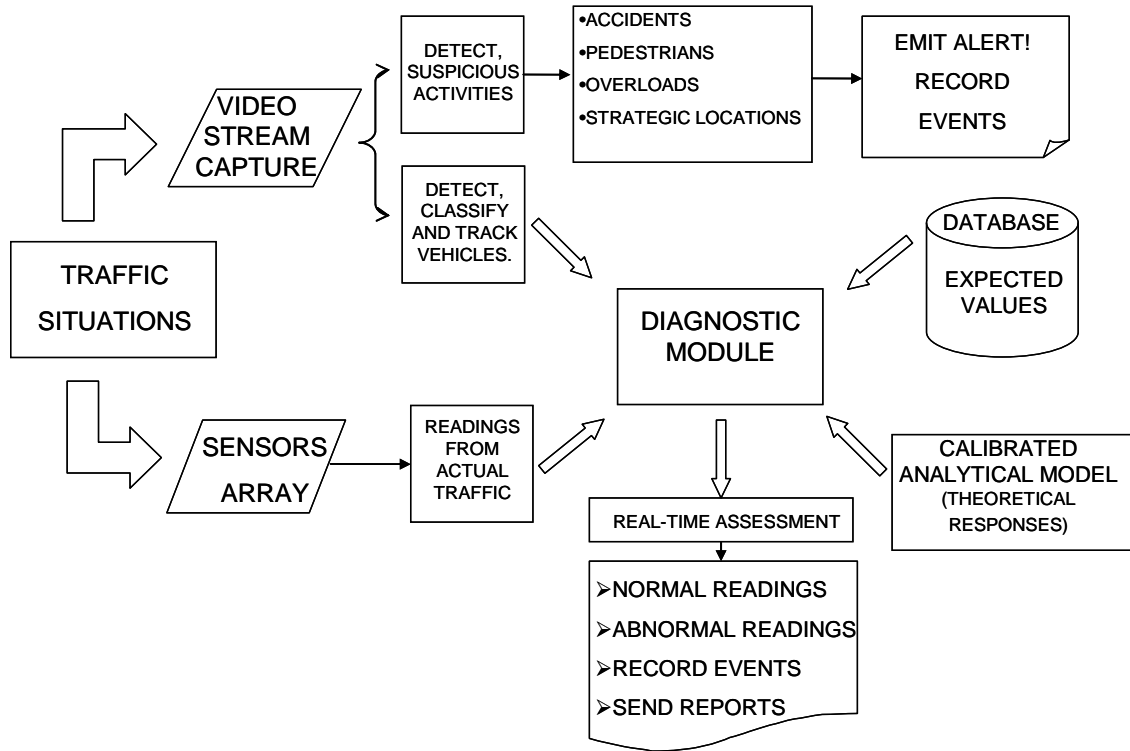


Figure 2. The Components of a Monitoring Framework with Computer Vision

Traffic is monitored and captured by fire wire cameras while sensors collect traditional data. Video stream is used in conjunction with computer vision techniques to determine the class, speed, and location of vehicles moving over the bridge and this information is synchronized with data from the sensors. Unit Influence Line (UIL) feature vectors are extracted for assessment and damage diagnostic. Additionally, video can be also used to detect suspicious activities, i.e. the presence of persons, vehicles and/or objects in critical or prohibited, predetermined locations.

All of this is done in a continuous manner. Thus, the bridge is monitored and its condition is assessed, preventing damage progression and catastrophes as well as keeping the most critical legacy data for further studies.

This feature is expected to prevent catastrophic failures by detecting any abnormal behavior, generation of image and numerical records, remote visual monitoring, tracking of structural behavior and help in scheduling condition-based maintenance.

2.3. Summary

In this chapter, a review of traditional approaches for SHM is presented. Visual inspections, benefits and shortcomings are discussed as well as some of the methods and procedures currently used for damage detection on structures. Then some of the previous experiences using video images and sensor data are reviewed. Finally a framework for structural health monitoring, which combines the analysis of video images by means of computer vision techniques, and traditional sensor data is introduced and described.

3. CHAPTER THREE: INTEGRATION OF VIDEO IMAGING AND SENSOR DATA FOR STRUCTURAL HEALTH MONITORING OF BRIDGES

3.1. Computer Vision Techniques Used for Structural Health Monitoring (SHM)

Computer vision can be defined as the process of analyzing images to obtain an understanding of the content such as what type of objects are present, where they are located and how they are related to the real world. The integration of imaging and optical devices with traditional sensing technology is a promising paradigm for SHM. Identifying moving objects such as vehicles from a video sequence is a critical task for all surveillance systems. Some kind of mechanism is required to detect what is happening in the field of view of the camera. Any moving or out-of-place object becomes of interest and has to be somehow detected. Once objects are detected, further processing is needed to indicate moving direction (tracking) and/or type of object (classification). In spite of many benefits of using video in conjunction with sensing technology, there are also many issues related with this approach in the case of monitoring of civil structures such as bridges. Some of the computer vision techniques, issues and possible solutions for applications on bridge monitoring are discussed in the following.

3.1.1 Detection Approach with an Example from a Real Life Bridge

In vision based systems, a common approach to identify moving objects is background subtraction, where each video frame is compared against a reference or background model. Pixels in the current frame that deviate significantly from the model are considered to be moving objects and belonging to the foreground. This pixel based

information is then clustered to identify regions, and also to label as well as to classify objects. Computer vision techniques have also been used for traffic monitoring and surveillance systems [41]. The common approach for these methods is to build a model of the scene background and detect deviations in each pixel feature value from the model to classify the pixel as part of either background or foreground. Variations of pixels in the image of static background scene can be easily modeled as a Gaussian distribution. Although, pixel intensity or color is the most commonly used feature for scene modeling, there are several others being used in computer vision applications and new approaches are also explored by various researchers. Independent of the method, these approaches basically follow the same scheme shown in Figure 3.

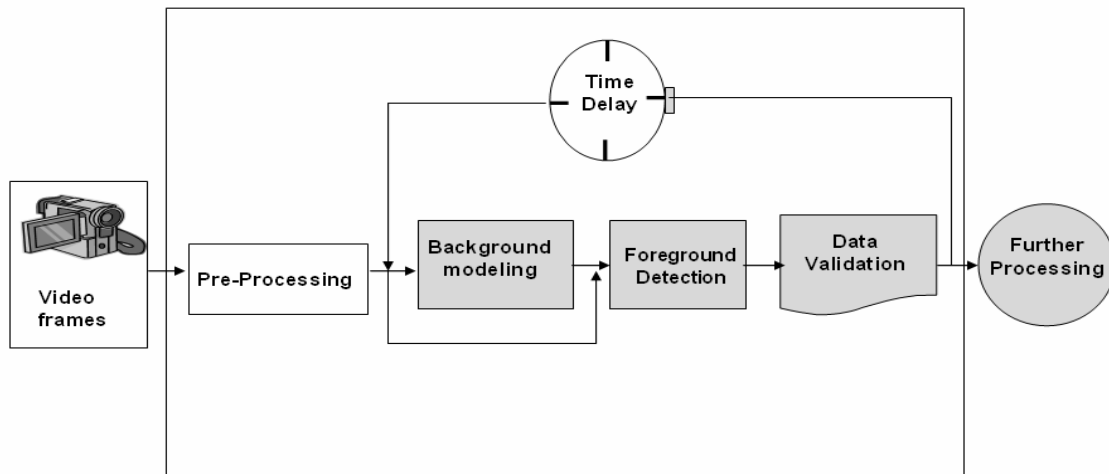


Figure 3. General Background Subtraction Method

Two key issues have to be solved when using background subtraction are determining the value for threshold (λ) and deal with illumination changes. Although background subtraction method has been well studied during the last decades, determination of the pixel-wise optimal threshold value is still object of research and discussion. Several systematic methods have been proposed for selecting threshold values

but at the end, user has to select the most appropriate one.

Thresholding for a bridge monitoring system application can be challenging due to illumination changes throughout the day as well as sudden changes due to fog, rain, and snow. Here, the writers discuss and illustrate their implementation for bridges with a set of RGB video (N=99 frames) which was used to create a background model. For every pixel/RGB channel, the image mean (Figure 4) and standard deviation (Figure 5) are calculated using the Equations 1 and 2 respectively.

$$\{\overline{R}_{i,j}, \overline{G}_{i,j}, \overline{B}_{i,j}\}_{n \times m} = \frac{1}{N} \sum_{k=1}^N \{R_{i,j}, G_{i,j}, B_{i,j}\}_{n \times m} \quad (1)$$

$$\{\sigma_{R_{i,j}}, \sigma_{G_{i,j}}, \sigma_{B_{i,j}}\}_{n \times m} = \sqrt{\frac{1}{N} \sum_{k=1}^n \left[\{\overline{R}_{i,j}, \overline{G}_{i,j}, \overline{B}_{i,j}\}_{n \times m} - \{R_{ij}, G_{ij}, B_{ij}\}_{n \times m} \right]^2} \quad (2)$$

Where $\{\overline{R}_{i,j}, \overline{G}_{i,j}, \overline{B}_{i,j}\}_{n \times m}$ is the matrix formed by the mean per pixel of the corresponding red, green and blue channels of the background. $\{R_{ij}, G_{ij}, B_{ij}\}_{n \times m}$ is matrix containing the red, green and blue intensities for each pixel in each one of the 99 selected frames, and $\{\sigma_{R_{i,j}}, \sigma_{G_{i,j}}, \sigma_{B_{i,j}}\}_{n \times m}$ is the matrix formed by the standard deviations for red, green and blue of every pixel.

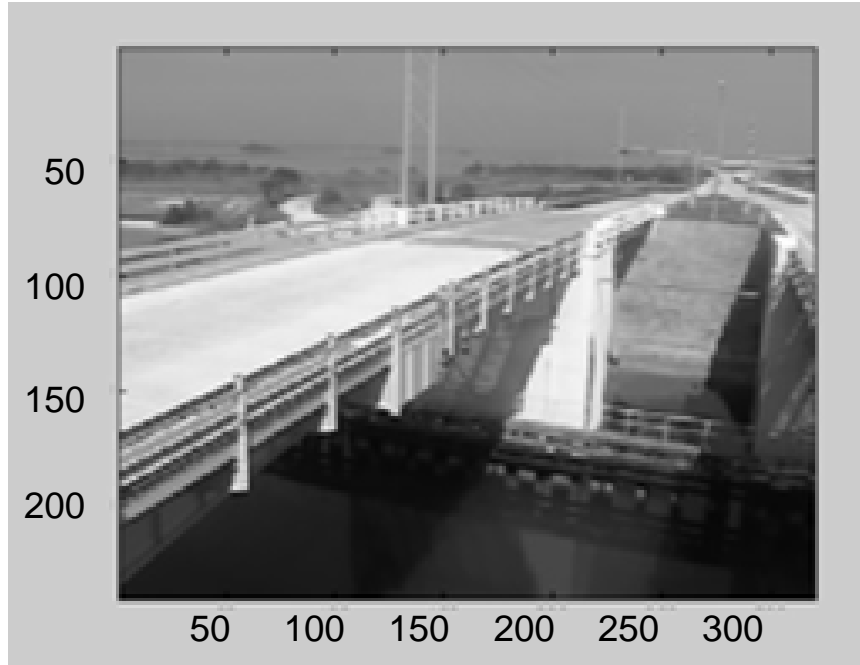


Figure 4. Image Mean for a Bridge in Florida

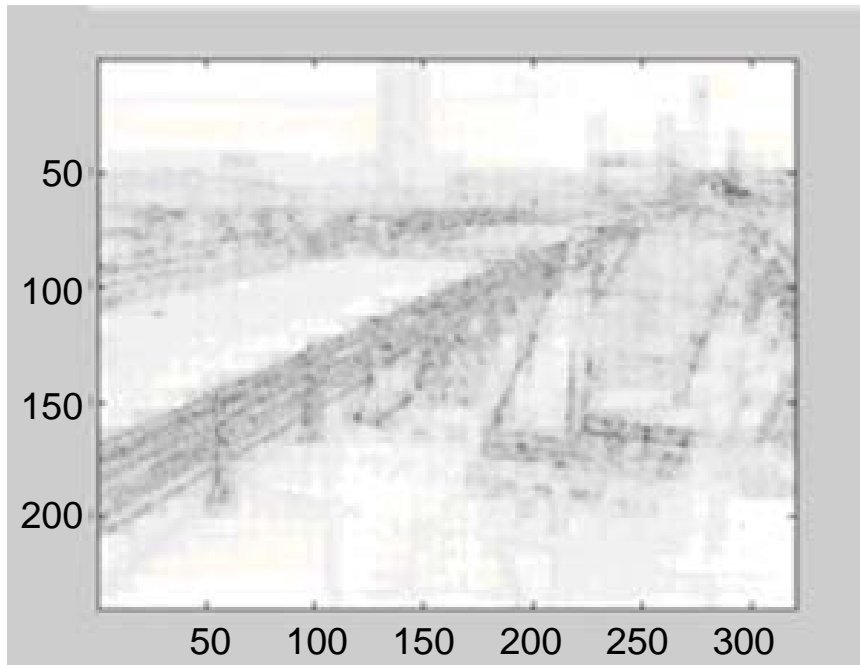


Figure 5. Image Standard Deviation

Per every new input frame a combined change indicator Δ (for every pixel) is determined by normalizing the RGB color space using the background model information as shown in Equation 3.

$$\Delta_{i,j} = \left[\frac{(I_{R_{i,j}} - \overline{R_{i,j}})^2}{\sigma_{R_{i,j}}} + \frac{(I_{G_{i,j}} - \overline{G_{i,j}})^2}{\sigma_{G_{i,j}}} + \frac{(I_{B_{i,j}} - \overline{B_{i,j}})^2}{\sigma_{B_{i,j}}} \right] \quad (3)$$

Here $I_{R_{i,j}}, I_{G_{i,j}}, I_{B_{i,j}}$ are the values of red, green and blue per pixel for each new input frame. Then, the value of Δ for every pixel (Δ is a matrix $n \times m$) is compared against the selected threshold (λ) to classify the pixel as belonging to the foreground ($\Delta_{i,j} \geq \lambda$) or as been part of the background ($\Delta_{i,j} < \lambda$).

Figure 6 shows background subtraction results for different threshold (λ) values. Note that foreground ($\Delta_{i,j} \geq \lambda$) is represented with white and background ($\Delta_{i,j} < \lambda$) which is stationary is represented with black pixels. It is noticeable that for λ values smaller than 1000, many false positives appear and for values of λ greater than 1000 vehicle shape starts to distort. For this reason a value, $\lambda=1000$ was chosen as the initial threshold.

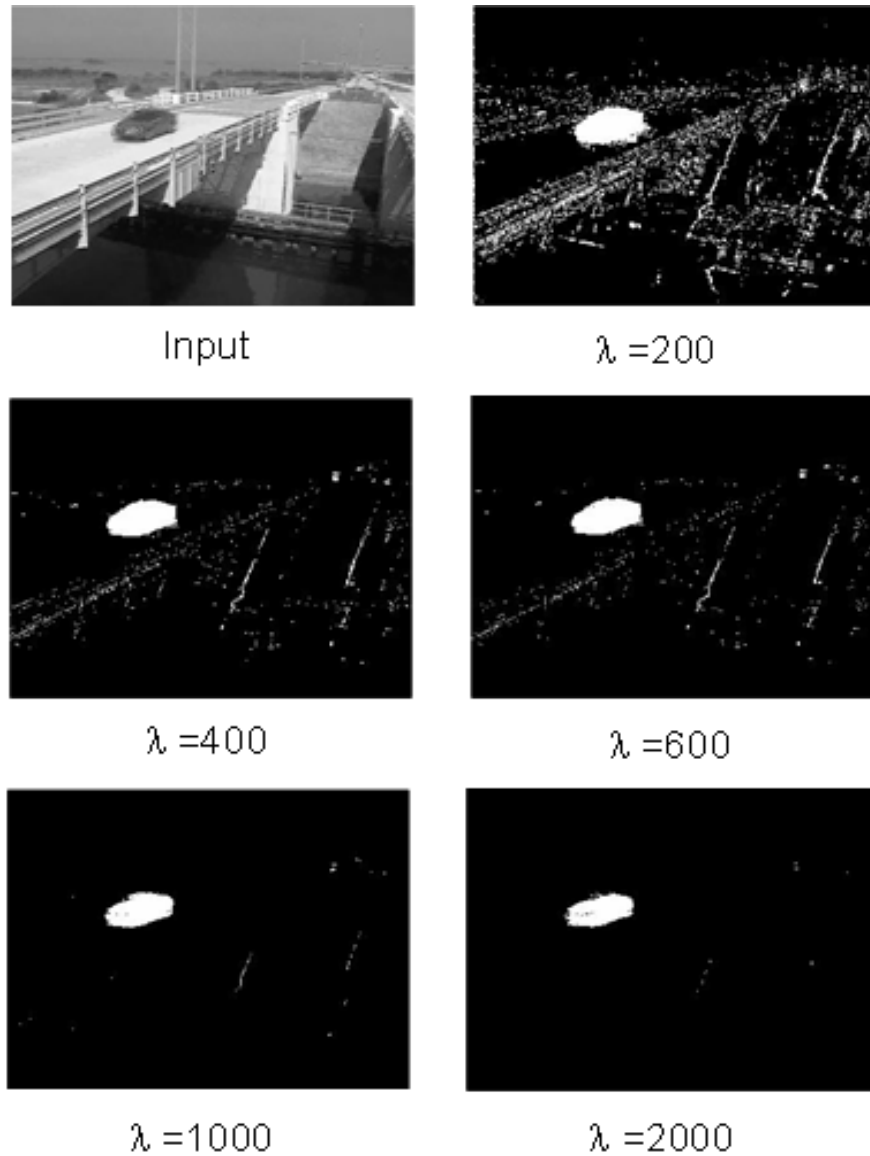


Figure 6. Background Subtraction Results for Different Threshold Values

Sudden changes in illumination conditions completely modify the RGB color characteristics of the modeled background. For this reason, most of all real time background subtraction methods would have difficulty modeling quick and large lighting variations for bridges. Thus background subtraction method would fail under partially

cloudy days if no corrective actions are taken. Figure 7 shows how the appearance of false positives increases dramatically with slightly changes in illumination.

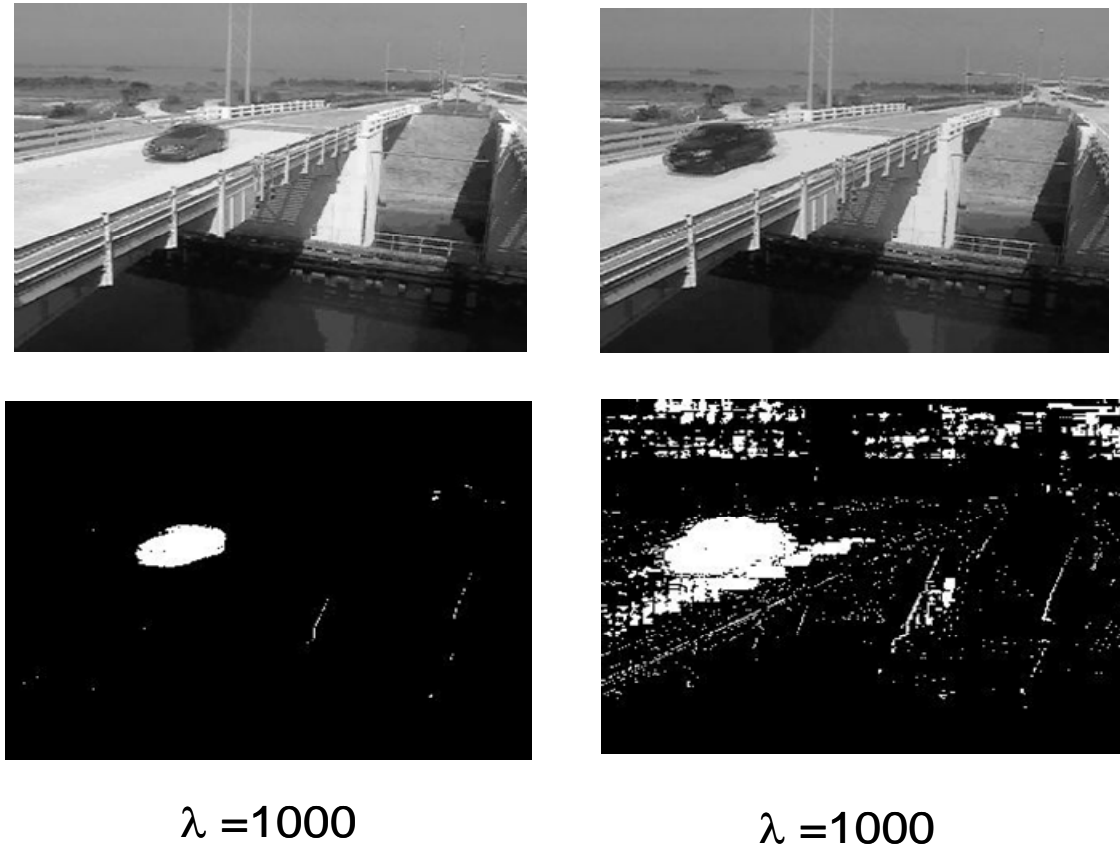


Figure 7. Background Results for the Same Threshold under Different Illumination Conditions

Gradual and slow changes can be solved by updating the background model by periodically incorporating new images into the analysis, changing the background mean and standard deviation producing new Δ values as λ is kept constant. The threshold could be also modified as a function of the spatial pixel location (x, y) , reducing its value for regions of low contrast and increasing it otherwise. Unfortunately, this solution can not be effective where there are sudden changes. While many researchers have studied this

problem, the proposed solutions are often computationally expensive. Computer vision for SHM of bridges with customized practical techniques can be implemented efficiently due to certain constraints and other known characteristics for a bridge and its environment. First, the monitoring area is limited only to the deck, making it possible to discard all false positives out of the region of interest. Objects projected exactly on the deck surface can be cataloged as shadows and be eliminated. For adjusting the threshold, statistical methods based on pixel counting of pre-determined regions are applied, by either increasing or decreasing λ accordingly [42].

3.1.2 Tracking Approach with an Example from a Real Life Bridge

Establishing the relationship between vehicles crossing a bridge (moving loads) in the 3D world and their projections on a 2D space (images) is the main goal for tracking algorithms employed for SHM. Once all camera parameters are determined, vehicles on the bridge can be tracked. Several methodologies have been proposed and proven to work very well, from snakes [43], through geodesic active contour level set based algorithm [44] and many others based on Scale-Invariant Feature Transform (SIFT) [45].

The first step is to perform a camera calibration process, allowing image and world coordinates to be mapped. Equation 4 shows how homogeneous image coordinates and homogeneous world coordinates are related by the intrinsic and extrinsic camera parameter matrices.

$$\begin{bmatrix} I_x \\ I_y \\ 1 \end{bmatrix} = \begin{bmatrix} -fk_x & 0 & o_x & 0 \\ 0 & -fk_y & o_y & 0 \\ 0 & 0 & 1 & 0 \end{bmatrix} \begin{bmatrix} r_{1,1} & r_{1,2} & r_{1,3} & t_x \\ r_{2,1} & r_{2,2} & r_{2,3} & t_y \\ r_{3,1} & r_{3,2} & r_{3,3} & t_z \\ 0 & 0 & 0 & 1 \end{bmatrix} \begin{bmatrix} W_x \\ W_y \\ W_z \\ 1 \end{bmatrix} \quad (4)$$

Where: I_x, I_y represent image coordinates, W_x, W_y, W_z are world coordinates, f is the focal length, k_x, k_y are the effective size of the pixel in mm, r represents the coefficients of the camera rotation matrix (3x3), t_x, t_y, t_z are the spatial translation of the camera, and o_x, o_y are the image center. All the intrinsic and extrinsic parameters can be determined by knowing a set of points in the image and real world, establishing a system of equations and using singular value decomposition to get the final solution. Although this is a very common approach, it requires a process which can be impractical for long term field monitoring for bridges. This 3-D problem is greatly simplified when reduced to a 2-D situation if the surface is assumed to be planar. Hence all the z coordinates are either the same or the difference is negligible [38]. Using the previous assumption, Lagrange Interpolation Method can be used to calculate the position of the vehicles over the bridge. The geometry of the camera and setup is shown in Figure 8. Now, it becomes evident that if Z is assumed to be constant along the bridge, image and real world can be correlated both in the plane XY, which defines the plan view of the bridge.

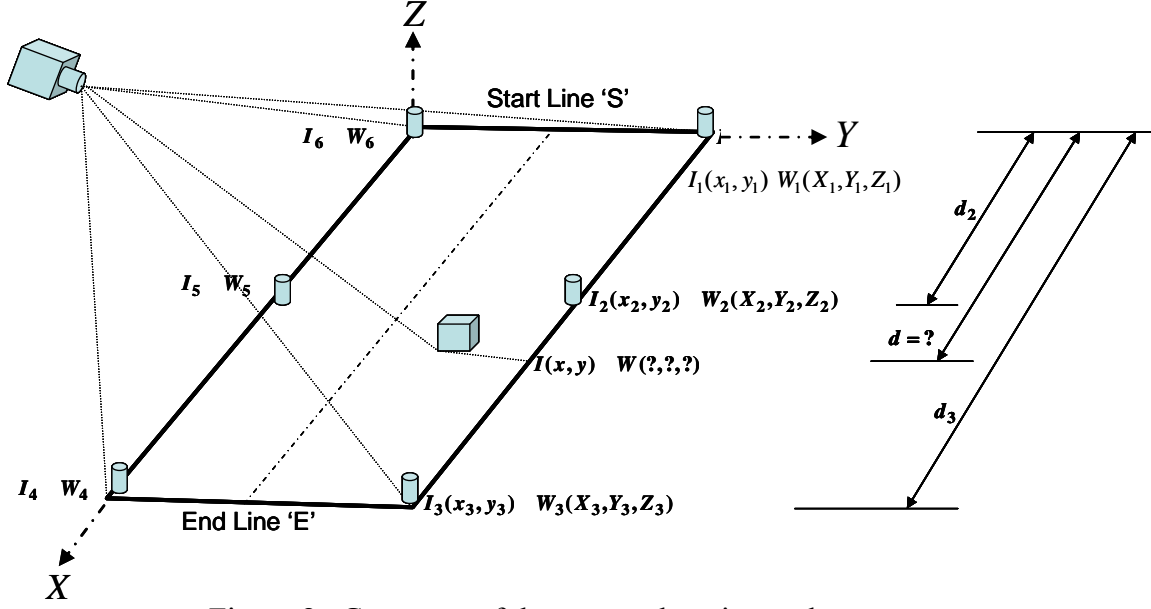


Figure 8. Geometry of the camera location and test set-up

Considering a set of $k+1$ data points $(d_{image_i}, d_{world_i})$; $i = 0 \rightarrow k$ where d_{image} is the distance in pixels between line 'S' and a set of known points in the image, and d_{world} is the distance in the real world between the line 'S' and the same set of points, then:

$$\left. \begin{aligned}
 d_{world(i+1)} &= \sqrt{(Wx_{i+1} - Wx_i)^2 + (Wy_{i+1} - Wy_i)^2 + (Wz_{i+1} - Wz_i)^2} + d_{world(i)} \\
 d_{image(i+1)} &= \sqrt{(Ix_{i+1} - Ix_i)^2 + (Iy_{i+1} - Iy_i)^2 + (Iz_{i+1} - Iz_i)^2} + d_{image(i)}
 \end{aligned} \right\} (5)$$

In Equation 5 we find the distance of the object with respect to the original start line 'S' in the real world and in the image, respectively to calculate the world distance from the line S (d_{world}) for a given image distance from the line S (d_{image}). Equation 6 can be used with $l_j(d_{image})$ being the Lagrange coefficients for a new input image

distance.

$$d_{world}(d_{image}) = \sum_{j=0}^k d_{world(j)} l_j(d_{image}) \quad (6)$$

The Lagrange basis coefficients can be obtained using Lagrange basis polynomials as given in Equation 7.

$$l_j(d_{image}) = \prod_{i=0, i \neq j}^k \frac{d_{image} - d_{image(i)}}{d_{image(j)} - d_{image(i)}} \\ = \frac{d_{image} - d_{image_0}}{d_{image_j} - d_{image_0}} \cdots \frac{d_{image} - d_{image_{j-1}}}{d_{image_j} - d_{image_{j-1}}} \cdot \frac{d_{image} - d_{image_{j+1}}}{d_{image_j} - d_{image_{j+1}}} \cdots \frac{d_{image} - d_{image_k}}{d_{image_j} - d_{image_k}} \quad (7)$$

A set of known correspondences between world and image spaces on the structure is used as reference and Lagrange coefficients are obtained following Equation 7. For SHM of bridges, several known constrains can be considered such as common motion, constant speed, known trajectories, and predefined motion regions leading to practical algorithms. Basic features like shape, size, color, and speed can be used to build a weighted correspondence matrix between two consecutive frames at times t_1 and t_2 . Matching is established between the two pair of objects giving the lowest cost.

Occlusion is another concern in computer vision tracking. For SHM of bridges, this issue can be minimized by placing the cameras, along the bridge in the traffic direction. However, even by finding the best location for the video source, there might be objects in frame t_1 which can not be paired to in frame t_2 due to occlusion. In this case, position of the occluded object can be calculated using linear velocity models and

distance-speed relationships. Figure 9 shows results of the proposed tracking algorithm in a real-life structure. For the same time interval between frames distance and speed are calculated.

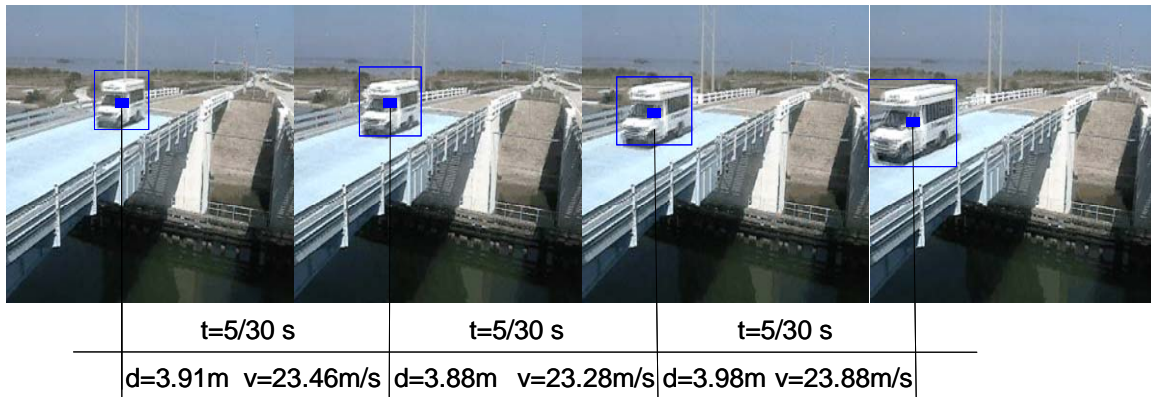


Figure 9. Results of Proposed Tracking Algorithm

3.1.3 Classification Approach

For SHM of bridges, vehicles are moving loads and vehicle classification is critical in traffic monitoring analysis. In order to establish input-output relationship (load and response as function of time and location), type of vehicle, magnitude and location of the loads transmitted to the structure through the wheels must be obtained. The goal is then to classify each moving object of interest within the input image as belonging to a certain group of vehicles. The first step to achieve this objective requires the detection and correspondence of each object. The tracking method discussed in the previous section provides the bounding box, centroid and motion path of each object over the frames. Classification can be made by computing the size (number of pixel) of the object for a particular location. This approach, assumes the only cause of change in the projected height of an object is the variation in its position respect the camera. Once the

size is known, it can be compared with the statistical distribution for the particular traffic population of the bridge, previously compiled and stored in a database. Further improvements by including geometry (shape) along with size can be also included when employing only size is not sufficient.

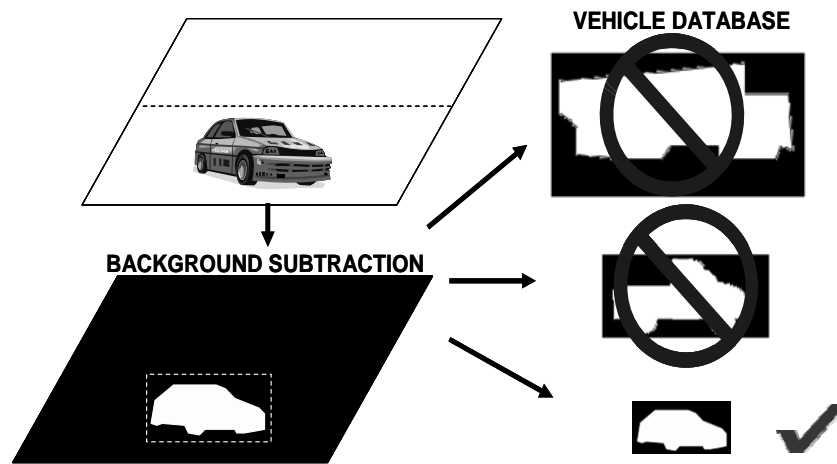


Figure 10. Classification of Vehicles

In addition, the number of wheel axles can be identified by using an additional camera located perpendicular to the traffic flow direction. By means of computer vision procedures, number of axles and distance between them can be determined and used as extra features for classification purposes, as explained in the rest of the dissertation.

3.2. Development and Synchronization of Damage Indices with Image Data

Condition assessment is one of the most challenging activities to be performed by civil engineers to objectively evaluate if structures are safe for the public use. In order to effectively assess the condition objectively, it is essential that some type of sensing technology and adequate index are employed for decision-making. Appropriate indices should be sensitive to damage, yet not to changes in ambient conditions or variations to

the testing method. An index should be easy to measure confidently and can be processed directly from measurement, with minimal assumptions or computational requirements. Finally, an index should be conceptual and thus easy to interpret [46]. Although there is no consensus on a comprehensive index and no single index can address all condition and damage identification requirements, unit influence line (UIL) can be considered to meet many of the previously mentioned properties for an ideal index [47].

3.2.1 Description of Unit Influence Line (UIL) as a Damage Index

UIL, which is commonly used by structural engineers, shows the variation of a response at any given point on a structure due to the application of a unit load at any point on the structure. Influence lines are generated by applying a unit load and moving it on the structure. The response due to this unit load at the location of interest is calculated and values are then plotted to generate the influence line for the function as shown in Figure 11. This fundamental concept is covered in elementary structural analysis courses, and it is widely used in bridge engineering design and load rating.

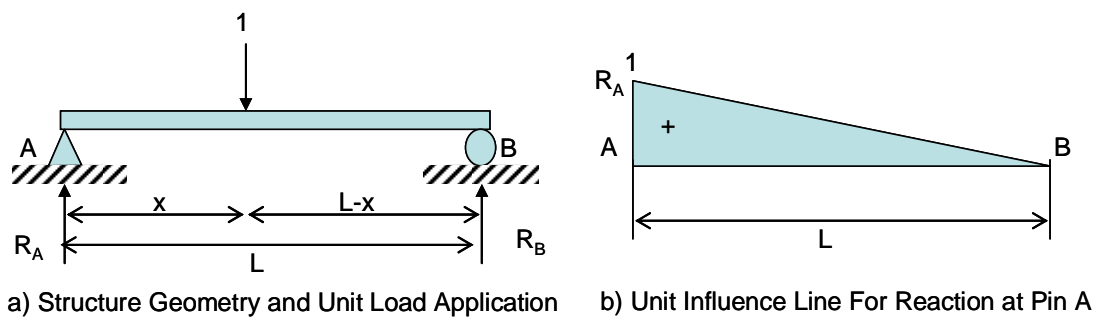


Figure 11. Example of UIL for the Reaction at the Pin Support of a Statically Determined Beam

When UIL is identified from SHM data by means of an inverse problem, UIL provides a signature with a normalized bridge response for the critical locations

instrumented by any type of sensor. By knowing the weight and location of each axle, and the structural responses, it is possible to extract the UIL of the structure using the following formulation.

$$\{r\}=[w]*\{u\} \quad (8)$$

Where $\{r\}$ is a vector containing the response of a certain location due to the moving load, $[w]$ is a matrix containing the axle weights with its corresponding distances, and $\{u\}$ is the UIL vector. Figure 12 shows an example of UIL extraction for Moment Response.

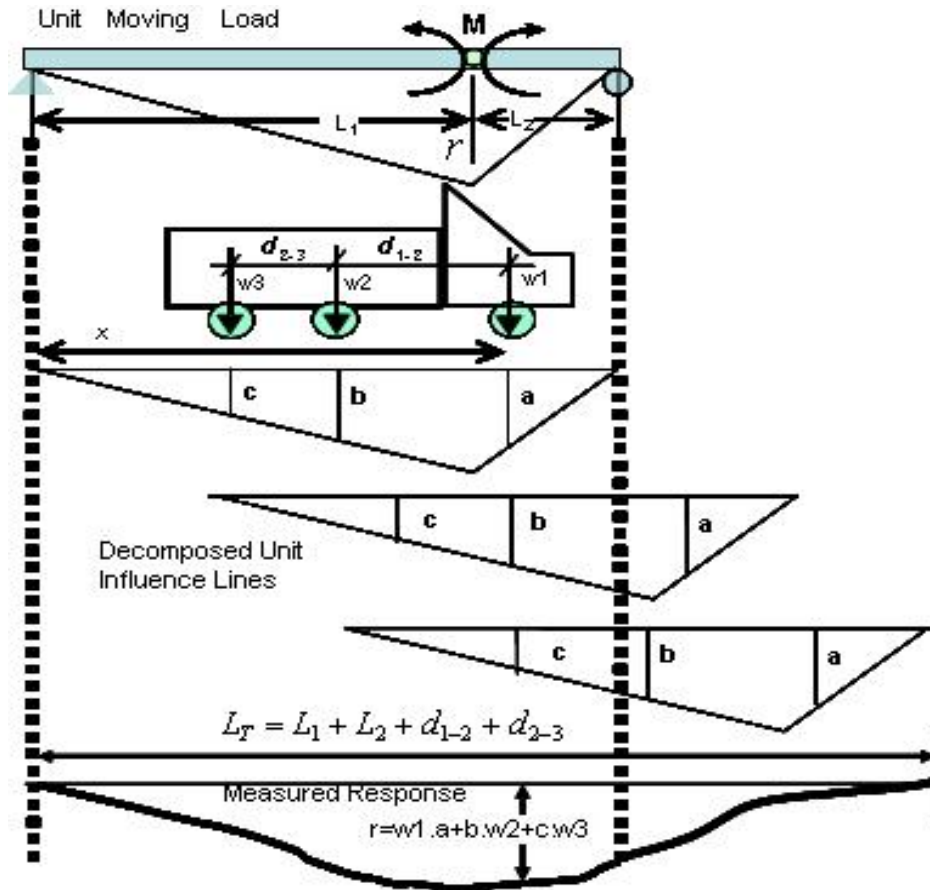


Figure 12. Example of UIL extraction for Moment Response (Adapted from [48])

A matrix containing the information of the weight/location of each axle is formed. This matrix has m rows corresponding to the number of unit steps Δx the bridge is divided into plus the extra number of Δx coming from the distance between the first and last axle of the truck ($m=L_T / \Delta x$). The number of columns is n i.e. the number of Δx corresponding to the length of the bridge ($n = (L_1 + L_2) / \Delta x$). Where n is also the number of discretized coefficients for unit influence along the actual length of the bridge. The value of each cell within the matrix is the weight applied from the axle to the structure at that particular location (Equation 9). Then, by knowing the responses $\{r\}$, Equation 10 can be established.

$$\begin{Bmatrix} r_1 \\ r_2 \\ \cdot \\ \cdot \\ r_m \end{Bmatrix}_{m \times 1} = \begin{bmatrix} w_1 & 0 & 0 & 0 & 0 & 0 & 0 & 0 & \cdot \\ \cdot & \cdot & \cdot & \cdot & \cdot & \cdot & \cdot & \cdot & \cdot \\ w_2 & 0 & 0 & 0 & w_1 & 0 & 0 & 0 & 0 \\ \cdot & \cdot & \cdot & \cdot & \cdot & \cdot & \cdot & \cdot & \cdot \\ w_3 & 0 & 0 & w_2 & 0 & 0 & 0 & w_1 & 0 \\ \cdot & \cdot & \cdot & \cdot & \cdot & \cdot & \cdot & \cdot & \cdot \\ 0 & w_3 & 0 & 0 & w_2 & 0 & 0 & 0 & w_1 \\ \cdot & \cdot & \cdot & \cdot & \cdot & \cdot & \cdot & \cdot & \cdot \\ \cdot & \cdot & \cdot & \cdot & \cdot & \cdot & \cdot & \cdot & \cdot \\ \cdot & 0 & 0 & 0 & 0 & 0 & 0 & 0 & w_3 \end{bmatrix}_{m \times n} * \begin{Bmatrix} u_1 \\ u_2 \\ \cdot \\ u_n \end{Bmatrix}_{n \times 1} \quad (9)$$

Unit influence line can be determined by taking the pseudo inverse, more formally the Moore-Penrose pseudo inverse, of the matrix $[w]$ and multiplying it by the responses:

$$\{u\} = [w]^{-1} * \{r\} \quad (10)$$

However, four criteria have to be achieved for the pseudo inverse to be defined:

1. – $[w][w]^{-1}[w] = [w]$
2. – $[w]^{-1}[w][w]^{-1} = [w]^{-1}$
3. – $([w][w]^{-1})^{TRANSPOSE} = [w][w]^{-1}$
4. – $([w]^{-1}[w])^{TRANSPOSE} = [w]^{-1}[w]$

Also, for the system to have a unique solution, the rank of $[w]$ has to be equal to the rank of the augmented matrix $[w|u]$ and equal to 'n'. If these criteria are not met, the system could have various solutions leading to erroneous results. In this case, the corresponding UIL values should be discarded.

3.2.2 Limitations and Uncertainties

Although UIL is a very conceptual method, there are limitations and uncertainties in the experimental process that may lead to errors. It is important to understand possible sources of uncertainties and limitations in order to employ UIL more efficiently. Some of the uncertainties and limitations are described in [46] as follows:

Uncertainty in synchronizing time with distance: By using video cameras and computer vision algorithms, small differences in the location of the axles can appear.

Uncertainty in the straight path of the truck: Vehicles do not necessarily follow a straight line while crossing over a bridge. Any small variation in their path along the transverse direction may cause experimental errors and affect the UIL.

Uncertainty in data filtering: Recorded data contains ambient, dynamic effects (from the bridge as well as from the vehicle suspension), noise coming from the data

acquisition system (DAQ), and other signals added to the static data.

Uncertainty in the weight per axle: Same vehicle can have infinite combinations of axle weight depending on how the load is distributed within them. Any difference in the weight distribution per axle can lead to a different UIL. Upper and lower bounds for the responses have to be established to indicate a safe condition for the bridge. If a weight in motion system is added, exact weights per axle can be known and this uncertainty is minimized.

Uncertainty in linear bridge behavior: The UIL method assumes a perfectly elastic behavior of the structure. Any nonlinear behavior would induce error and uncertainties to the method.

Uncertainties due to environment: Environmental conditions such as temperature and humidity would affect the stiffness and behavior of a bridge. Development of intrinsic forces due to temperature changes or a modification of boundary conditions can lead to variations in the response; hence its UIL would also change.

3.3. Laboratory Demonstration

3.3.1 *Structure Description and Instrumentation (UCF 4-Span Bridge)*

An experimental setup was designed and constructed by the researchers to demonstrate sensing and video monitoring framework along with the data analysis method. The set up is a four span bridge-type structure consisting of two 120 cm approach (end) spans and two 304.8 cm main spans with a 3.18 mm thick, 120 cm wide steel deck supported by two HSS 25x25x3 girders separated 60.96 cm from each other.

Supports were designed in such a way that they could be easily changed to roller, pin or fixed boundary conditions as shown in Figure 13.

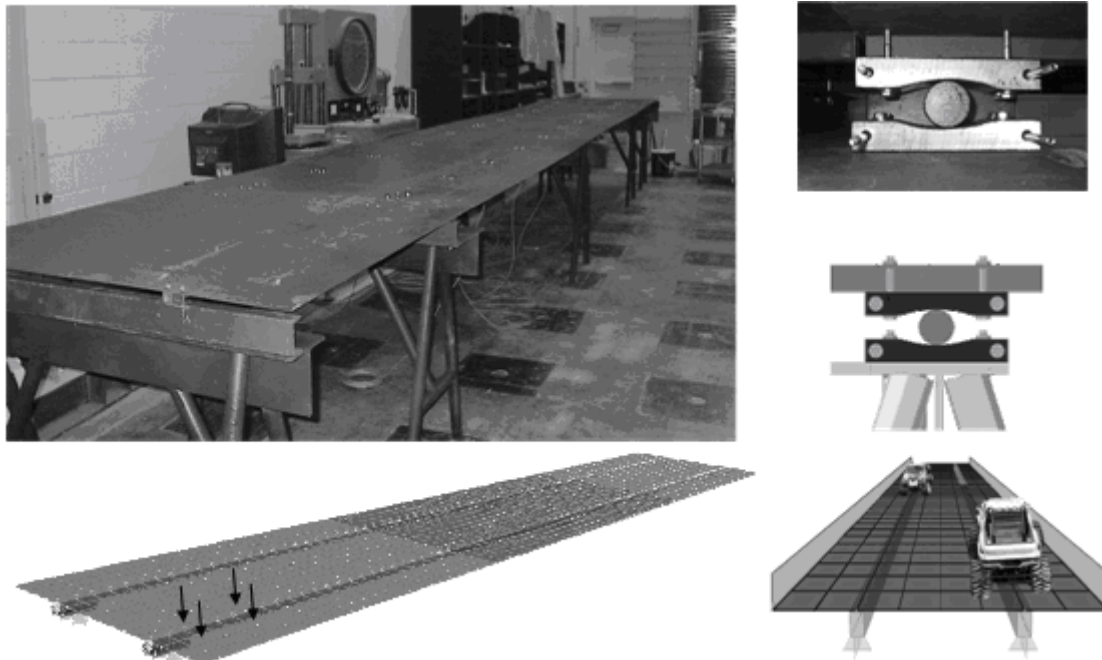


Figure 13. Experimental Setup, Finite Element Model and Boundary Conditions

Girder and deck can be connected together at will by using bolts at different locations to modify the stiffness of the system and to simulate damage. Radio controlled vehicles can crawl over the deck with different loading conditions (from 4.02 kg to 15.71 kg). Wheel axis distance and speed are also variable. While a video camera is used to identify and track the vehicles, a set of strategically located sensors collects the data to be correlated with the video stream in real-time. It is important to mention that although the structure is not a scaled down bridge model, however, its responses are representative of typical values for medium-span bridges. A more comprehensive description of this structure as well as the analytical model can be found in [2].

This laboratory setup is instrumented with various sensors as shown in the

instrumentation plan (Figure 14). A data acquisition system collects data while a USB type camera collects video stream data at a rate of 15 Hz., 20 foil type strain gages are sampled at a rate of 1kHz and are averaged every 100 points to minimize noise for an effective rate of 10 Hz. Figure 15 shows the Data Acquisition System (DAQ) and the execution of the tests. There are also a total of sixteen accelerometers, and two dynamic tiltmeters collecting data at the same sampling rate as the strain gages. It should be noted that only strain and tilt data are used in this study for the demonstrations.

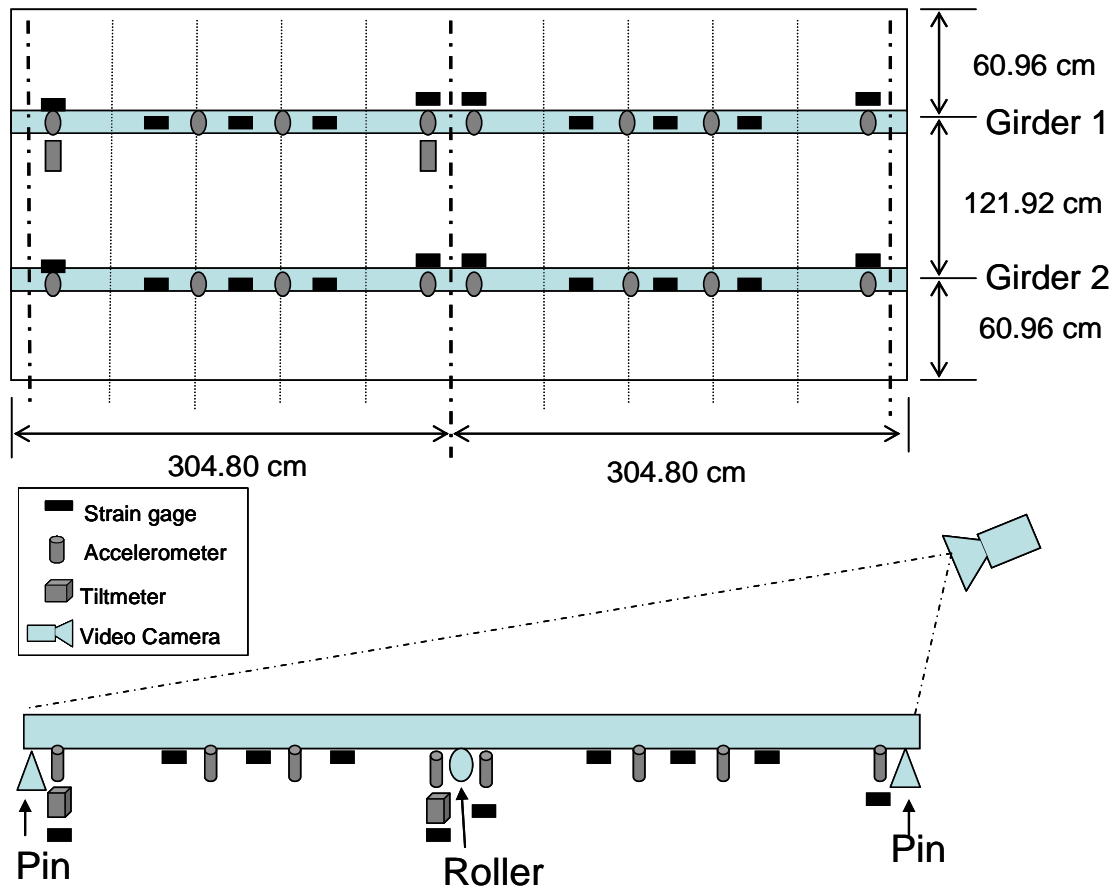


Figure 14. Sensor array



a) DAQ System

b) One of the Test Vehicles

Figure 15. Data Collection

3.3.2 Data Filtering

UIL analysis is based on static response of the bridge caused by traffic load; hence, dynamic response component has to be eliminated by filtering out the dynamic components of the signal. Dynamic load effects are due to road roughness and imperfections on the pavement that can cause impact forces exerted from the vehicles on the bridge. Another issue is the redistribution of the axle weights while in motion, due to differential deflections of the bridge, especially for large heavy-loaded trucks. Also, as a vehicle moves over the bridge, its engine and suspension generates vibration that behaves itself as a dynamic system, introducing the additional dynamic component to the data. Some of these effects can be eliminated whereas the others have to be considered negligible. Filtering is performed by changing the time domain data into frequency domain by applying Fourier Transformation (which was done using Fast Fourier Transform (FFT) in this case). When using this procedure, separation of static and

dynamic components is possible as shown in Figure 16. It is shown that the first two modes of vibrations of the bridge are in the vicinity of 5 Hz and 7.5 Hz. The modes are also identified from the Finite Element (FE) analysis and these are also shown in the figure. By inspecting this dynamic response, the cut off frequency for a low pass filter can be identified. After this stage, zero padding the to responses above the cut off frequency and Inverse Fourier Transform (IFT) of the frequency domain data to time domain gives the processed data for the UIL analysis.

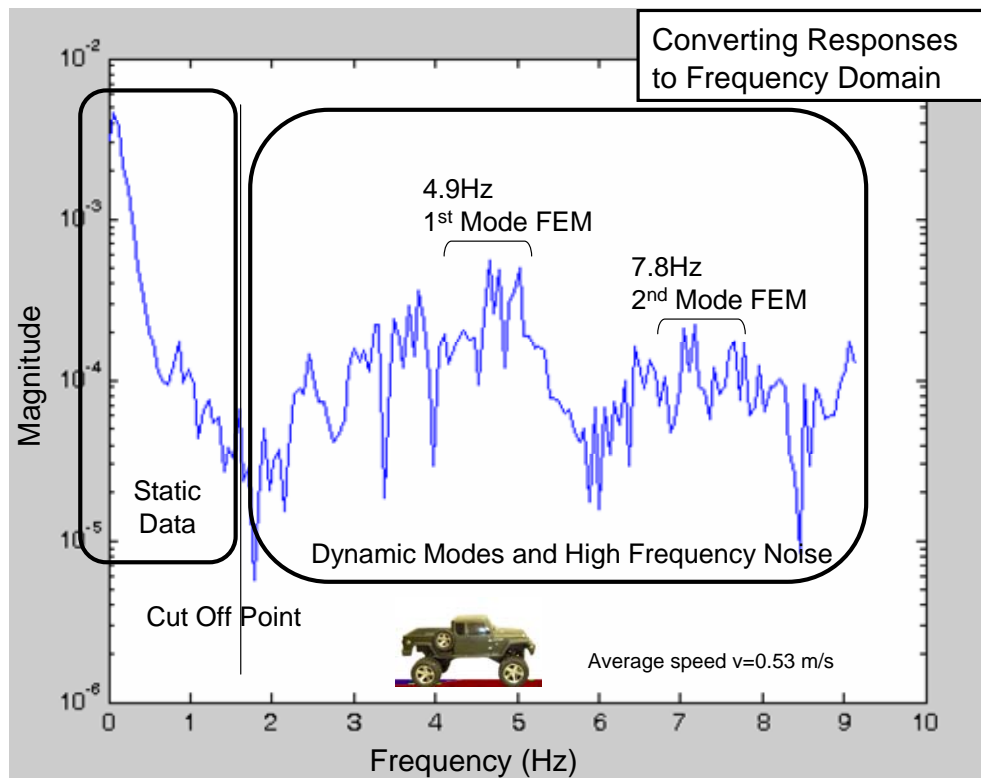


Figure 16. Conversion of Responses to Frequency Domain

The new data are converted back to the time domain and the results of filtering are shown in Figure 17 and Figure 18 for four different sensor measurements after

dynamic components and high frequency components are filtered out.

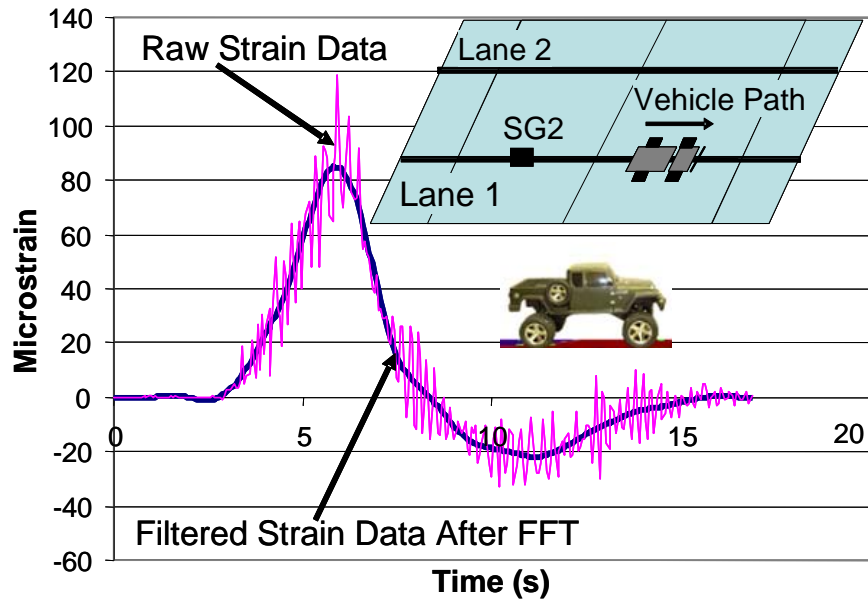


Figure 17. Raw & Filtered Data for 2-Axle-Vehicle (Lane 1-SG2)

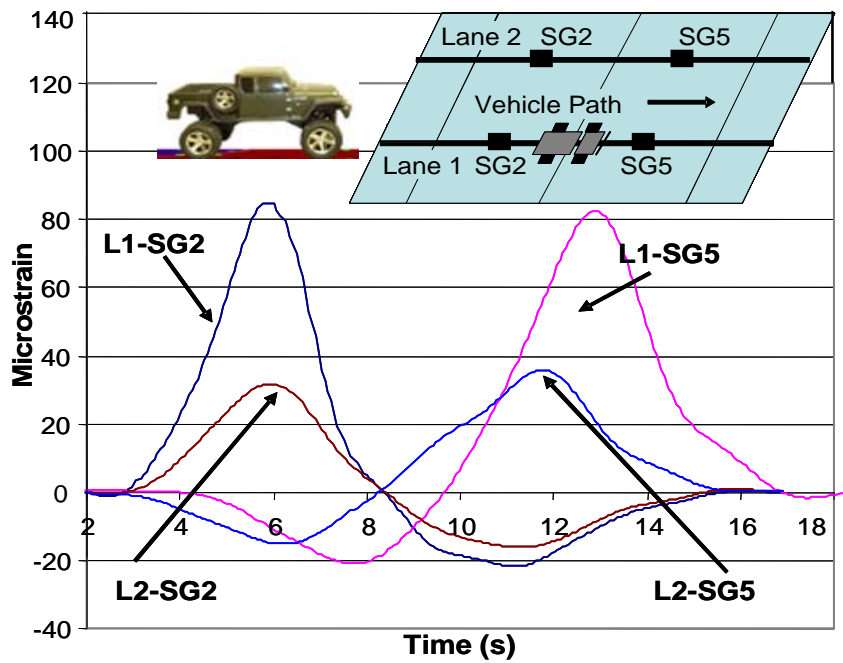


Figure 18. Strain Data for 2-Axle Vehicle (Filtered)

3.4. Integration and Implementation of Computer Vision and Condition Index in the Laboratory

A very novel characteristic of this study is the fact that structural responses obtained by means of sensors are synchronized with the moving load which is determined by using video processing and computer vision algorithms. Detection, classification and tracking of the loads are shown and explained in the following.

3.4.1 Detection of the Vehicles

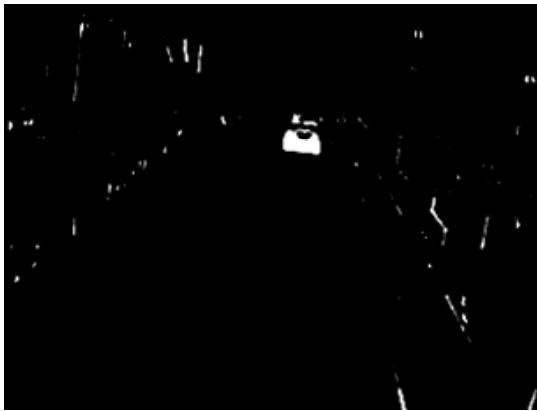
First, background subtraction is performed as explained in section 3.1. Results are shown in Figure 19. A background model is created by using 99 frames and standard deviation and mean image (Figure 19a) are calculated. Then for every new input frame (Figure 19b) Background subtraction is performed (Figure 19c). Threshold for pixel differences is applied; connected component algorithm allows detecting different possible interest objects by finding interconnected pixels. Objects are now thresholded size-wise. Any object lying outside of the region of interest (bridge deck) is discarded (Figure 19d). Morphological filtering is applied to fill holes and define the shape of the remaining object (Figure 19e). Finally, a bounding box is drawn in the input frame to show detected object (Figure 19f). Size (in pixels) and image coordinates of the box (es) are saved in a file for each one of the studied frames, corresponding to the vehicle(s) in motion.



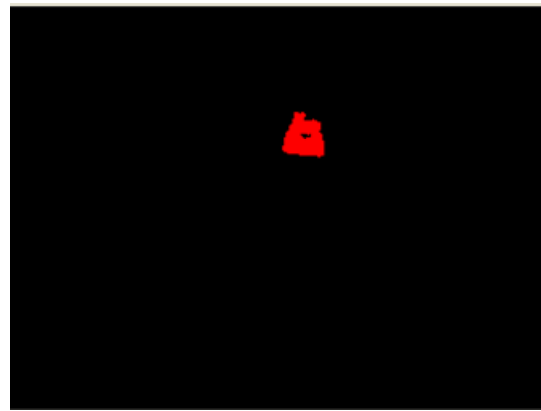
a) Background model



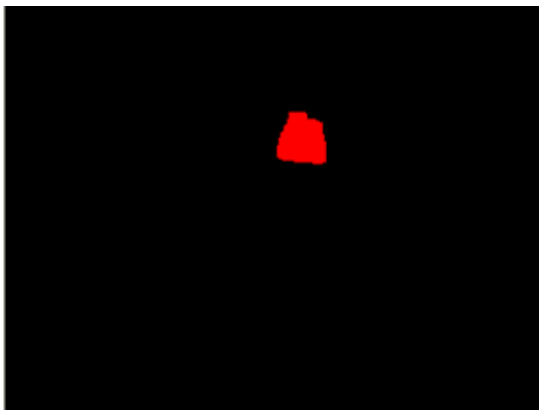
b) Input Frame



c) Background Subtraction



d) Threshold & Conn. Comp



e) Morphological Filtering



f) Detected Vehicle

Figure 19. Vehicle Detection Results

3.4.2 Classification of the Two Trucks Used in the Laboratory

As explained before, the goal of this task is to classify each vehicle as belonging to a certain group. In this way, the approximated load transmitted to the structure can be

estimated. For this case study, two different vehicles were used and the exact number and weight per axle for each vehicle were known. For a real life application, a program was developed and tested in the laboratory, using a video camera perpendicular to the traffic and computer vision techniques. This program, based on pattern matching, is able to determine the size, number of axles, and distance between axles as shown in Figure 20 and Figure 21. If the exact weight per axle is required, weight in motion can be added as part of the system.

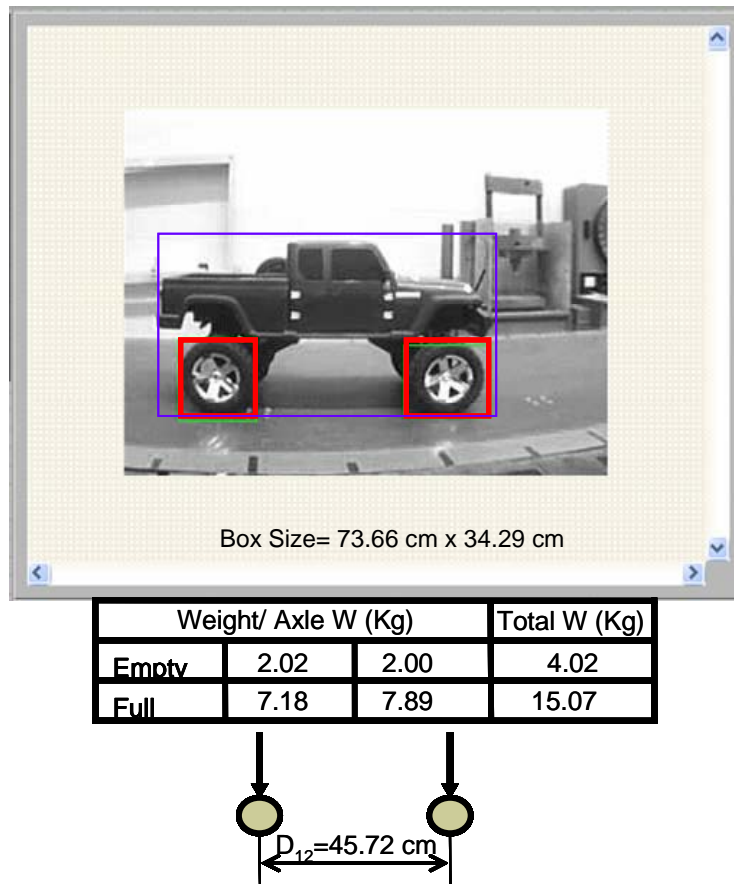


Figure 20. Characteristics of 2-Axle Vehicle Determined using Computer Vision.

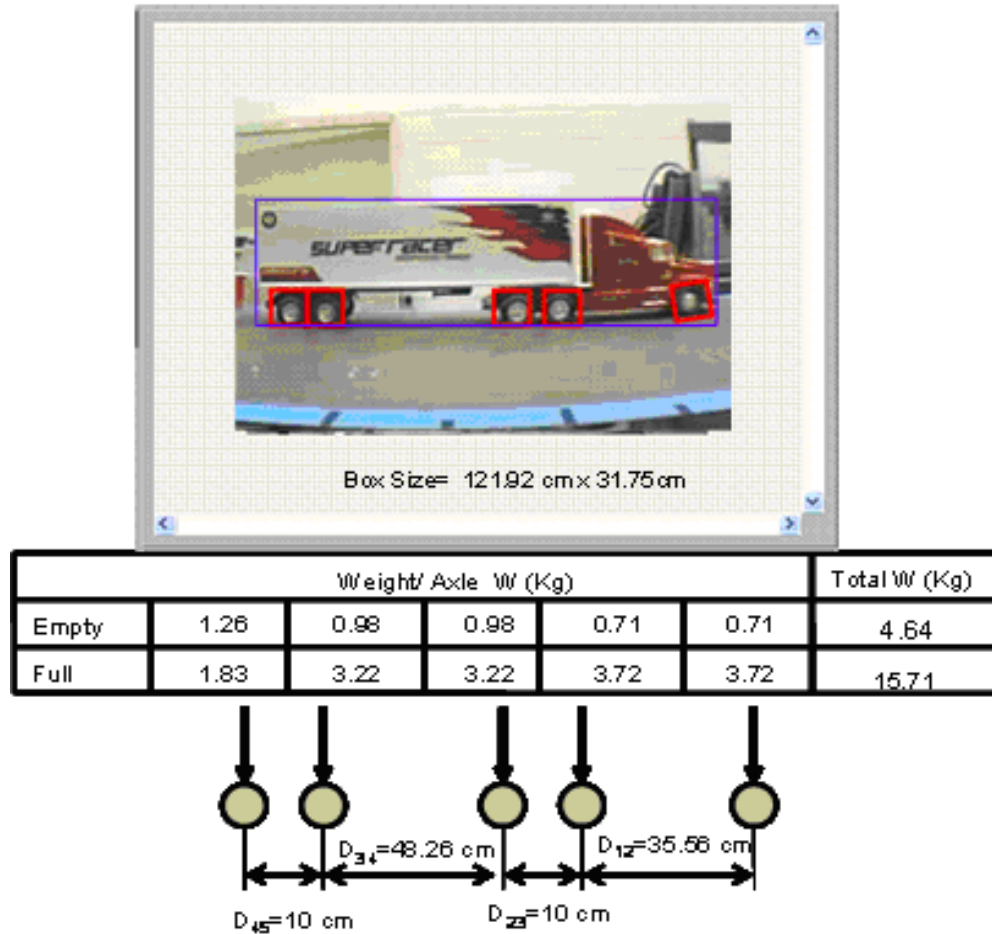


Figure 21.Characteristics of 5-Axle Vehicle Determined using Computer Vision.

3.4.3 Tracking of the Moving Vehicles on the Laboratory Bridge

A set of known points on the structure is used as reference (10 points for this example). These beacon points can be either selected by a user (Figure 22a) or detected automatically using pattern matching algorithms. Once the vehicle is detected, position in the image of the vehicle lower-leftmost pixel is determined and its distance d_{image} to the line S is calculated by using Equation 5. This distance is entered in Equation 6, obtaining the position of the vehicle (moving load) on the structure. Tracking is performed by matching the moving objects in two consecutive frames based on size, color, common motion and speed. Figure 22b shows the path of the vehicle while moving over the

structure, calculated using the described procedure. Figure 23 shows calculated instantaneous speed for both test vehicles. One of the advantages when using this method is that if by any reason, such as excessive wind, the camera moves and loses its calibration, recalibration can be performed in an automated way by detecting the reference points and correlating the image coordinates again with the corresponding real world.

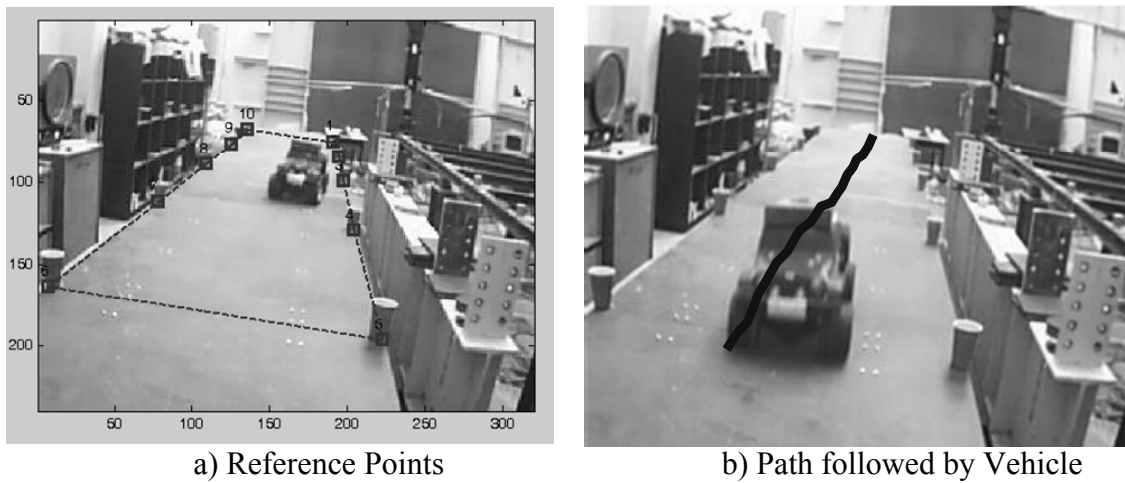


Figure 22. Tracking of the 2-Axle Vehicle

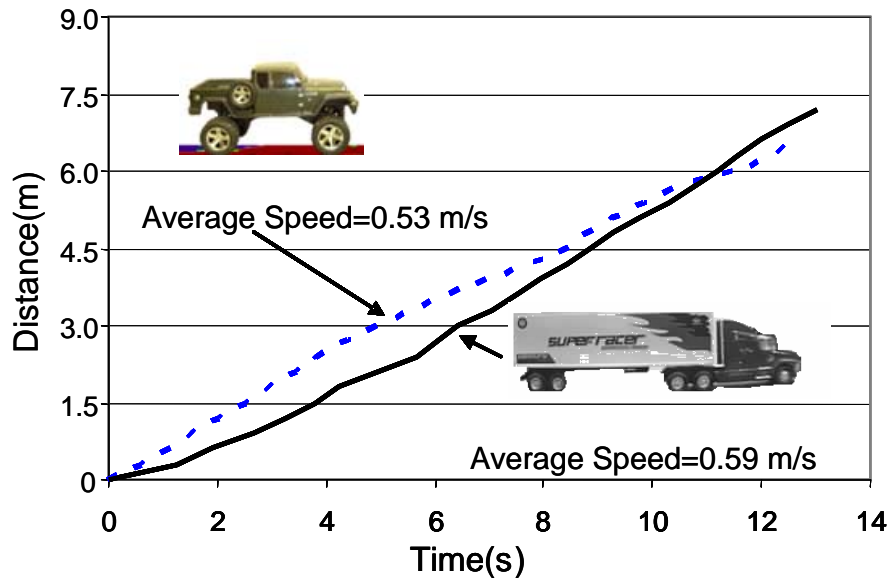


Figure 23. Calculated Instantaneous Speed for the Test Vehicles.

3.5. Load Location And Response Synchronization

Data image from the video camera can be decomposed in individual frames, each one captured in a particular time instant. As shown in Figure 24.



Figure 24. Video Image Frame Sequence with Time Stamp

The final goal is to obtain a direct correlation between the different locations of the vehicle over the bridge and the corresponding responses. By using computer vision algorithms, the vehicle is detected and classified as explained previously. The position of the front axle (and hence all other axles) is determined for each frame. Now, location of the front axle while vehicle is crawling over the bridge is determined with a time stamp. Finally, a MATLAB algorithm matches the time stamps of the location with those of the

sensors, relating the distance with responses. Figure 25 shows the strain readings from sensor SG2 for two different trucks. Each data point represents the response when the front axle is at that particular location on Lane 1. Due to the different truck load and axle configurations, the magnitudes and the truck position creating the maximum response are different.

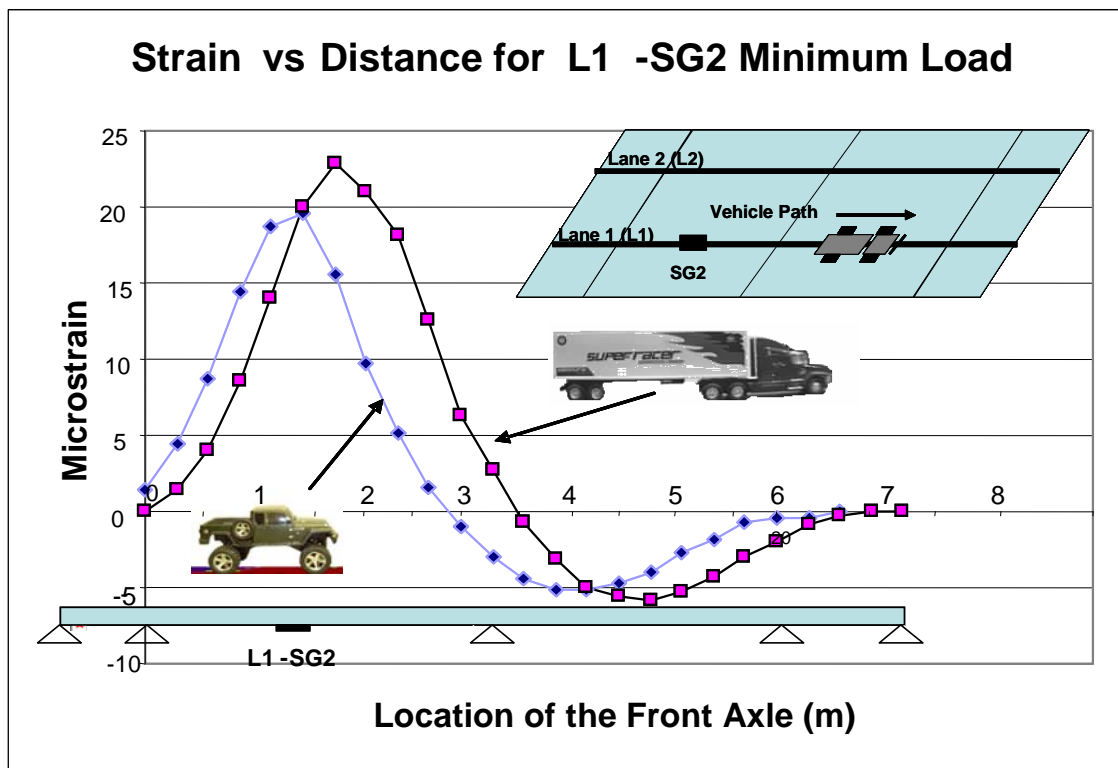


Figure 25. Strain vs. Distance for L1-SG2 (Both Vehicles with Minimum Load Capacity)

3.6. Identifying Unit Influence Lines from the Monitoring Data in the Laboratory

UIL provides a signature with a normalized bridge response for the critical locations instrumented by any type of sensor. One of the main advantages of using the method described in this study for condition assessment is the fact that with every vehicle crossing over the bridge, comparison between the previously obtained UIL and the most

recent one can be done.

To verify the synchronization of image data with measured responses, static tests were conducted by moving the front axis of the vehicle by one foot increments, recording the responses corresponding to them, and calculating the UIL for each case (Figure 26 and Figure 27). For this static test, the positions of the trucks were pre-determined and the structural responses were tagged with respect to these positions.

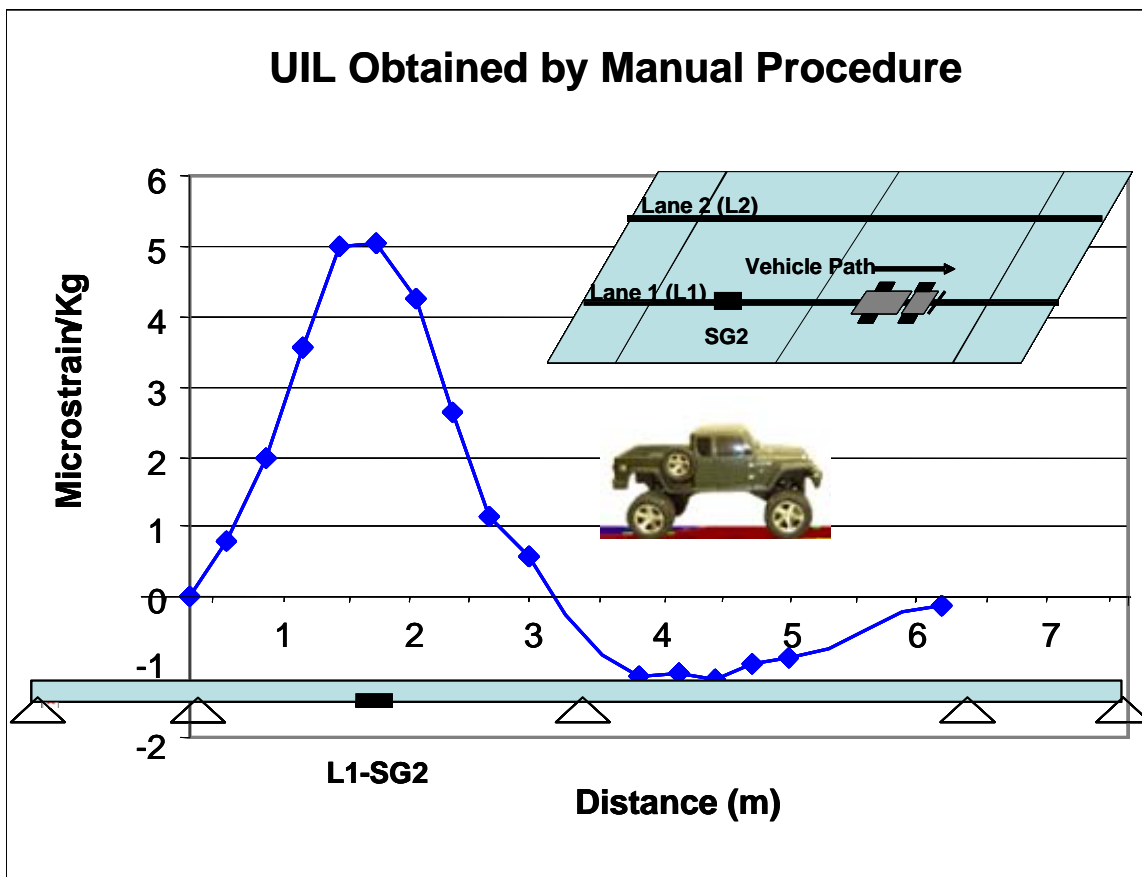


Figure 26. Unit Influence Line sensor L1-SG2 for 2-Wheel -Axle Vehicle. Manual Procedure

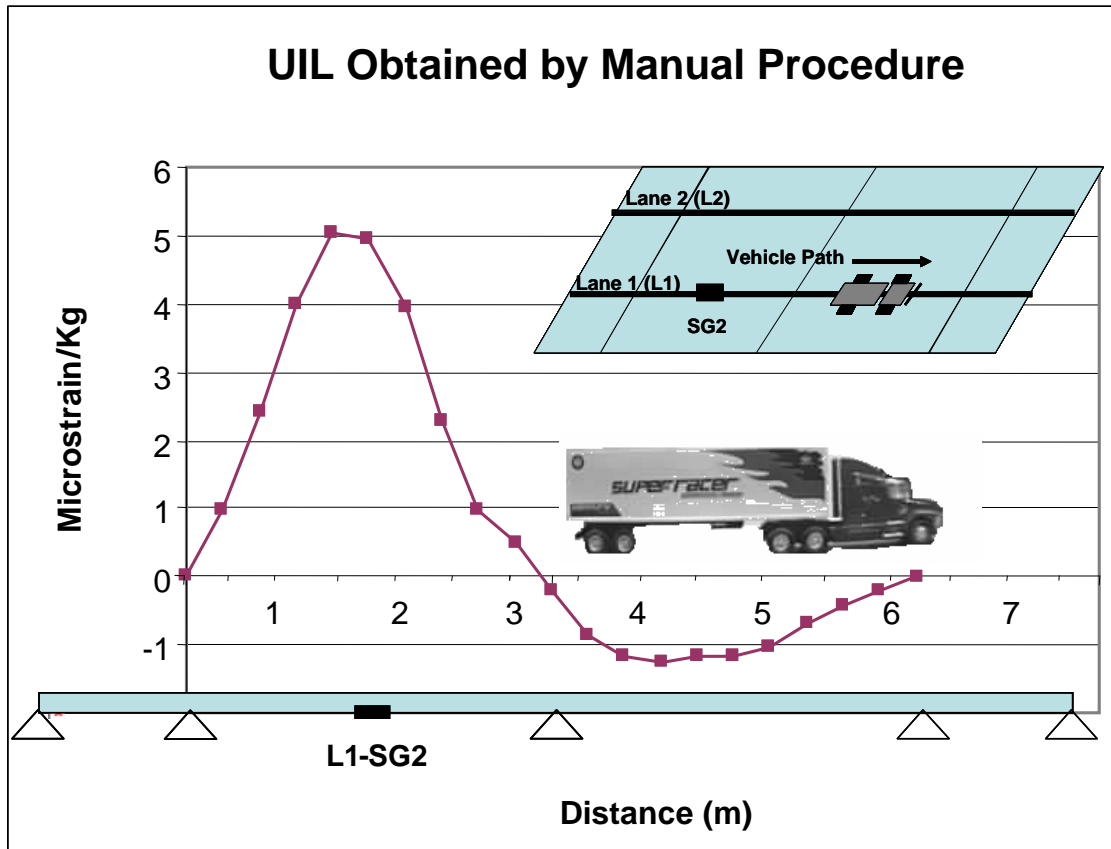


Figure 27. Unit Influence Line sensor L1-SG2 for 5-Wheel -Axle Vehicle. Manual Procedure

Subsequently, the computer vision system was used to determine the UIL by calculating the distances as the vehicles crawled over the bridge. The structure response was correlated with the input force and location by means of synchronized computer image data as shown in Figure 28 and Figure 29.

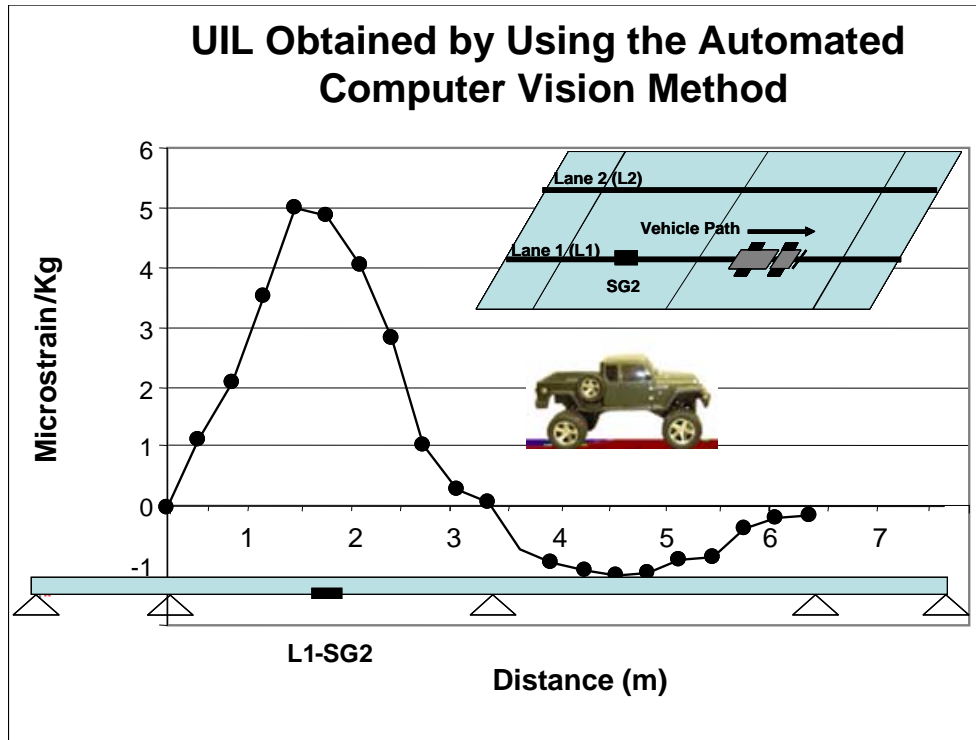


Figure 28. Unit Influence Line sensor L1-SG2 for 2-Wheel -Axle Vehicle. Automated Computer Vision Method

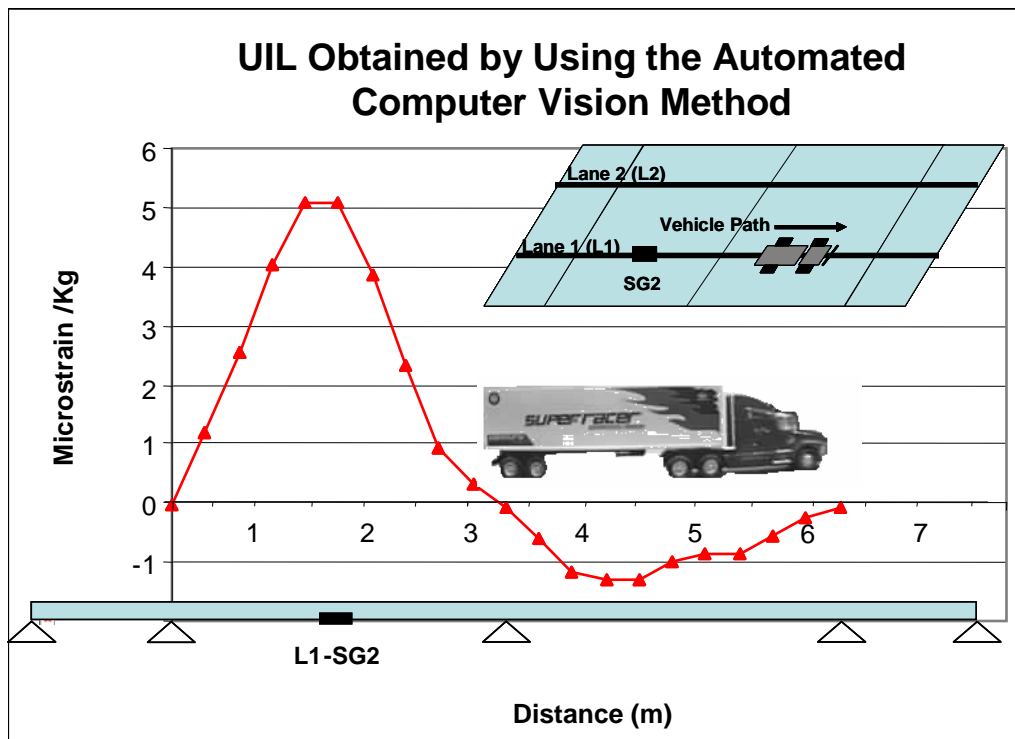


Figure 29. Unit Influence Line sensor L1-SG2 for 5-Wheel -Axle Vehicle. Automated Computer Vision Method

Both the static load test data and the load test with computer vision synchronization are analyzed to obtain UIL, as well as for different trucks. It should be emphasized that the exact location and type of vehicles are determined using computer vision algorithms. Locations are manually recorded for the static case. Figure 30 shows excellent agreement between static and dynamic cases. In addition, it is seen that UIL as a normalized index is identified almost identically for two different truck types.

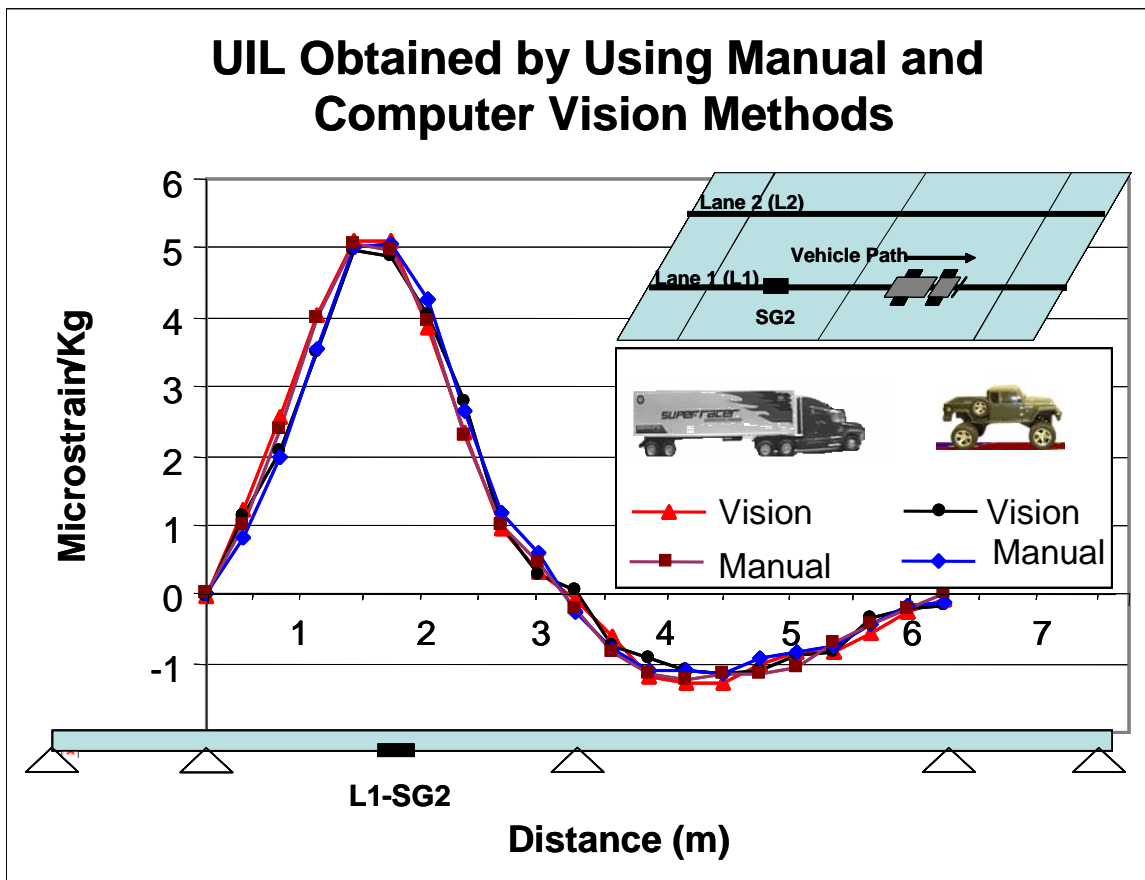


Figure 30. UIL Results for all Studied Cases

3.7. Summary

In this chapter, a conceptual damage index is formulated using the computer image and the sensor data for tracking the structural response under various load conditions. An experimental laboratory bridge model is utilized to demonstrate the application of video imaging and traditional sensor data for SHM along with the analysis methods. Video images and computer vision techniques are used to detect, classify, and track two different types of vehicles crawling over the bridge while sensors measure the corresponding responses. It is shown that a successful integration of computer vision techniques and sensor data on a four span bridge model loaded with different vehicles is achieved. With this method, a normalized response, Unit Influence Line (UIL), is obtained for each sensor location as function of the vehicle position that are determined using computer vision algorithms simultaneously with the sensor data. It should be noted that the vehicle type in terms of number of axles are also determined by computer vision algorithms as discussed in this chapter. Laboratory studies show a very good correlation between the UIL extracted using pre-determined load positions and those identified by computer vision. The algorithms, approaches and results given in this chapter, present very promising results for the application of the computer vision and UIL method on a real-life bridge as well as for using this information for damage detection and condition assessment for decision making.

4. CHAPTER FOUR: COMPUTER VISION AND SENSOR DATA ANALYSIS FOR DAMAGE DETECTION

The previous chapter presented the formulation of a conceptual damage index called Unit Influence Line (UIL), which is obtained by using the computer image and the sensor data for monitoring the structural response under different load conditions. Video images and computer vision techniques are used to detect, classify, and track vehicles on the bridge (input loads) while strain and tilt data are simultaneously collected as the structure response (output). In this chapter, UILs are obtained and used as features for damage identification. Statistical analysis is performed as outliers detection algorithms identify and localize induced damage on the UCF 4-span bridge model.

4.1. Statistical Analysis - Outliers Detection.

An outlier is an observation with an abnormal distance from other values in a random sample from a population. Outlier detection is one of the most common methods used in SHM to detect variations from measured structural behavior. In this paper a new approach for using UIL as damage feature is developed along with Mahalanobis distance-based outlier detection algorithm. Introduced by P. C. Mahalanobis in 1936, the Mahalanobis distance is based on correlations between variables by which different patterns can be identified and analyzed. It is a useful way of determining similarity or difference of an unknown sample set to a known one. It takes into account the covariance among the variables in calculating distances, hence it is scale invariant. A larger distance from the rest of the sample population of points indicates more dissimilarity. The Mahalanobis distance (Md) of a multivariate vector $\vec{x} = (x_1, x_2, \dots, x_n)$ to a distribution

with mean $\vec{\mu} = (\mu_1, \mu_2, \dots, \mu_n)$ and covariance matrix $S_{n \times n}$ is defined in (11).

$$Md = \sqrt{(x_i - \mu_i)_{1 \times n} S^{-1}_{n \times n} (x_i - \mu_i)^T_{n \times 1}} \quad (11)$$

If Md is greater than a pre-set threshold level, the vector is considered to be an outlier. For this study, the Mds of the UIL populations are compared against each other to determine the outliers that represent the change due to damage. The threshold is set for each sensor as the minimum Md value that includes all the extracted UIL within the set for $t_0 < t < t_1$. This will be explained in more detailed in the following sections.

4.2. Description of the Experiments

Two different remote controlled vehicles were used for this experiment, each one under two loading scenarios as shown in Figure 31. Every vehicle crawled over the undamaged structure for a total of 15 times for each load case to simulate monitoring over long term and collecting large data sets. In this way, a total of 60 UIL could be extracted, ensuring a sufficient number of feature vectors (UILs) for the analysis before the structure was damaged. Then, same procedure was repeated for the damaged structure.

Weight per Axis(kg)			Weight per Axis (kg)					
Axis 1	Axis 2	Total	Axis 1	Axis 2	Axis 3	Axis 4	Axis 5	Total
<i>EMPTY</i>			<i>EMPTY</i>					
2.02	2.00	4.02	1.26	0.98	0.98	0.71	0.71	4.64
<i>LOADED</i>			<i>LOADED</i>					
7.18	7.89	15.07	1.83	3.22	3.22	3.72	3.72	15.71

Figure 31. Loading Scenarios

4.2.1 *Damage Scenarios*

Different damage scenarios were considered and implemented on the UCF-4-span bridge as shown in Figure 32. These cases were chosen because they represent some of the most common damages affecting bridge performance based on our private conversations with the Department of Transportation (DOT) engineers. The first three cases (Figure 32a, b, and c) involve changes in boundary conditions corresponding to a case usually found when rollers or pinned supports of the bridge (Figure 33a) become corroded or blocked by cinders and the structural configuration of the bridge changes. These alterations cause stress redistribution, affecting the different structural elements and may subject them to additional forces. In the bridge model, this case was simulated by fixing the supports as shown in Figure 33b. Missing bolts and section stiffness reduction are also cases presented by DOT engineers. Cases 4 and 5 simulate the loss of connectivity between composite sections and also can generate localized stiffness reduction. For case 4, only four bolts were loosened (Figure 32d) while for case 5, eight bolts were released (Figure 32e). Figure 33d shows the bridge model when bolts were retired for testing. Case 6 is another example of changes in boundary conditions. Here, the rollers at the central support were change from roller to elastomeric pad (Figure 32 f and Figure 33 c).

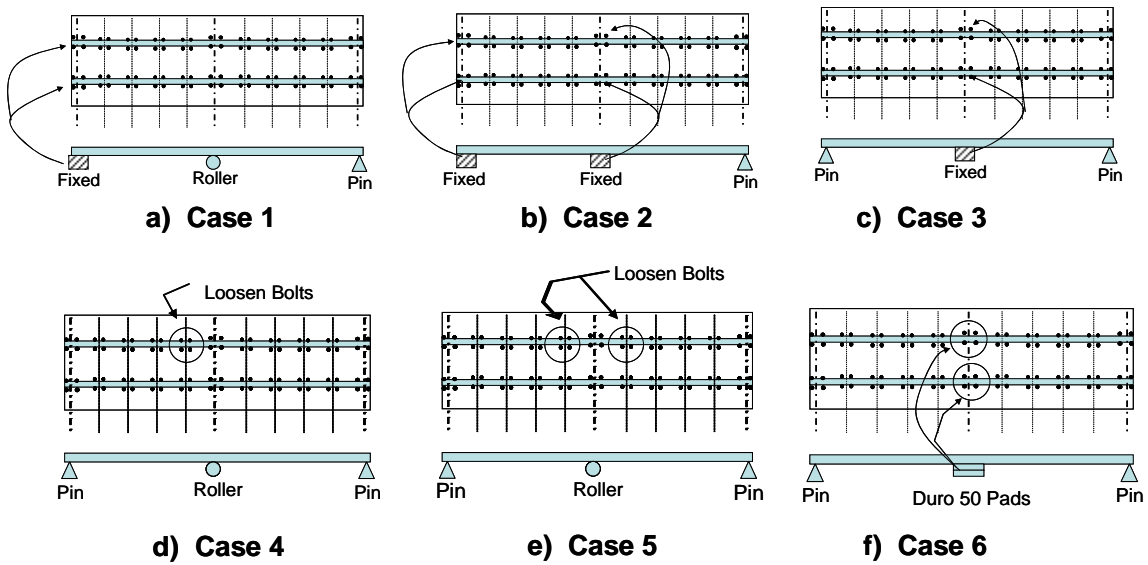


Figure 32. Studied Damage Cases

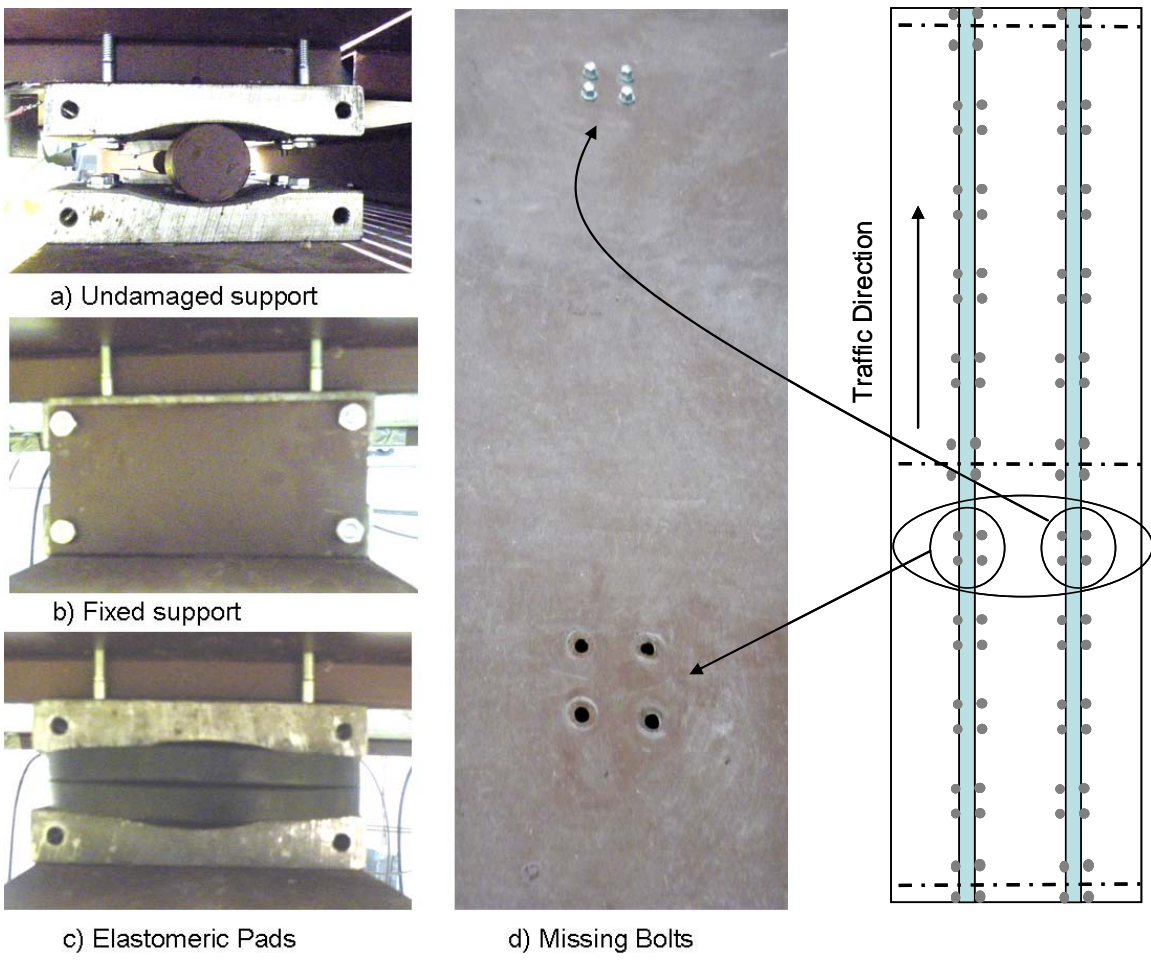


Figure 33. Simulated Damage Cases

4.3. Damage Detection Using a Statistical Distribution of UIL Vectors as Damage Feature

4.3.1 *Unit Influence Lines Extraction*

As previously explained, data is typically collected in time domain. In order to use measured vehicle responses to extract UILs, a direct correlation between responses and load location is needed. The raw data for the measured responses are a combination of static and dynamic responses, and noise (Figure 34a). Static responses have to be determined filtering out the other components. As explained previously, filtering is performed by changing the time domain data into frequency domain using Fourier Transformation (Figure 34b). The resultant signal is converted back to the time domain by applying the Inverse Fourier Transformation as shown in Figure 34c. Subsequently, the computer vision algorithm is used to detect and track each one of the test vehicles by calculating the location versus time as the vehicles crawl over the bridge (Figure 34d). Finally, the structure response is correlated with the input force and location by means of synchronized computer image data and UIL are extracted as shown in Figure 34e [37].

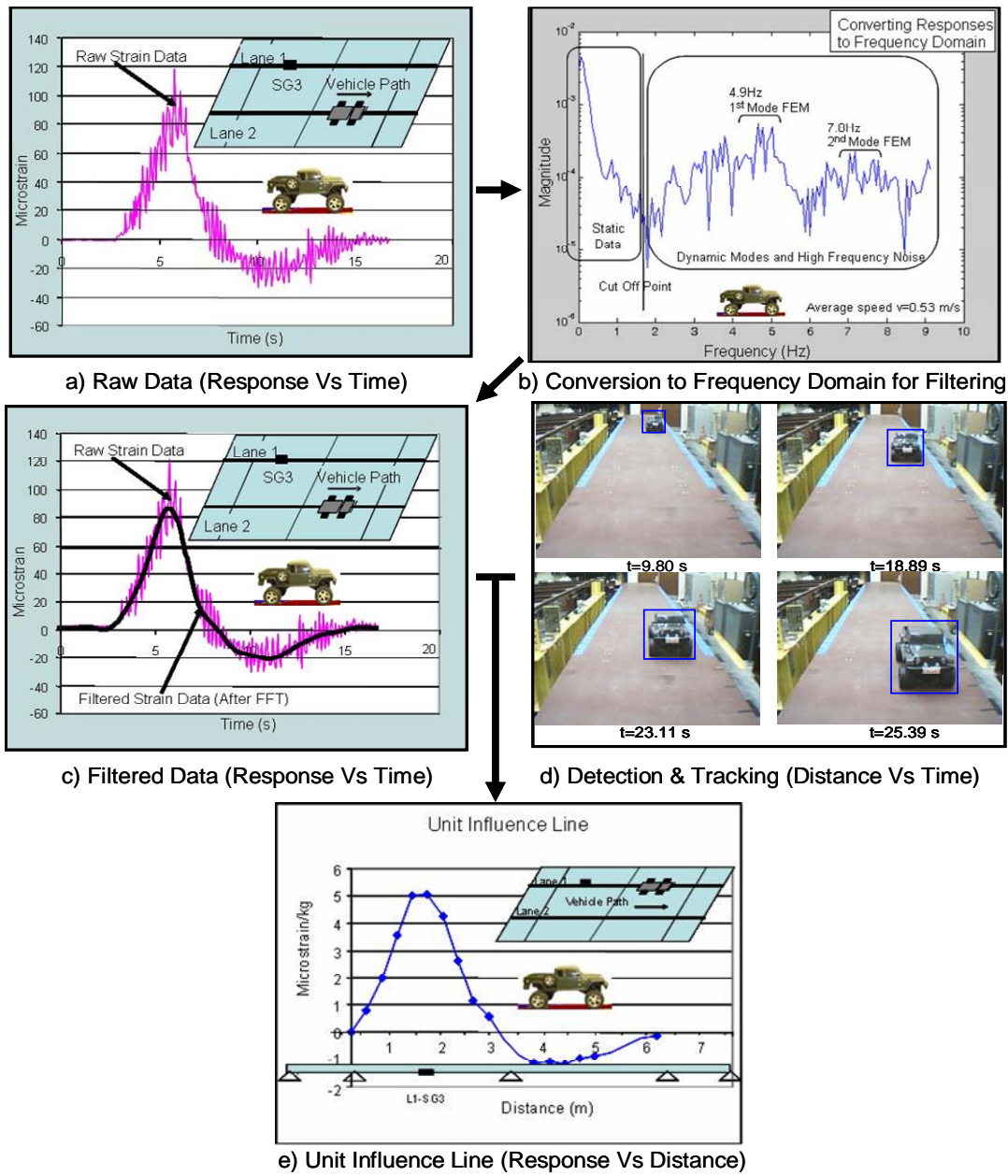


Figure 34. Procedure for Unit Influence Line Extraction

4.3.2 Overview of Outlier Detection from UIL Population for Damage Detection

In this section, the theoretical basis of the proposed method is introduced. First, video images are used to detect, classify and track the vehicles (input loads) crawling over the bridge model while sensor data (responses) is captured and correlated with the loading position. A set of UIL is extracted for an initial time interval ($t_0 < t < t_1$) where

the structure is undamaged. Out of this first set of UIL (represented in Figure 35 as y_{ij}), the mean for each UIL points (μ_i) and covariance matrix for the whole set (S) are calculated. For each UIL, Mahalanobis distance is calculated to determine the variation of the set with respect to the rest of the feature sets, and a threshold is established in such a way that all UILs within the initial set ‘y’ are inliers. Then, at a new time interval ($t_1 < t < t_2$) where damage is assumed to occur, a new set of UILs is extracted (x_{ij}), Mahalanobis distance is calculated and thresholded to detect possible damage on the structure. In Figure 35 a summary of the process is shown where y_{ij} and x_{ij} denote unit influence line coefficients obtained at two different times; ‘i’ identifies the test number and ‘j’ refers to the load location.

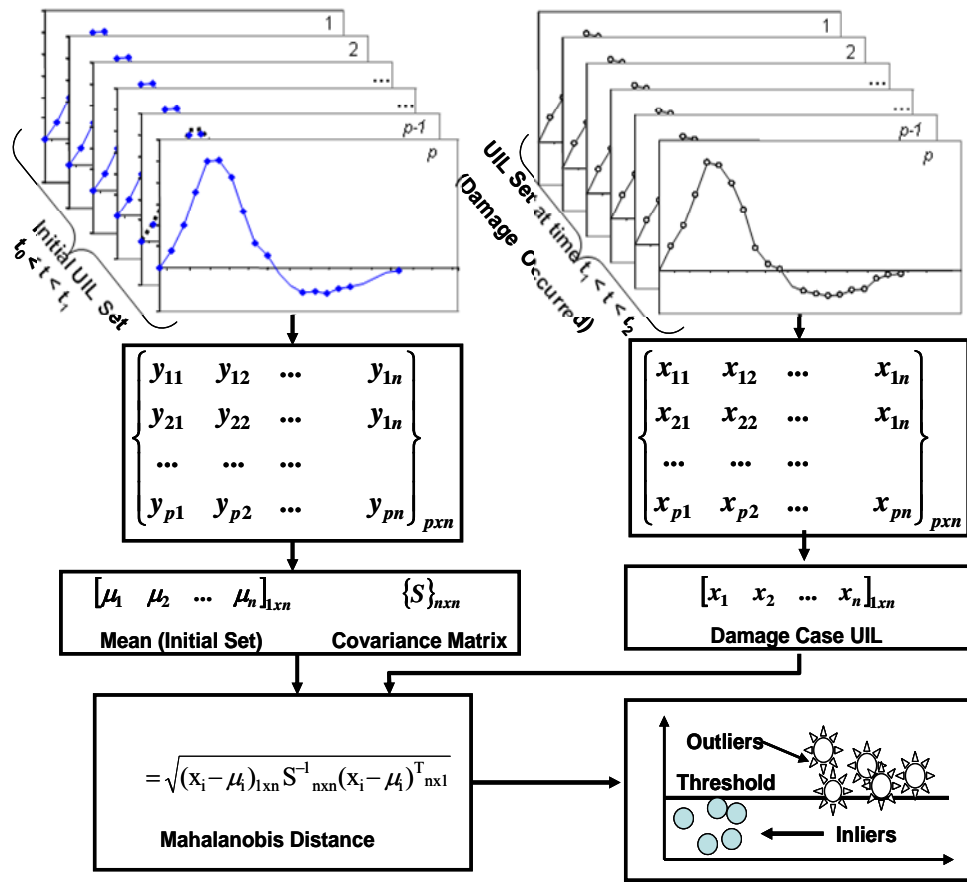


Figure 35. Overview of the Methodology

4.4. Outliers Detection-Clustering

After applying and processing the different damage cases, influence lines were obtained as explained in the previous section. Mahalanobis distance was calculated and results are plotted in Figures 36-41. In general, it can be seen that almost every sensor show some kind of variation with respect to the baseline data set population collected at $t_0 < t < t_1$. It is also noticeable that the sensors closer to the damaged area show a greater Mahalanobis distance than those farther away. Even though strain gages provide a localized response, the method shows sufficient information for the different channels to determine the damage location from the relative distances from the thresholds.

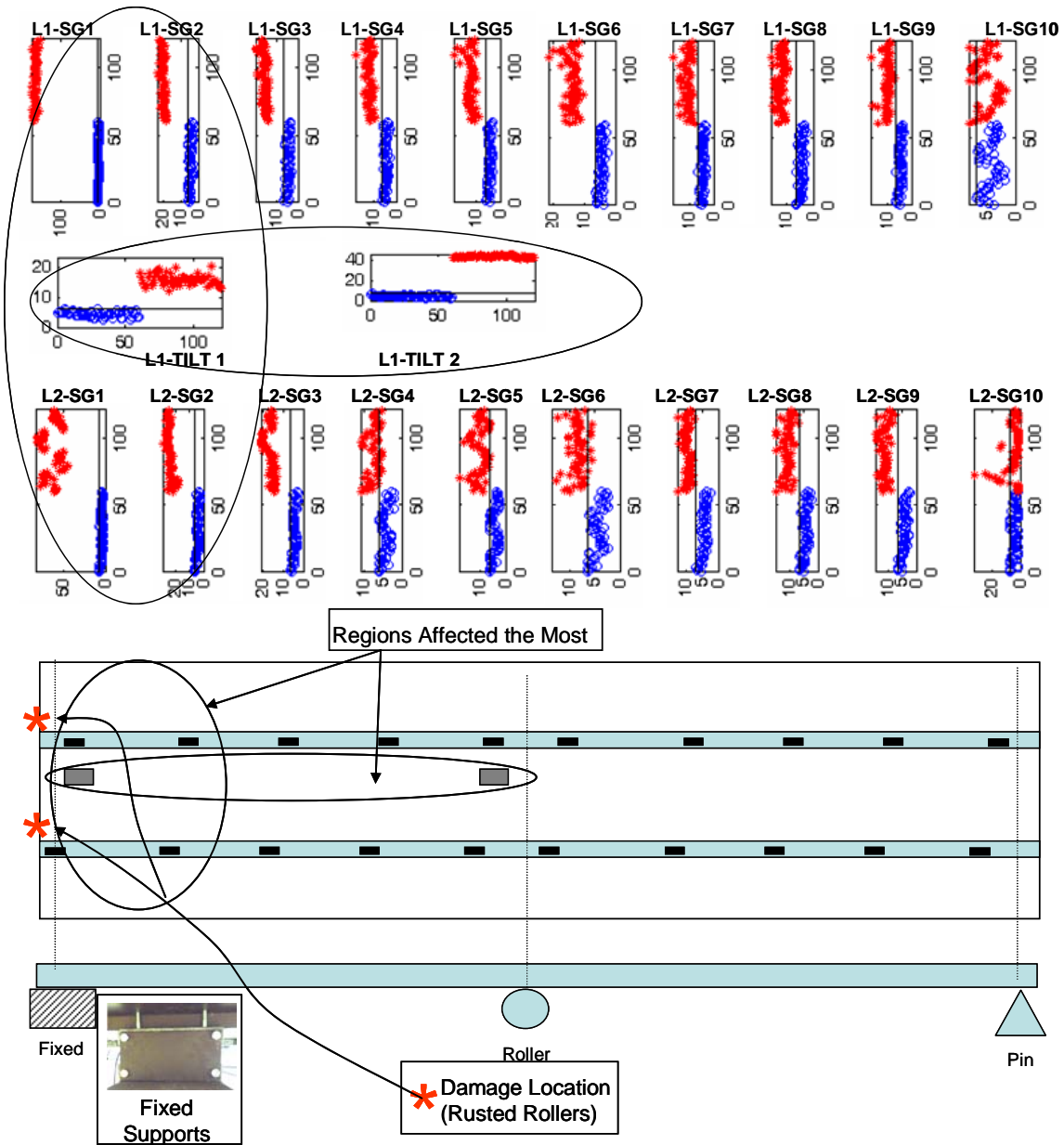


Figure 36. Damage Case 1: Rusted Rollers (First Support)

In Figure 36 the outlier near the vicinity of the first support (where damage is induced ($t_1 < t < t_2$)) indicates that the change in structural behavior is greater compared to others. When damage progresses by fixing the middle support also (Figure 37), it is seen that outliers start to separate with greater distances for the middle location sensors as well.

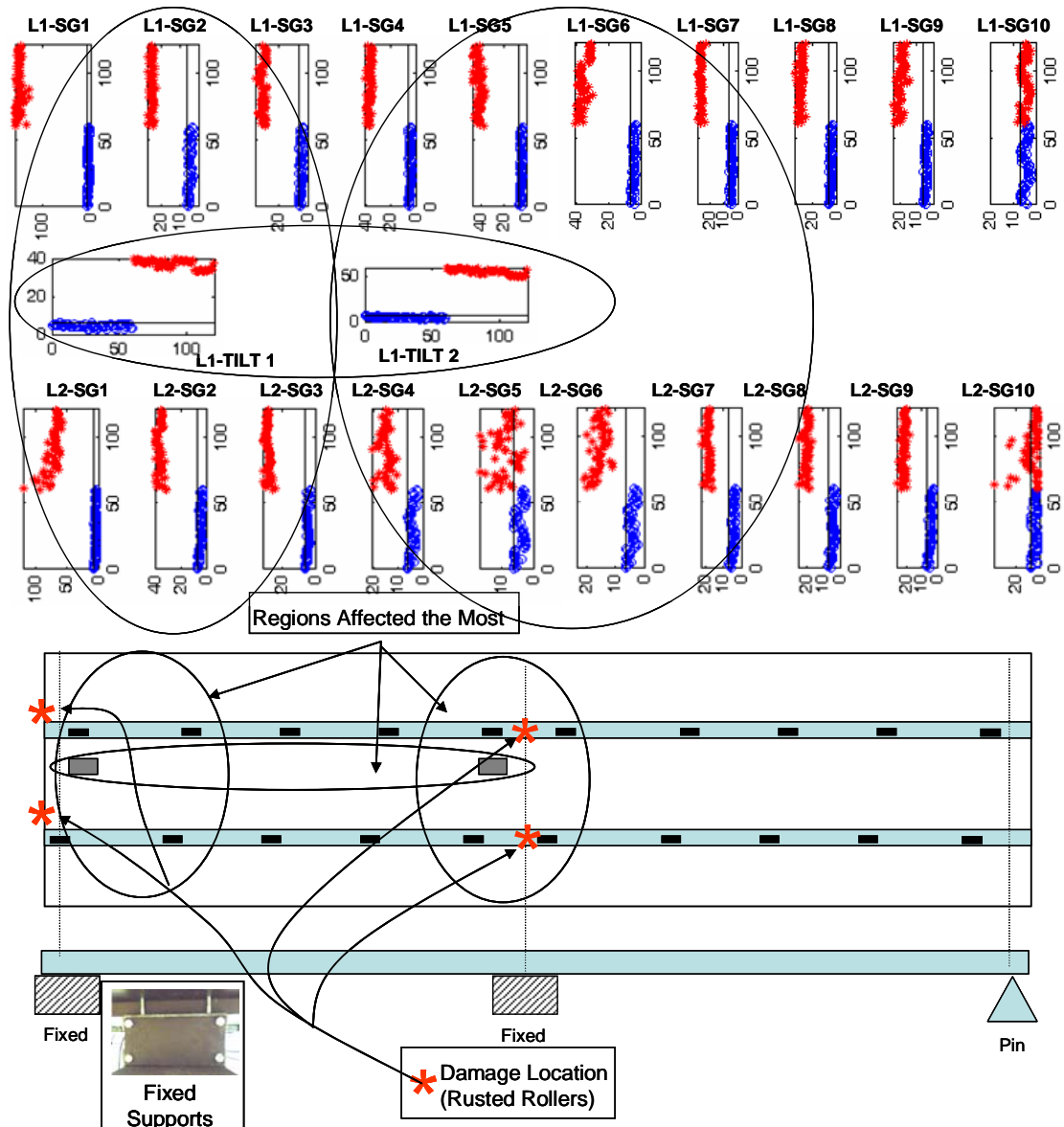


Figure 37. Damage Case 2: Rusted Rollers (First and Second Support)

In Figure 38 presence of significant amount of outliers for all sensors can also be seen. The distances these outliers are plotted from the threshold show how much the readings deviate from the undamaged case at $t_0 < t < t_1$. This approach is an efficient means of handling large sets of data in a very rapid way. Once the thresholds are exceeded, it is an indication of a change and further evaluation of UIL that indicates this change can be evaluated to determine the effect of this change (e.g., stress response due

to a design truck applied to UIL) on the bridge.

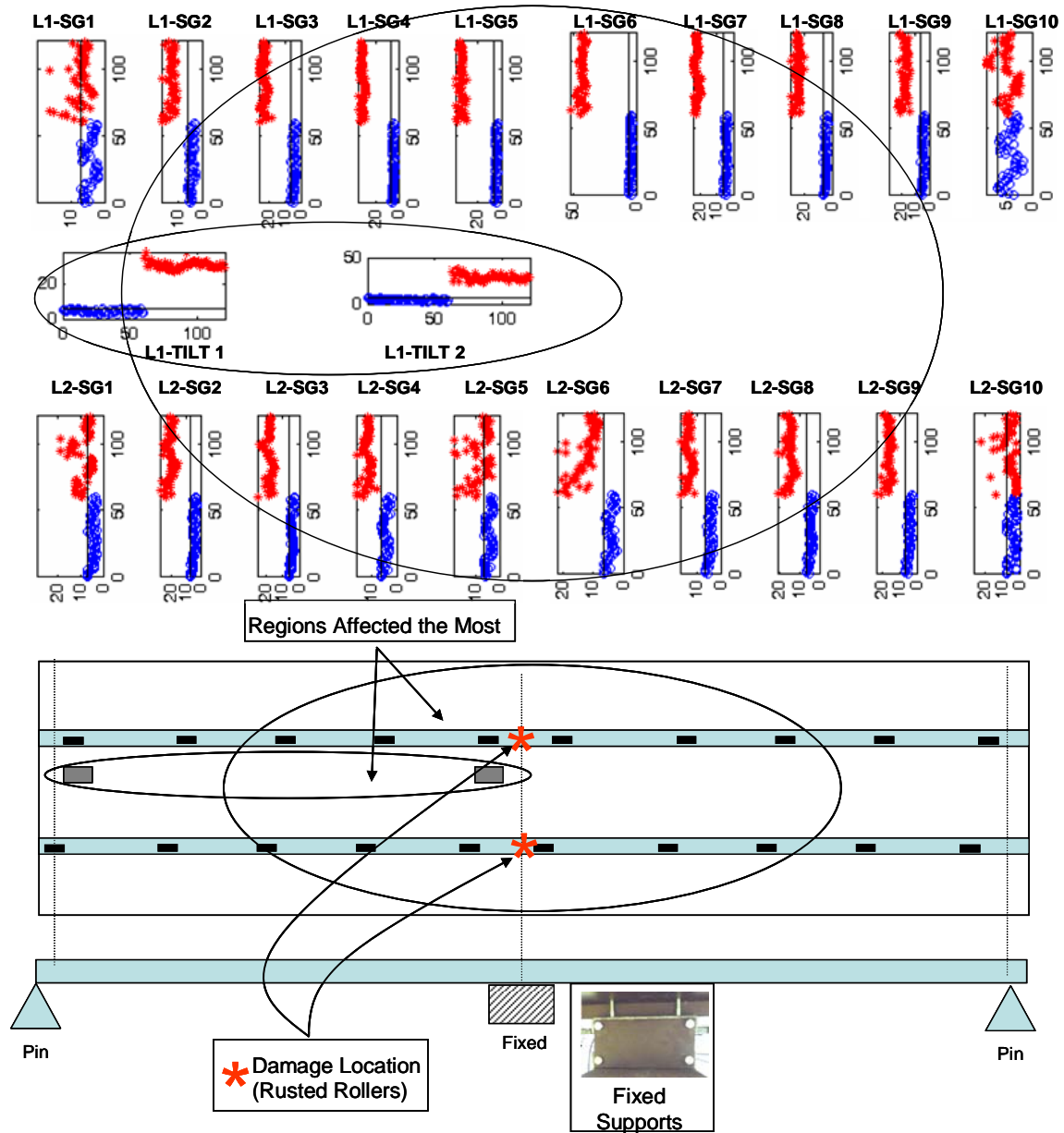


Figure 38. Damage Case 3: Rusted Rollers (Second Support)

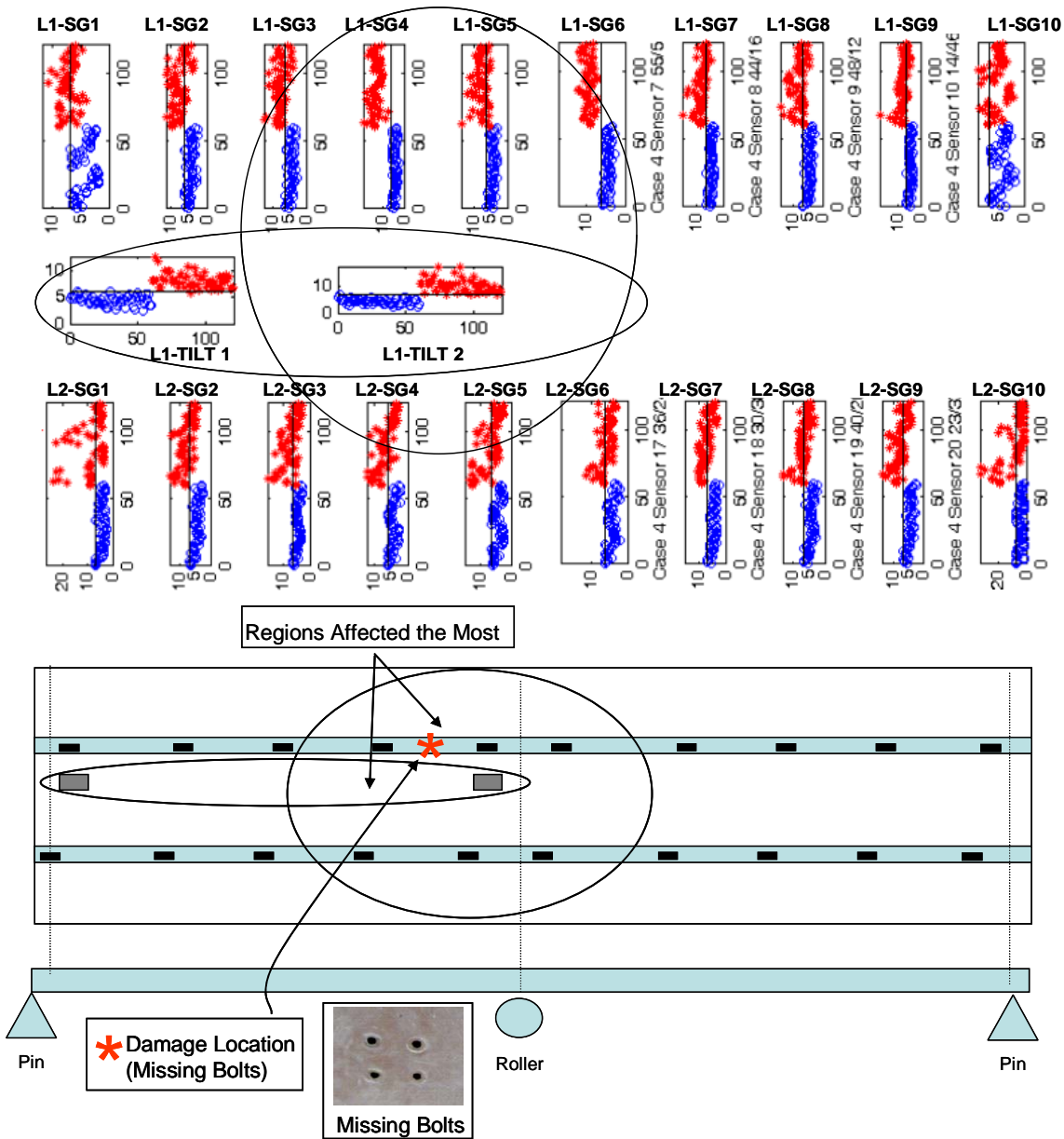


Figure 39. Damage Case 4: Missing Bolts (One Location)

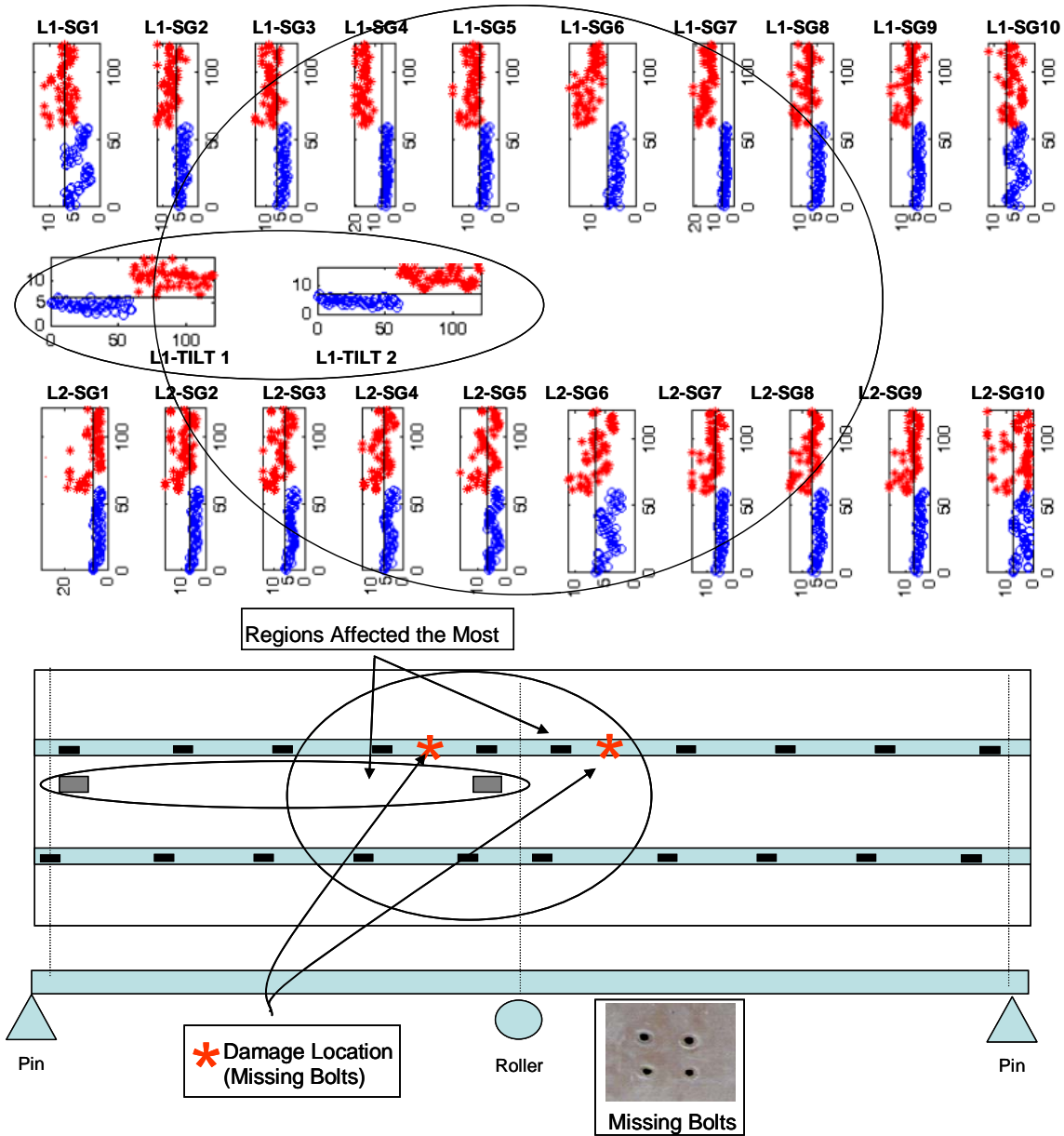


Figure 40. Damage Case 5: Missing Bolts (Two Locations)

Missing bolts causes loss of connectivity between deck and girder, affecting the composite section behavior and inducing a stiffness reduction of the structure in those localized regions. For most occasions, if only few bolts are missing, the structure properties may not be expected to change significantly, making it difficult to detect. However, as the damage progresses the structural integrity can be compromised rapidly.

Figures 39 and 40 present the results for case 4 (4 removed bolts) and case 5 (8 missing bolts) respectively. The application of the proposed detection algorithm shows that even for the case 4, with only four missing bolts, significant variation of the UILs feature vectors was detected and shown through the outliers plots. In Figure 40 the separation of outliers from threshold line becomes more apparent in the vicinity of the damage.

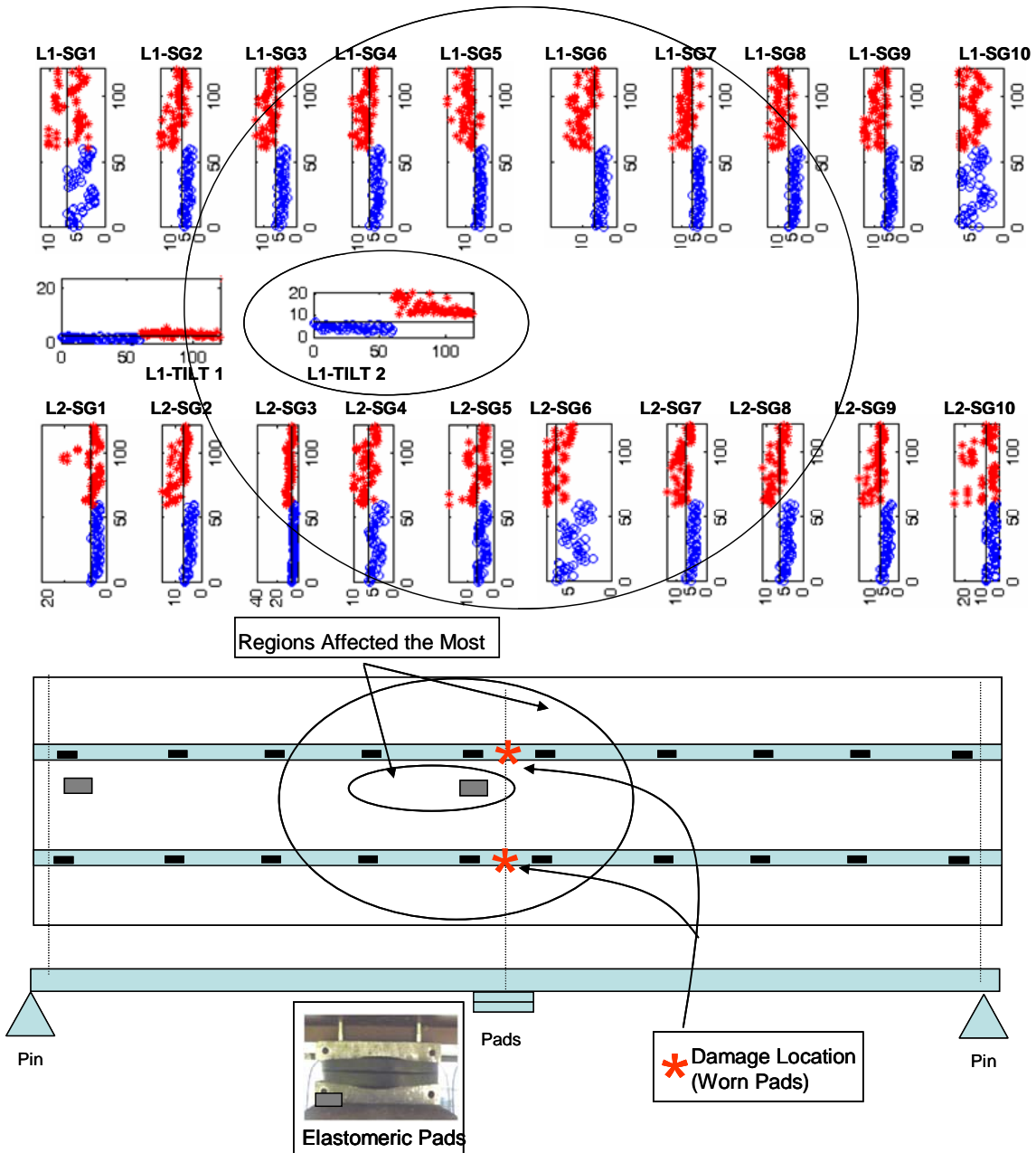


Figure 41. Damage Case 6: Worn or not Fully Settled Pads (Elastomeric Pads)

Substitution of central rollers for elastomeric pads simulates those situations where support pads are worn or not fully settled (Case 6). This is also one difficult case to detect; however, in Figure 41 one can observe that outliers are present and their number as well as their distance from the threshold increase for those sensors closer to the affected region showing change of structural behavior along with some type of

location and intensity information.

4.5. A New Method for Identification of Damage

In the previous section, Mahalanobis distance-based outlier detection algorithm is presented with figures (Figures 36-41) showing the sensors which are more affected by a particular damage case. Although the inspection and evaluation of outliers provides valuable information, it might be tedious in some cases. As a result, it is more desirable to find a more effective method to not only show differences between different sets of measurements but also better pinpoint the approximate area where damage exists. Since Mahalanobis distance (Md) is scale invariant, it is possible to plot all sensors in a single representative graph. First, the mean of the Md values for the set corresponding to $t_0 < t < t_1$ and the mean of all outliers for the set $t_1 < t < t_2$ are calculated (Figure 42). If all of the calculated Mds from the set ($t_1 < t < t_2$) are outliers, the distance between their mean divided by the mean of the Md set for $t_0 < t < t_1$ can be considered as the normalized change, a new index which can be denoted as \bar{N}_d . Therefore, \bar{N}_d is a normalized indicator between Mds calculated for UIL sets obtained at two different times ($t_0 < t < t_1$ and $t_1 < t < t_2$) during the monitoring of the structure.

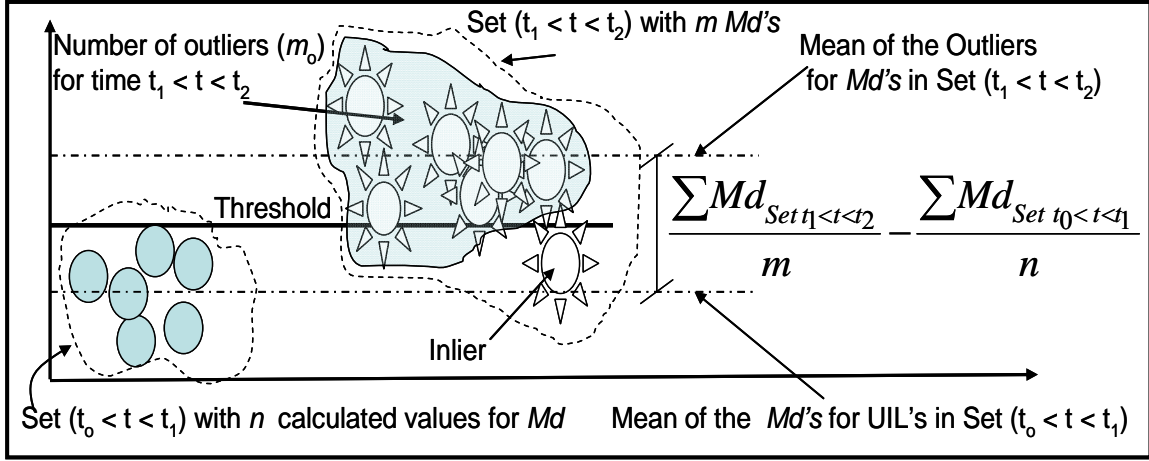


Figure 42. Distance Between two UIL Sets

If there is any inlier within the UIL set ($t_1 < t < t_2$), as shown in

Figure 42, then the normalized distance \bar{N}_d has to be affected by the relation between the number of outliers (m_o) and the total number of points within the set (m) as written in Equation 12.

$$\bar{N}_d = \frac{\left| \frac{\sum_{i=1}^{m_o} Md_{i(t_1 < t < t_2)}}{m_o} - \frac{\sum_{i=1}^n Md_{i(t_0 < t < t_1)}}{n} \right|}{\frac{\sum_{i=1}^n Md_{i(t_0 < t < t_1)}}{n}} \left(\frac{m_o}{m} \right) \quad (12)$$

Figure 43 through Figure 49 show the plots of index \bar{N}_d for all sensors and for all damage cases studied. The sensor locations are shown in the figures along with the damage location and types. The bar diagram shown on the top of the bridge and its instrumentation figure corresponds to \bar{N}_d for each sensor. As discussed before, the first damage case corresponds to changes in the boundary conditions due to rust in the rollers.

This damage case was simulated by fixing the supports accordingly. By simply inspecting Figures 43-49 it can be noticed that the plot for \bar{N}_d distance shows the approximate area where the damage occurred.

As can be seen from Figure 43, when the boundary conditions are fixed, the \bar{N}_d corresponding at the boundary location UIL set indicate major separation from the initial case (set $t_0 < t < t_1$ corresponding to roller boundary conditions). We also notice that the two \bar{N}_d s at the support location have different level of effect due to changes at the boundary conditions.

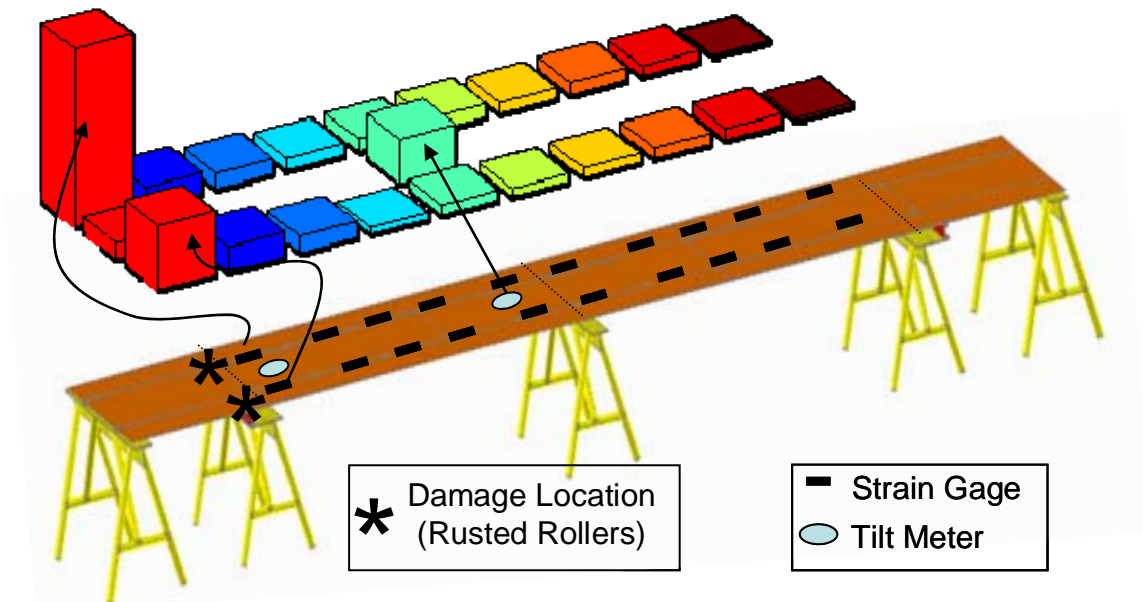


Figure 43. Damage Identification for Case 1 (Rusted Rollers on Left Support)

A closer look at Figure 43 (damage Case 1) shows that the tiltmeter 2 (close to the central support) presents more variation than the one located at the vicinity of the left support, where the damage was induced. At this point, it is important to analyze the

reason for this outcome and evaluate if this corresponds to a physical case or it is a shortcoming of the proposed method.

Figure 44 shows the influence lines obtained for the undamaged and damaged case 1. The variation in the UILs for both sensors is shown as the shaded grey area. It can be easily seen that even though the induced damaged happened at the left support, the change in UIL is greater for the tiltmeter located at the central support. The tiltmeter 1 senses a greater change while the moving load is on the first span, closer to it. However, once the load crosses the central support, the variation for the measured rotations is small. Tiltmeter 2 detects changes happening as the load moves through both spans of the continuous structure, hence \bar{N}_d appears greater for this sensor.

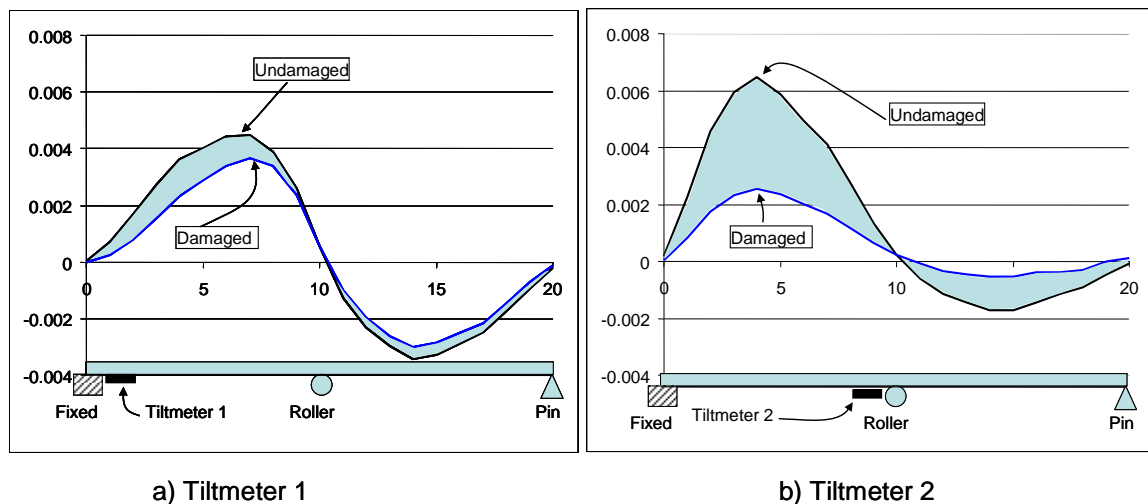


Figure 44. UIL for Tiltmeters 1 and 2 (Undamaged Case and Case 1)

Also, it is evident in Figure 43 that Girder 1 shows more relative change than Girder 2. The reason for this is that all UILs were obtained when the vehicles were crawling on top of Girder 1. The small values for strain and rotation on Girder 2 as well

as all uncertainties described before, affect Girder 2, revealing damage only at the vicinity of damage with relatively less \bar{N}_d magnitude compared with the \bar{N}_d magnitude or Girder 1 as shown in the bar chart in Figure 43.

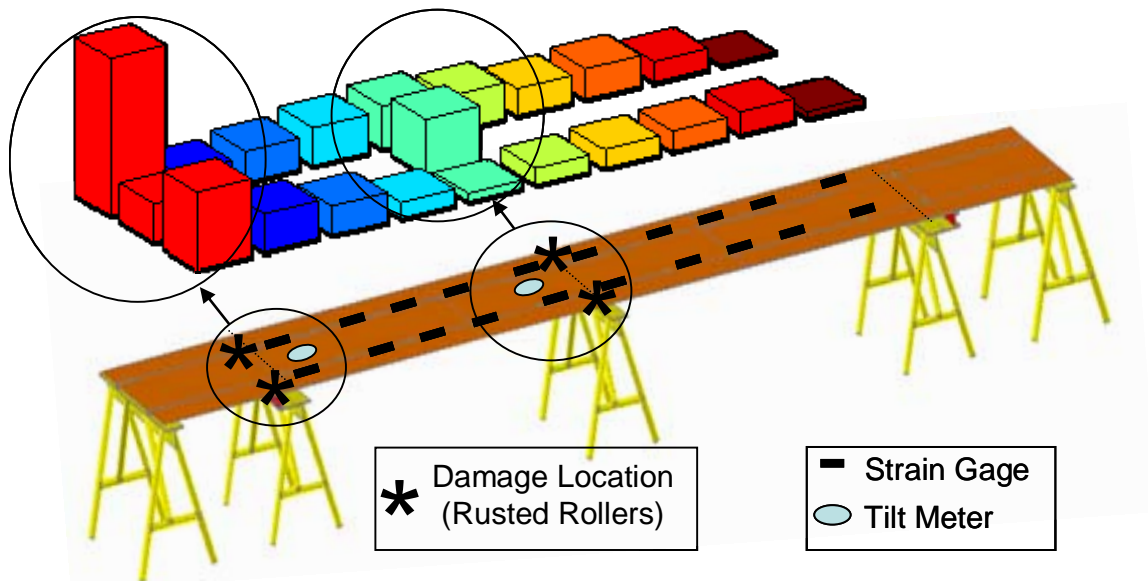


Figure 45. Damage Identification for Case 2 (Rusted Rollers on Left and Central Support)

Figure 45 shows the \bar{N}_d plot for the case where damage was induced by fixing the left and the central support (Case 2). Same as before, the height of the bars corresponding to the strain sensors increases as their location is closer to the damage region. Also, similar behavior as that of Case 1 is observed for the tiltmeters, where the magnitude of \bar{N}_d is larger for the intermediate tiltmeter measurement.

In Figure 46 the bar diagram for index \bar{N}_d at Girder 1 shows a distribution that can be easily determined and located around the central support. Once again, both tiltmeters present significant change which is expected due to the global nature of the

rotational response when corresponding degree of freedom is restrained. For Girder 2, it also can be inferred that some change has occurred but its location is not as clear.

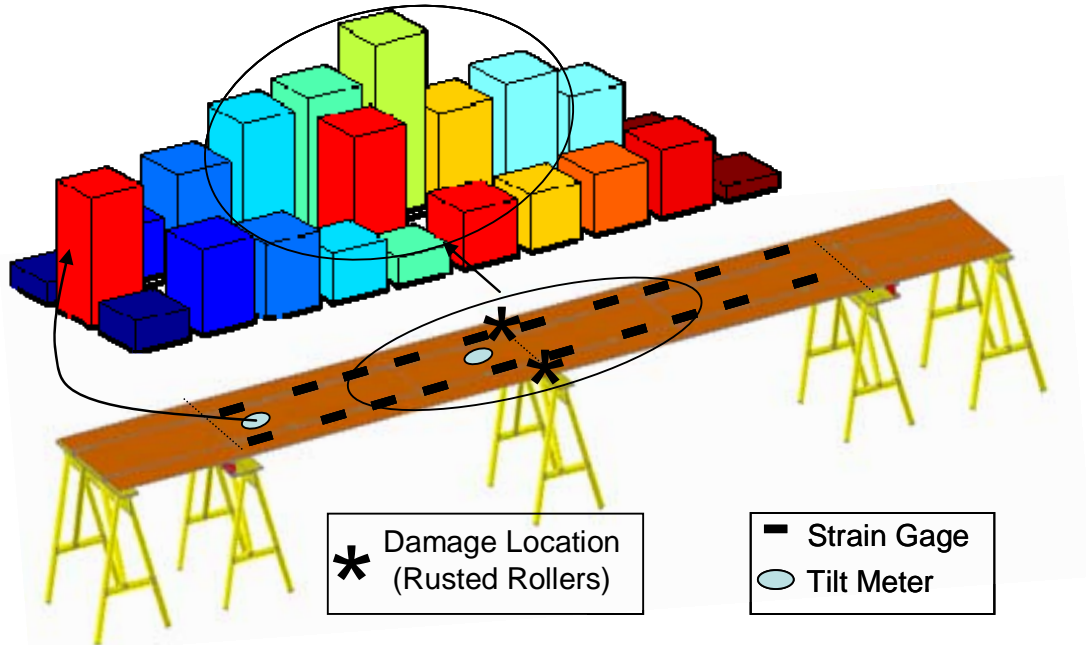


Figure 46. Damage Identification for Case3 (Rusted Rollers Central Support)

Figures 47-48 correspond to damage cases 4 and 5. As previously described, these cases simulate missing bolts causing loss of connectivity between composite sections with the corresponding stiffness reduction. For case 4, only four bolts were disconnected and 8 bolts were retired for case 5. Once again, by simple inspection, the plot of \bar{N}_d allows to detect the approximate region where the damage is present.

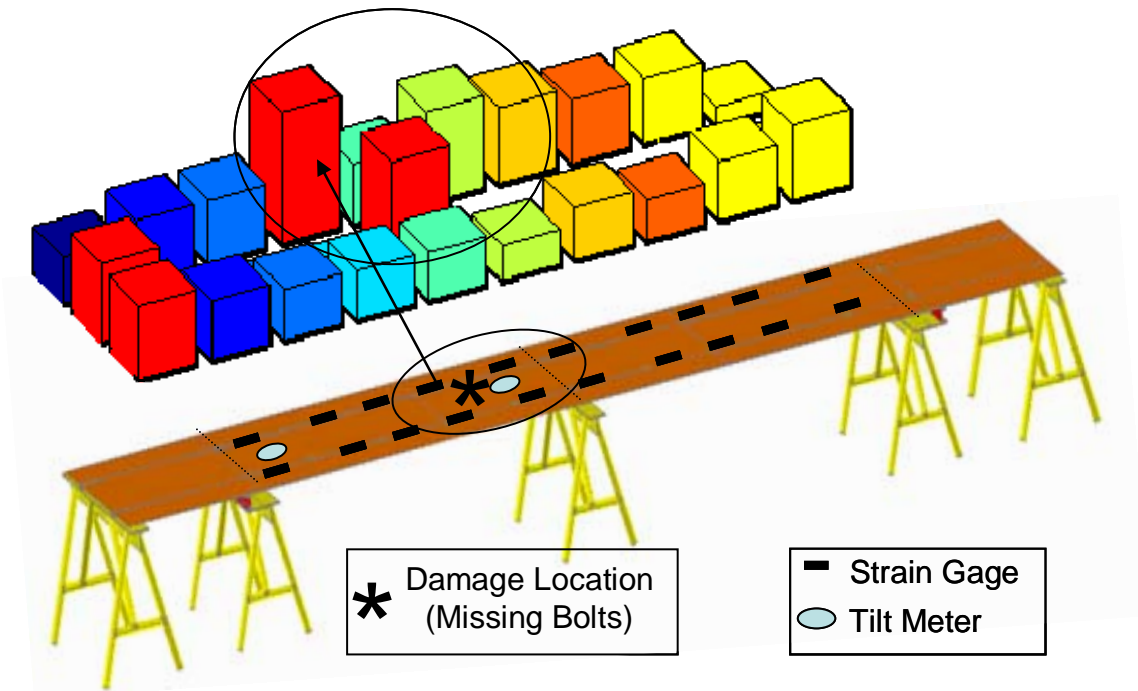


Figure 47. Damage Identification for Case 4 (4-Missing Bolts)

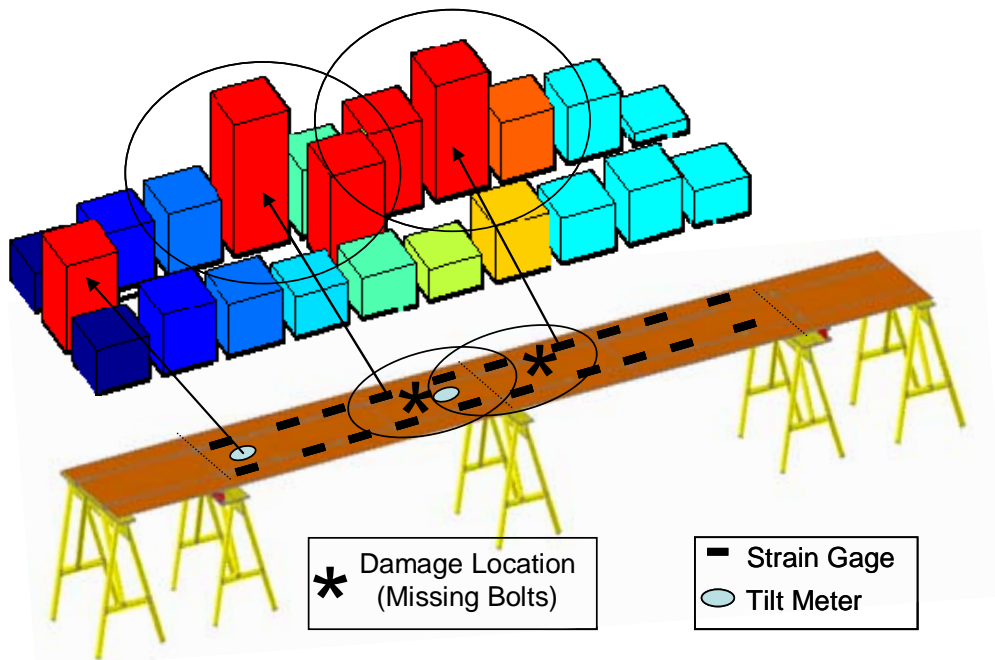


Figure 48. Damage Identification for Case 5 (8-Missing Bolts)

Finally Figure 49 shows the results of the damage detection method for changed boundary conditions. Worn or not fully settled pads of the supports are simulated by replacing the central roller with elastomeric pads as shown previously. Even though this is a challenging case for detection, here it is also identified the approximate region where the damage is present, leading to conducting further and more extensive examination and analysis.

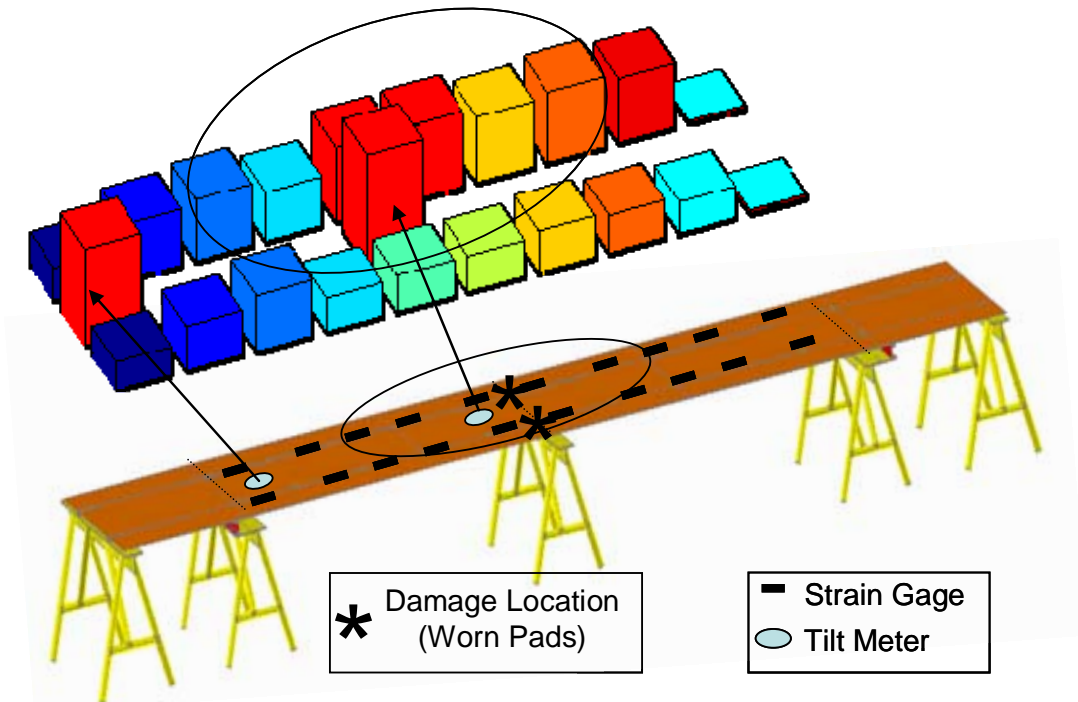


Figure 49. Damage Identification for Case 6 (Worn/Not Fully Settled Pads)

4.6. Summary

The Integration of computer imaging with traditional sensing technology provides a method to monitor the structures continuously by using UIL as a normalized bridge response for the critical locations instrumented by any type of sensor. The UIL sets can further be employed for statistical analysis for each measurement location using a Mahalanobis distance based outlier detection algorithm. In this chapter, a new method was also proposed to more effectively identify, localize and quantify (in a relative sense) induced damage.

The results presented in this chapter show that the methodology discussed herein was able to sense changes on the experimental test set-up. Even small and localized damage cases like missing bolts (Case 4) were successfully detected. It should be noted that the sensor spatial resolution is also important to capture the behavior. Damage detection was also possible by calculating and plotting a new index, normalized distance \bar{N}_d . With these plots, by simple inspection, the possible area where the damage occurred can be identified and more rigorous analysis can be prescribed.

Based on the analysis of strain and rotation data, it is observed that tiltmeters showed a clear indication of structural variations for all the studied cases. Due to its global nature, UILs for rotation proved to be more sensitive than strain even when loading and damage were not very close to the tiltmeters. However, their use for damage localization by using \bar{N}_d could lead to misinterpretation if employed alone. On the other hand, UILs for strain provide a more localized response making it possible to be used as a more efficient measurement to pinpoint damage. Although structural changes can be

detected with a few sensors, the method for damage localization improves if exists a dense spatial resolution for the strain gages.

5. CHAPTER FIVE: REAL LIFE APPLICATIONS

One of the objectives of this dissertation was the validation of the methods and algorithms first in the laboratory and for real life structures. Our research group is currently conducting a research project on developing methods and technologies for structural health monitoring of a movable bridge (Sunrise Bridge) located in Fort Lauderdale, Florida. Movable bridges are unique structures due to the complex interaction of their structural, mechanical and electrical systems. These mechanisms provide versatility to movable bridges; however, their intricate interrelations combined with the harsh environmental effects also produce some inherent drawbacks. Movable bridges are reported to have experienced significantly higher maintenance costs than regular fixed bridges, due to their special operational demands, structural designs, and interaction of different systems.

This chapter presents the real life implementation and results of a monitoring system where the data analysis and damage identification methods are demonstrated. Video images are analyzed by means of computer vision techniques to detect and track vehicles crossing the bridge. Traditional sensor data is correlated with computer images to extract Unit Influence Lines (UIL), which are used as index for load rating analysis and damage detection. For load rating, truck tests are commonly carried out to obtain more reliable load rating for decision-making by bridge owners. In this chapter, a practical method for this test and analysis is presented using UIL and operating traffic to obtain a more reliable load rating. For the damage detection, the several commonly observed conditions that are of concern for maintenance and operation were simulated on

the bridge temporarily. The results from these conditions are presented.

5.1. A Review of the Structural Health Monitoring System of a Movable Bridge

Heavy movable structures involve large machinery in which most operational speeds are low and critical forces are large. Bascule type movable bridges, which this study focuses on, are probably one of the most common types. A movable bridge is a structure, which has been designed to have two alternative positions and which can be moved back and forth between those positions in a controlled manner as a way for land traffic to cross a waterway while ensuring a path for the waterborne traffic [49, 50]. The main advantage of this type of structure is that because of its moving condition, the bridge can be constructed with little vertical clearance, avoiding the expense of high piers and long approaches. Moving components of movable bridges are operated by various types of machinery to open the passageway for waterborne traffic. Mechanical and electrical components fuse with the structural elements, creating a very unique type of structure often referred to as kinetic architecture.

The very same moving condition that gives its versatility to a movable bridge is the main responsible for significant drawbacks and problems associated with the operation, and performance [51]. First, deterioration is an issue since movable bridges are subject to harsh conditions. They are located over waterways, and often close to the coast, which constitute conditions suitable for corrosion, causing section losses. Also, wind forces are significantly higher in the coastal regions. Another important reason for the deterioration observed in movable bridges is that movement causes friction and wear of the structural and mechanical components. Fatigue is also one of the problems due to

the reversal or the fluctuation of stresses as the spans open and close. Any member or connection subject to such stress variations should be carefully inspected for fatigue failure [52]. Even with regular maintenance, continuous downgrading of movable bridges is inevitable.

The second major concern is the unexpected breakdowns, which cause problems for both, land and maritime traffic. Another concern is the high maintenance costs associated with the complex operation system, mechanical parts requiring special expertise, and with deterioration causing more extensive repair. In Florida, it is estimated that the unit maintenance cost of a movable bridge can be up to 100 times that of a fixed bridge [51]. Almost all parts need to be frequently checked and maintained. Also, unexpected failures increase the life cycle cost of the movable bridges. Difficulty in repair is an issue for movable bridges. Even a minor malfunction of any component can cause an unexpected failure of bridge operation. Electrical and mechanical problems may require experts and may be difficult as well as time consuming to fix. Due to the complex mechanisms of the movable system, repairs may be very costly. Consequently, a small movable bridge population owned by an agency may require considerable maintenance budget. Timely repair of the bridge is of major importance since the malfunction of the bridge would disrupt traffic, blocking either one or both transportation routes.

Coupled with analytical models, the SHM paradigm offers an automated method for tracking the health of a structure by combining damage detection algorithms with structural monitoring systems. Such a system can monitor the structural, mechanical and even electrical components of a movable bridge and generate warning flags to indicate a worsening in certain conditions. Infrastructure owners may use these flags as a

mechanism to monitor/assess maintenance performance. The data may be used by the contractors in scheduling preventive maintenance to maximize the service life of the equipment and the structure. In addition, the root causes of the structural and mechanical problems can be determined, and future designs can be improved using the information generated by the monitoring system.

5.1.1 Description of the Structure

Florida has a large population of movable bridges due to the waterways and coastal topography. Most of these bridges are owned by the Florida Department of Transportation (FDOT). The FDOT has an inventory of 98 movable bridges including 3 lift type, 94 bascule type, and 1 swing type bridges.

Bascule bridges constitute by far the majority of movable bridge types. Based on this analysis and interaction with FDOT structures and maintenance engineers, a bascule bridge in Fort Lauderdale known as ‘Sunrise Bridge’, was selected for monitoring since it belongs to the largest class within the population with representative geometry and condition of movable bridges in Florida (Figure 50).



Figure 50. Sunrise Bridge

The structure 860466 is the Westbound span of two parallel spans on SR 838 (Sunrise Bridge), crossing the Inter Coastal water way in Fort Lauderdale, FL. This span was constructed in 1989. It has double bascule leaves, each 73'10" (22.49m) long approximately, and 53'4" (26.15 m) wide, carrying three traffic lanes and opening about 15 times a day.

Sunrise Bridge is of the most common bascule type, with a rack-and-pinion mechanism. The bascule leaves are lifted horizontally at the point of the trunnions, which are the pivot points on the main girders. The weight of the span is balanced with a counterweight that minimizes the required torque to lift the leaf. The counterweight is made of cast-in-place concrete. In the closed position, the girder rests on a support called

‘Live Load Shoe’, or LLS, on the pier and traffic loads are not transferred to the mechanical system. The movable bridge also involves fixed components, such as reinforced concrete piers and approach spans. The counterweight of the main girder stays below the approach span deck in the closed position. When the bridge is opening, the leaves rotate upwards, and the counterweight goes down. The driving torque is generated by an electrical motor, which is then distributed to the drive shafts via the gear box. The gear box involves an assembly of gears operating similar to automobile differentials, and provides equal lifting of both sides. The drive shafts transmit the torque to the final gear called the pinion, engages the rack assembly which is directly attached to the main girder.

5.1.2 Design of the Sensor Network

As a part of the on-going research project for FDOT, main issues for the maintenance of electrical, mechanical and structural components of the movable bridge were identified. Based on these, an extensive sensor network is designed and implemented to monitor various parts of the bridge. A total of 168 sensors are deployed to the bridge for monitoring the electrical, mechanical and structural components as well as collecting environmental data [40]. The electrical and mechanical components are monitored with accelerometers, strain rosettes, tiltmeters, microphones, infrared temperature sensors, ampmeters, video cameras, and pressure gages. Structural components are mainly monitored with accelerometers, high speed strain gages and slow speed vibrating wire strain gages. Video cameras and a weather station are also part of the monitoring system. The detail of the installed sensors is as follows.

Accelerometers: A total of 40 PCB accelerometers are installed. Sixteen sensors

are placed on the main girders to measure vertical (12) and horizontal (4) acceleration. Another six on each gearbox and four accelerometers on the electric motors to monitor alignment and vibrations to reflect the performance of the mechanical and electrical components. Also, two accelerometers are installed on each rack and pinion base for detecting excessive vibration and checking the base integrity.

Dynamic strain gages: 36 Hitec weldable dynamic strain gages have been attached to main girders, floor beams, and stringers.

Vibrating wire strain gages (VWSG): 36 Geokon VWSG are strategically distributed on main girders, floor beams, and stringers; continuously collecting slow speed temperature and strain data. Figure 51 shows the location of some of the strain gages used in this study. For identification of the sensors a number was added to the end of the denomination: 1 means the sensor is installed in the top flange of the main girder, 2 for the bottom flange (main girder) In the same way, 3 and 4 are for top and bottom respectively in the case of either stringers or floor beams.

Strain Rosettes: 22 Hitec strain rosettes are used in total. Four of these sensors are placed on girders at the live-load shoe locations to correlate with traffic, another two at the receiving encasing for the span locks for checking alignment and integrity, and eight sensors at the trunnions vicinities for studying the shear on these critical regions. Eight rosettes at the main shafts allow correlating with tiltmeters and monitoring the torque, balance, and friction number on each opening/closing operation.

Tiltmeters: A total of eight 801 uniaxial Tuff tiltmeters are used. Four are located at the trunnion regions to measure inclination angle during opening/closing and another

four are placed one at the tip of each girder for checking the alignment of both leaves.

Pressure gages: Four TPS sensors are placed at the span-lock hydraulic system for checking variations in the oil pressure which can indicate problems related to alignment between the span-lock bar and the receiver.

Infrared Temperature sensors: Two non-contact IT Omega transmitters are installed for detecting abnormal levels of heat on the motor brakes.

Amperage meters: Six current sensors are installed to monitor the amperage consumption of the motors during the opening/closing operations, serving at the same time as triggers for data capture.

Microphones: 4 microphones are installed to detect acoustic print of possible lack of lubrication issues of gear boxes and trunnions.

Video cameras: Two fire wire cameras collect video stream data; one is dedicated to monitor the traffic and the other to detect corrosion on the open gears.

Weather station: an Orion weather station is also installed to monitor ambient temperature, humidity, rain intensity, rain duration, wind intensity, and wind direction to correlate with all the other measurements. Figure 52 shows the installed monitoring system.

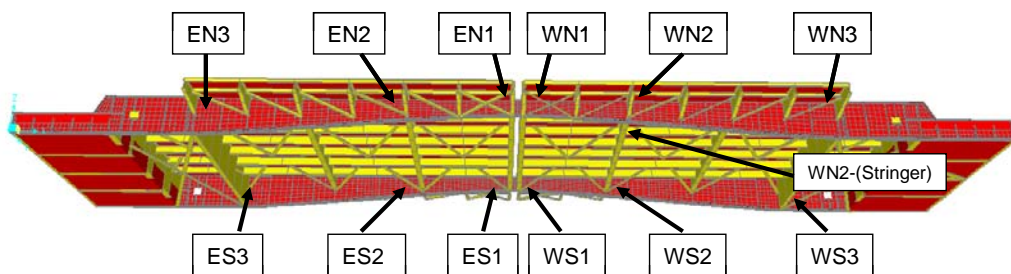


Figure 51. Location for Some of the Strain Gages

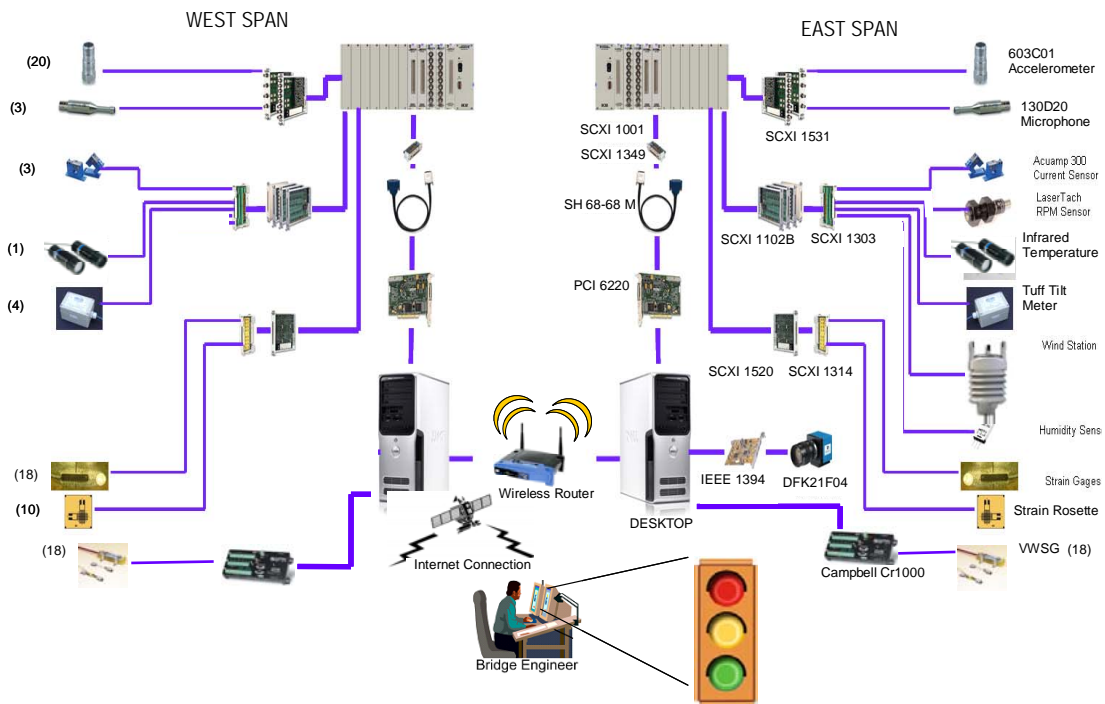


Figure 52. Monitoring System

Development of the finite element model (FEM), shown in Figure 53, provided the possibility of investigating different damage scenarios and determining instrumentation locations.

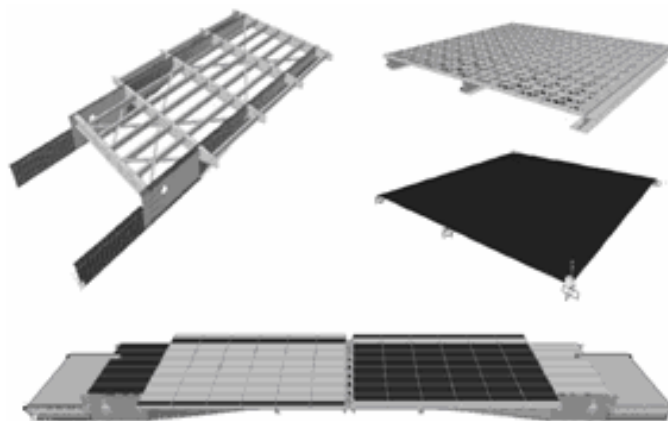


Figure 53. Finite Element Model

Figure 54 shows a typical sensor installation as well as the video camera position and traffic direction.

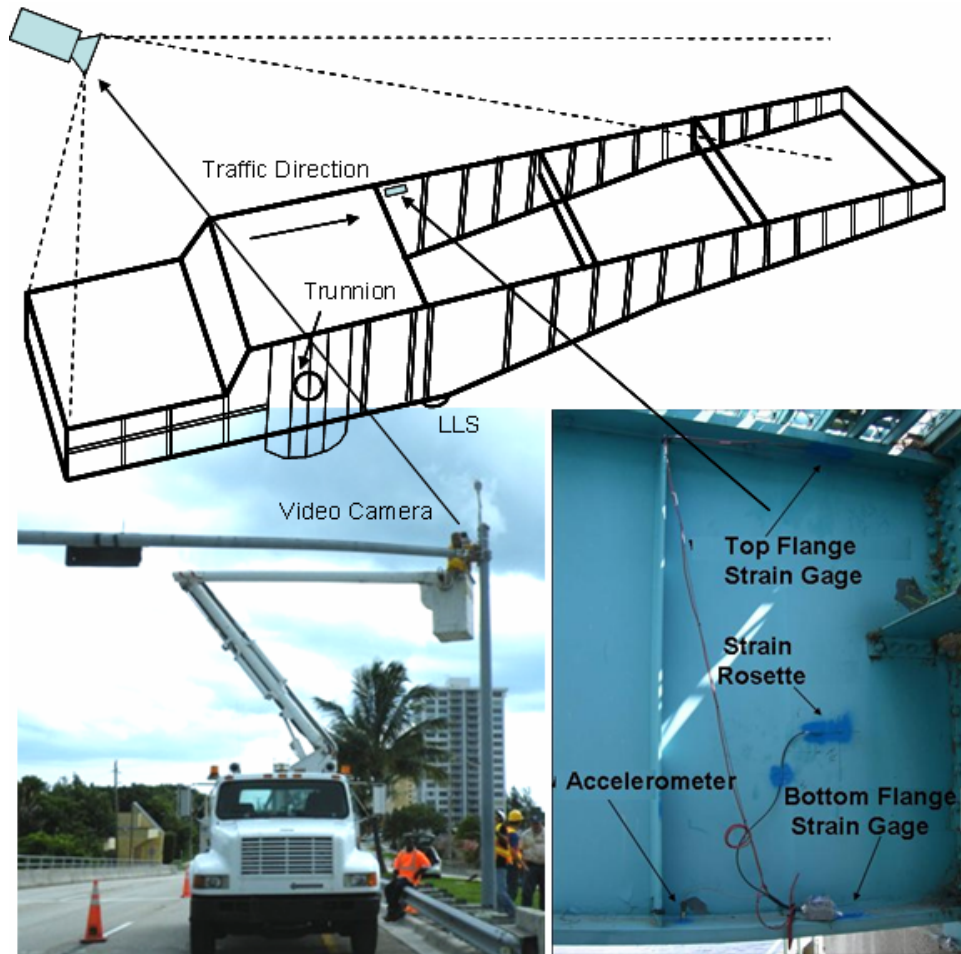


Figure 54. Strain Gage Location and Video Camera.

5.1.3 Instrumentation and Data Collection

As stated before, instrumentation include structural, mechanical, and electrical components. Data is recorded during every opening and closing of the bridge leaves. For each opening/closing event, shaft torsion, leaf angle, strain, acceleration, current of the motors, and temperature of the breaks are collected using the DAQ and stored in the computers located at each side. Also, video cameras monitor the open gear for signs of corrosion, lack of lubrication and/or indentations. Therefore, real-time acquisition and

tracking of the bridge balance for each opening and closing event is possible, providing the bridge owners immediate information on the status of the mechanical system. Deterioration can be controlled by applying preventive maintenance before the machinery sustains excessive wear, hence, being able to predict damage. When the bridge is closed, in normal operation, traffic is also monitored by a firewire video camera. At the same time, structural strain gages and accelerometers are collecting data from the traffic induced effects. Both, vision and sensor data are correlated and Unit Influence Lines (UIL) are extracted to be used as a feature for damage detection and load rating.

5.1.4 Data Acquisition System Configuration

The data acquisition system requires a special design for proper collection of the data. An analog filter of 100 Hz is applied to all strain gages and a 2.5 kHz analog filter is applied to acceleration data. A digital bandstop-butterworth 5th order filter with a lowpass cutoff frequency of 58 Hz and a high pass cutoff frequency of 62 Hz are applied as well to all measurements to account for 60 Hz electricity noise. Data is collected at 256 Hz for all channels.

5.1.5 Field Installation

SHM of large structures involves much more than laboratory tests where issues such as coordination, access, redundancy are relatively easy to control. The technical challenges associated with field implementation of a SHM program for bridges are commonly related to installation, operation, and maintenance of the various components of the monitoring system as well as the coordination and cooperation with the bridge owners. In addition, the distance between sensors and the DAQ system creates a complex

wiring issue; how to effectively relay the signal from sensor to computer. In this project, a multi conductor cable with individually shielded, twisted, and grounded pairs protected by a PVC outer jacket was used. The PVC outer jacket was rated for outdoor use and both sunlight and oil resistive; providing confidence for long-term use in a harsh environment.

Another major challenge in the implementation of SHM system in real life is the coordination of fieldwork with infrastructure owners in such a way that installation process impacts the land and maritime traffic minimally. Figure 55 shows a typical installation of sensors using a snooper truck.



Figure 55: Sensor Installation on Girders

5.1.6 Data Transmission and Synchronization

Since two leaves of the movable bridge are physically separated from each other,

it is necessary to provide data transmission across the waterway to monitor both spans of the bridge simultaneously. For the first reason, separate DAQs are used for each side, collecting the data from the corresponding sensors. A Digital Subscriber Line (DSL) internet connection was established at the East side of the bridge. This connection is terminated in a wireless access point. The West side gains connection to this access point by using a standard 802.11 PCI wireless card. A static IP address is provided by the DSL vendor ensuring a consistent internet presence. For the initial phase, standard Microsoft Remote Desktop is used to communicate and full control of both computers. Communication and transmittal of data between the two separated DAQ systems is accomplished through a combined 4-port switch plus RangeBooster type G wireless router. Figure 56 illustrates the data transmission. For security, this network is password protected.

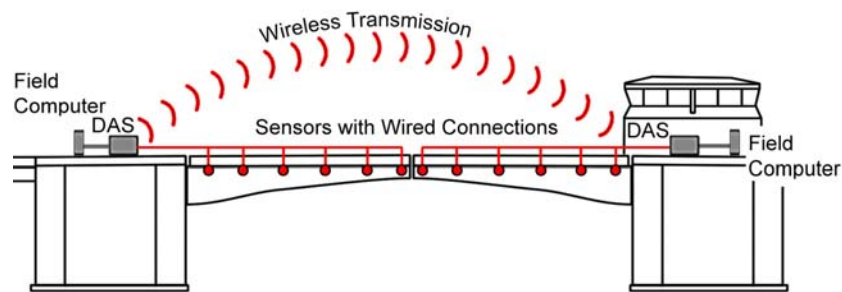


Figure 56: Scheme for Data Transmission

As stated before, one of the main issues of working on this movable bridge is the data transmission and synchronization. First, both computers are coarse-grained synchronized by using a standard Network Time Protocol (NTP). This NTP continuously measures the wireless network latency between both computers located at each side of the bridge, compensating the subrogated slave computer to the master in real time . This

procedure allows a starting point where the timing offset is in the order of 4ms.

Further refining is obtained by using a Global Positioning System (GPS) timing receiver at each side. The receiver is a full 12-channel, parallel tracking, embeddable GPS receiver designed to provide precise GPS or UTC time which is needed for synchronization. The timing accuracy provides plenty of headroom for future requirements. Rather than sharing time from a single timing source, with the resultant delays and loss of accuracy, precise time (synchronization) at every location can be achieved regardless of how isolated or remote the location of the monitoring system is.

These GPS not only provide location information but also supply a global time reference accurate up to the micro second order of magnitude. Every second, each GPS outputs a pulse whose leading edge is synchronized. These signals are captured simultaneously with other sensor data and embedded within the data files. By matching pulses on both computers, desired synchronization is achieved.

5.2. Data Analysis from Operational Traffic for Load Rating

Bridges are the critical links of the transportation networks. Any damage or collapse of a bridge not only results in loss of property and human fatalities but also has severe effects on the regional economy. Deterioration of civil infrastructures in North America, Europe and Japan has been well documented and publicized. In United States, 50% of all the bridges were built before 1940 and approximately 42% of those, present structural deficiency [53, 54].

Some of those bridges may be strengthened or rehabilitated, while others simply need to be replaced. Load rating analysis is a commonly used approach to evaluating live

load carrying capacity of bridges, and decision-making such as load posting or replacement. Most of the time, load rating analysis is performed using a simplified analysis or more detailed analysis such as using Finite Element Models. In addition, truck load test based load rating is also conducted on the structure to more accurately assess its load carrying capacity. In such a case, the structure is instrumented with a variety of sensors, and a heavy vehicle of known load is positioned for pre-identified load conditions and also crosses the bridge at crawl speed. The structure response is continuously monitored during several of these passages, along with the position of the vehicle. Results are analyzed and also used to calibrate numerical models which help to predict the behavior of the structure under different loading configurations.

A manual for bridge rating through load testing was published previously [55] through a National Cooperative Highway Research Program (NCHRP) project as a guide for the nondestructive load testing of bridges for improved rating. In this guide, two types of nondestructive load testing are described for the purpose of bridge load rating: diagnostic and proof. Diagnostic load testing involves loading the bridge in question with a known truck load at set positions and measuring the bridge response. Proof load testing is performed by setting a limit or goal for the bridge while vehicle loading is increased gradually until the target is reached. Both types involve mobilization of load trucks as well as lane closures.

One of the most desirable characteristics of any bridge monitoring system is the ability to continuously verify the structure safety with minimum or no interference to the normal operation. This section explains and demonstrates a new application for performing experimental bridge load rating by using operational traffic without the

necessity of neither bridge closures nor using any particular type of vehicle. This approach does not require a Weigh-in-motion (WIM) system, which might be costly in terms of the equipment and its installation. The incorporation of imaging and optical devices to a traditional SHM system, allows detecting, tracking, and identifying vehicles from captured video sequences. At the same time, these moving loads are synchronized with sensor data to extract Unit Influence Lines which are used to predict the bridge response under the AASHTO HL-93 rating truck, which is a standard truck used for load rating. Here, operating and inventory load rating are calculated. The complete process is explained in the following.

5.2.1 Detection

As explained before, detection was performed by using background subtraction, where each video frame (Figure 57b) is compared against a reference or background model (Figure 57a). Pixels in the current frame that deviate significantly from the model are considered to be moving objects and belonging to the foreground (Figure 57c). This pixel based information is then clustered to identify regions, filtered, and also to label as well as to classify objects (Figure 57d). A detailed explanation as well as all formulation used for the authors can be found in previous sections of this dissertation as well as in [37, 38]. For the load rating analysis, the data during the crossing of the passenger bus given in Figure 57b is used to extract UIL and then obtain HL93 based load rating.



Figure 57. Background Subtraction and Filtering

5.3. Classification

Classification was performed by following the procedure explained before. Once the vehicle type has been identified, the number of axis, distance between them, and weight per axle empty and loaded are obtained from the data base. Figure 58 illustrates the process. The bus that is detected, is then identified as the a Riverside Transit Agency (RTA) passenger bus with axle and load data as given in the following.

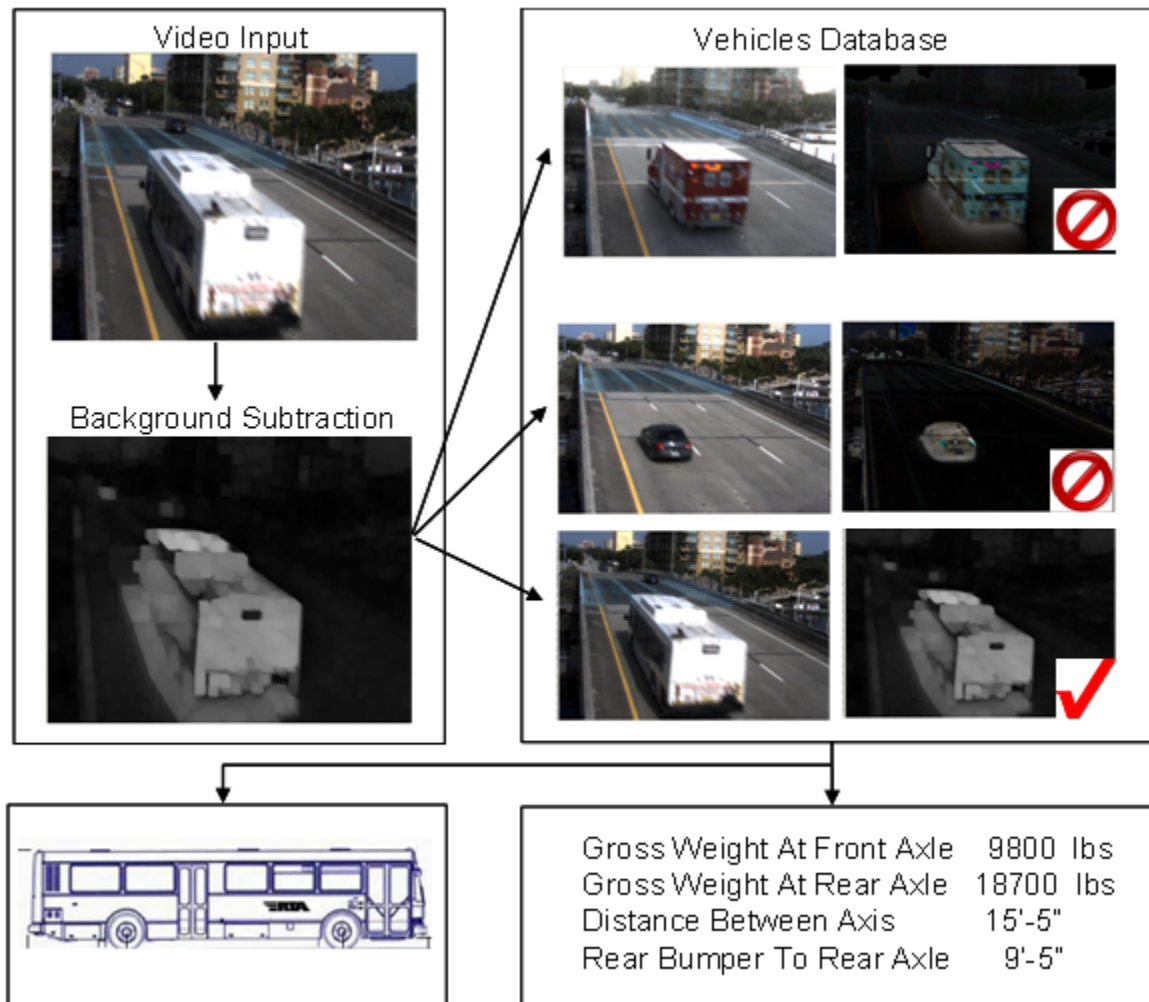


Figure 58. Classification of Vehicles

5.4. Tracking

Figure 58 shows the tracking algorithm detecting and following a bus while crossing the bridge. Tracking is critical to synchronize the measured responses with the location of the vehicle when obtaining the Unit Influence Lines.

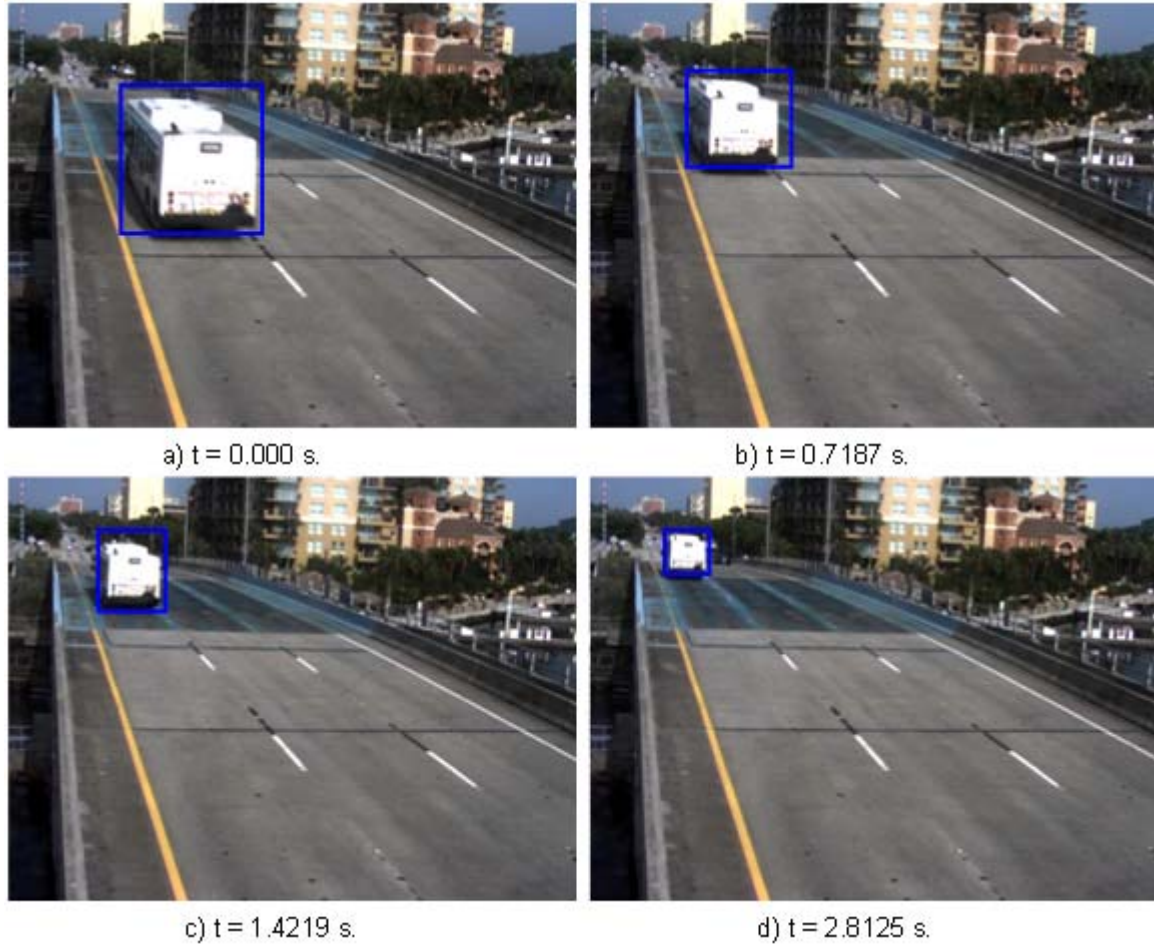


Figure 59. Results from the Tracking Algorithm

5.4.1 Load Location and Response Synchronization

Once the strain data is collected in time domain, filtering is applied by changing the raw data into frequency domain using Fourier Transformation. Then, dynamic and high frequency noise components are cut out while static component is kept and transformed back into time-domain. Vehicle is identified and location versus time of the moving load is obtained by means of computer vision algorithms. Figure 60 shows filtered responses of the vehicle and the FEM simulated strain values correlated with the front axle location of the identified bus (assuming is fully loaded) for the critical section under investigation.

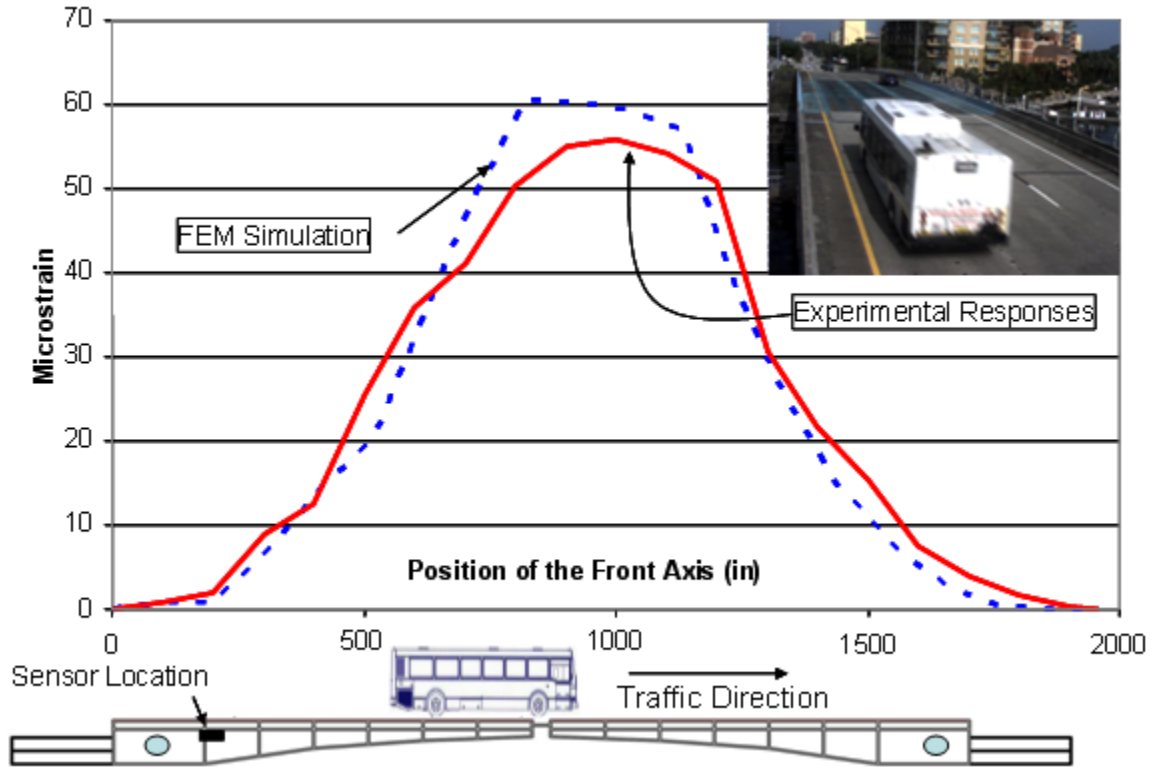


Figure 60. Measured Responses and FEM Simulation

5.4.2 Unit Influence Lines Extraction

Once the response of the bridge is obtained and correlated with the location of the vehicle, UIL can be extracted. One important fact is that the real bus loading is unknown. For this reason, two calculations can be performed. The first one assumes that the bus is empty and the second one with the bus fully loaded. Based on both assumptions, UILs are extracted as shown in Figure 61.

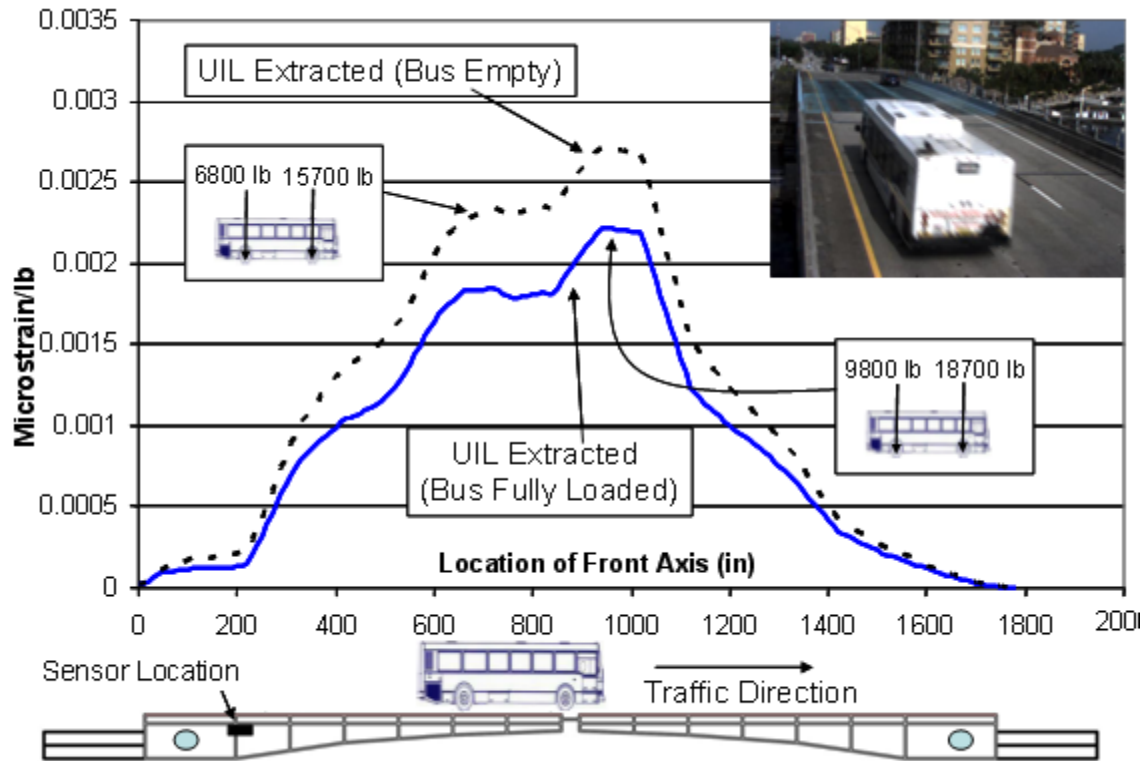


Figure 61. Unit Influence Lines for Bus (Assuming Empty and Fully Loaded Bus)

In Figure 61, the two UILs are plotted for the empty and the full bus assumptions. It is noticeable that the UIL for the empty bus has greater coefficients than the one for the loaded case. The reason is that both UILs have been extracted for the same measured response, hence, the UIL corresponding to the smaller load has to be larger and vice versa.

5.4.3 Rating Truck Response Prediction

Once UILs are obtained by using operational traffic, Equation (10) can be used again to obtain the predicted response of the bridge due to the rating vehicle HL-93. This time, $[w]$ is formed with the axis weight and distance information corresponding to the

vehicle HL-93. Figure 62 shows the obtained results in the form of three curves: the first one represents the predicted moment response of the bridge for the HL-93, calculated by using the UIL generated from the bus assumed empty (strain values are also shown); the second curve shows the expected bridge response by using the UIL extracted from the bus assumed fully loaded, and the third curve shows the FEM simulation for the bridge response under HL93 vehicle. Due to the uncertainty of the real bus loading, two bounds are formed and the actual response should be in between these limits. FEM results show a very good correlation with the experimental data.

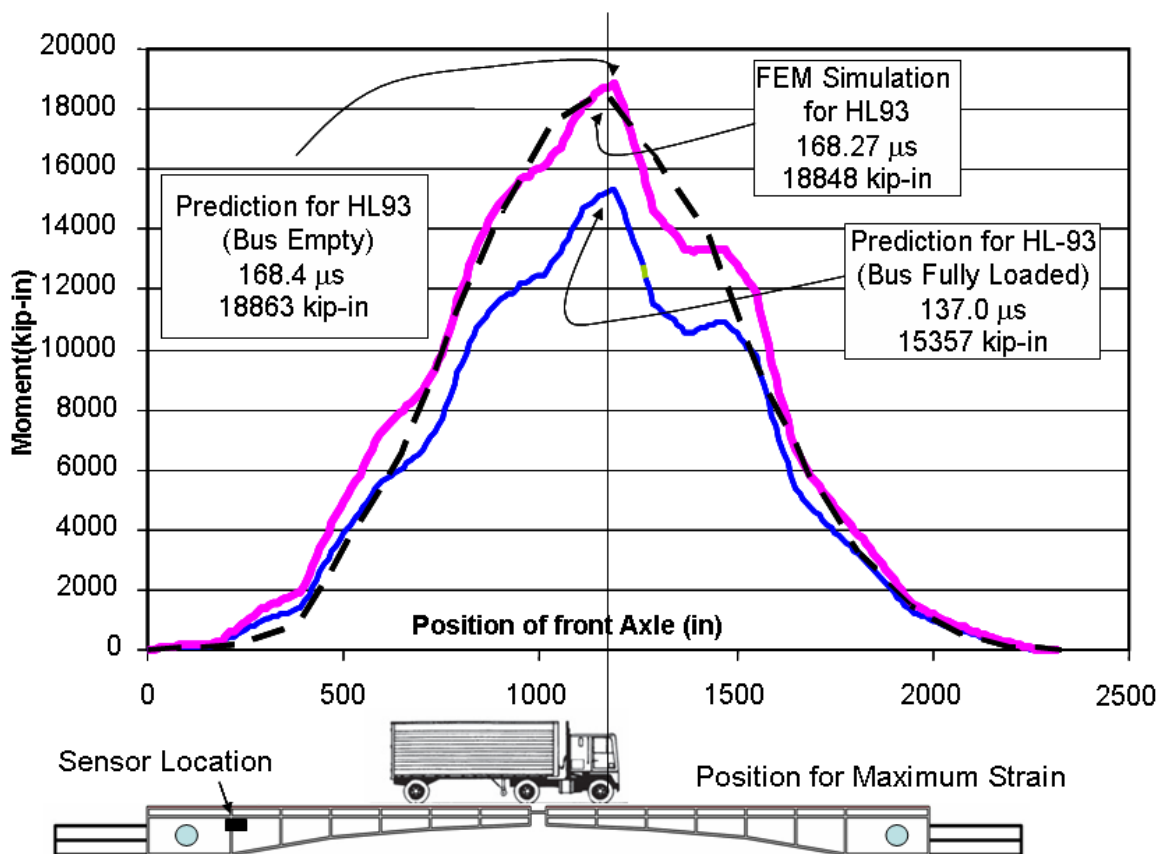


Figure 62. Predicted Responses for HL-93 by using UILs Obtained with the Operational Traffic

5.4.4 Load Rating Results

Load rating of the movable bridge was calculated for the indicated section following the AASHTO Guide [56]. Bending capacity, including lateral torsional buckling effect, and shear capacity were calculated as deterministic values. Predicted maximum and minimum moment values coming from the strain at the selected location were used. The load rating can be expressed as the factor of the critical live load effect to the available capacity for a certain limit state. The general formula for the rating factor is;

$$RF = \frac{C - \gamma_{DC}DC - \gamma_{DW}DW \pm \gamma_p P}{\gamma_L LL(1 + IM)} \quad (13)$$

Where C is the factored moment capacity, DC is the moment produced by the dead load of structural components, DW is the moment produced by the load of the wearing surface, P is a dead load concentrated at a single point, LL is the live load effect, IM is the impact factor, and γ 's are the safety factors. The load factors change according to the type of load rating, i.e., inventory or operating load rating. The load ratings for the girder were calculated at the section FB-A, located at the Live Load Shoe (LLS) in the bottom part of the top flange as indicated in Figure 63.

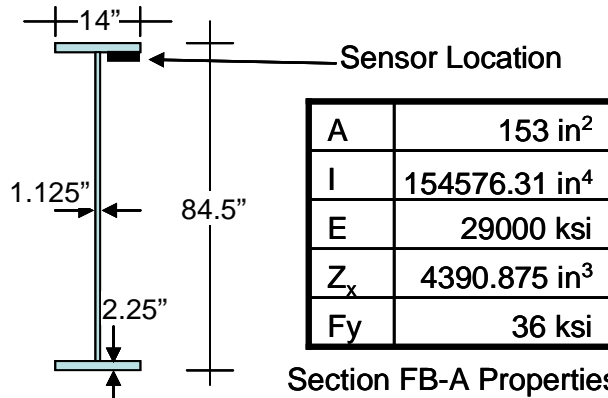
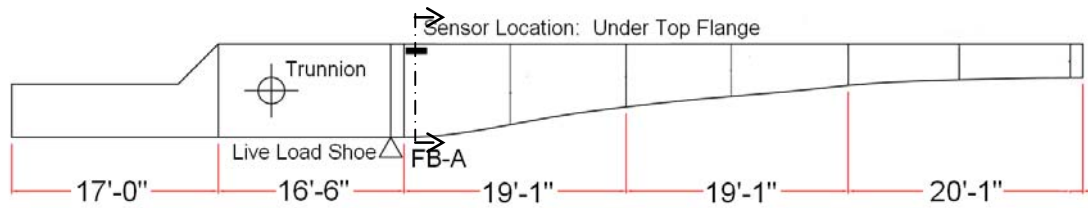


Figure 63. Studied Location and Section Properties

The capacity of the sections was calculated based on the ultimate moment capacity;

$$M_u = F_y Z_x \tag{14}$$

where M_u is the ultimate moment capacity; F_y represents specified yield strength and Z_x is the plastic section modulus. The yield strength of the steel was given as 36.0 ksi. The plastic modulus was calculated from section sizes in the drawings. Then, applying Formula (14), the section moment capacity was found to be $M_u=158072$ kips-in.

Moments at the studied section due to Dead Load and Lane Load were determined using the Finite Element Model of the bridge as $M_{DL}=15409.33$ kips- in and $M_{LL-LANE} =9794.73$ Kips-in respectively. Since the experimental data collected at the critical response location for this example is strain, it has to be converted to moment values in order to apply the load rating equation. By using the strain-stress relationship

$\varepsilon = \sigma/E$ and the flexural stress formula $\sigma = M.c/I$, then it can be established;

$$M = \varepsilon EI/c \quad (15)$$

where ε represents the experimental strain at the critical section, c is the distance from the centroid to the studied location, I is the moment of inertia of the section and E is the modulus of elasticity. The dynamic impact factor is used as 33% for both inventory and operating ratings. The load factors change according to the rating type as shown in Table below.

Table 1 – Load Factors

Load Factor (γ_L)	Load Rating Case	
	Inventory	Operating
DC	1.25	1.25
DW	1.25	1.25
LL+IM	1.75	1.35

According to the condition of the structural members of the bridge based on condition state or sufficiency rating, the condition factor allows for a reduction in the load rating up to 15%. Due to the latest inspections to the bridge, the condition factor, γ_c , is 1.0. The system factor (γ_s) was also taken as 1.0. By applying Equation (13), the load rating capacity of the section FB-A was calculated for each position of the truck. Figure 64 shows the results for inventory load rating as the truck crosses the bridge. Three curves are shown: The first for the maximum load rating, calculated by using the predicted behavior of the bridge for the HL-93 truck, determined with the experimental UIL assuming the bus was fully loaded. The second curve represents the minimum load

rating by using the predicted bridge response under the HL-93 assuming that the bus was empty. The third curve shows the FEM simulation for the HL-93. Results for the most critical truck location show an experimental inventory load rating ranging from 2.07 and 2.37 and a FEM inventory load rating of 2.08. Operating Load Rating was also calculated in the same way and critical values are also shown.

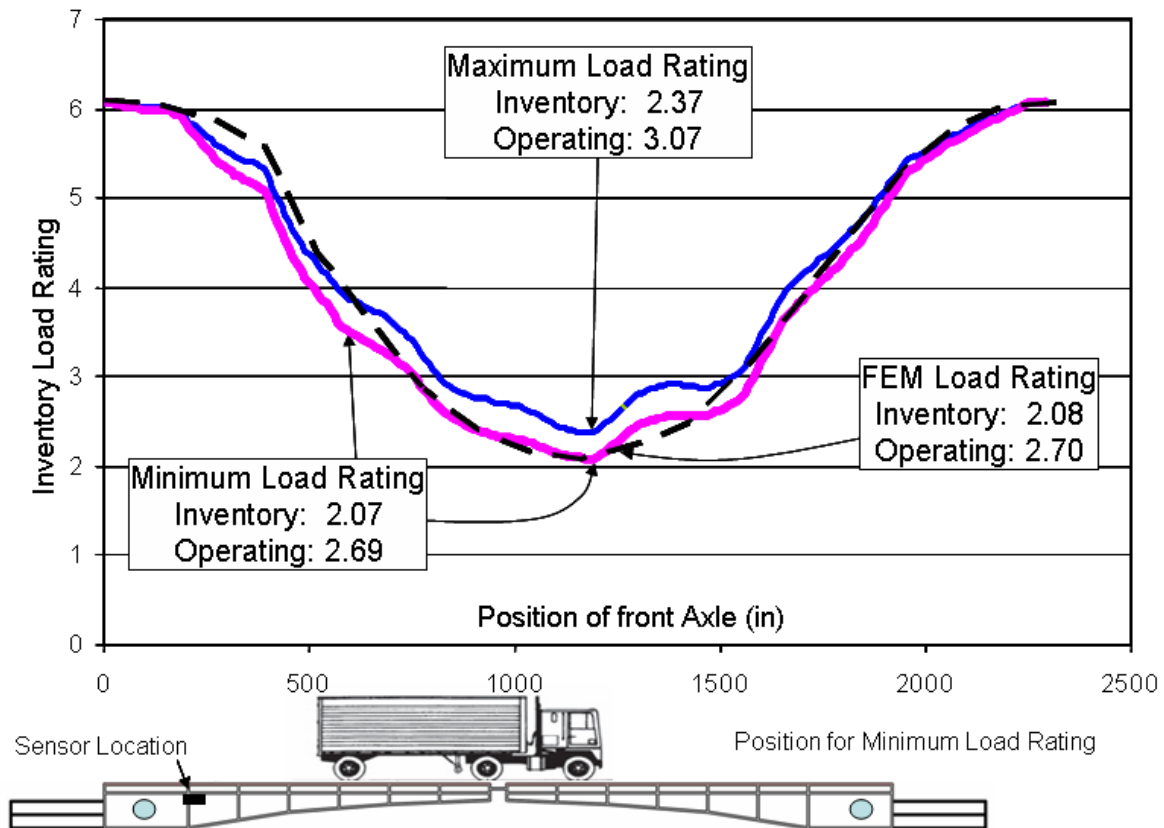


Figure 64. Load Rating Capacity for Section FB-A with respect to Truck Location

5.5. Damage Detection on a Movable Bridge

In this section, real life damage detection studies are conducted on the movable bridge by temporarily inducing structural alterations. As part of the previously mentioned ongoing project [40], some of the most common maintenance problems were identified,

and implemented on the bridge with the support of the FDOT engineers.

The first condition corresponds to a case that occurs when the Live Load Shoes (LLS) are not fully seated and a gap exists between the LLS and resting support pads. This causes misalignment, and problems for proper opening and closing of the leaves. Also, due to the inadequate support conditions, bouncing occur in the girders creating additional stressed due to impact as well as stress redistribution subjecting the structure to non desirable forces.

The second issue is similar to the first one but in this case, it happens when the Span Lock bar (SL) connecting the leaves at the center is not perfectly shimmed and a gap exists between the SL and the receiver. Once again, this situation causes a loss of connectivity between the two leaves as well as possible dynamic impact and stress redistribution.

Before continuing, a brief explanation of the LLS and SL is presented with the aim of facilitating the comprehension of the further analysis.

5.5.1 Live Load Shoes

Live load shoes are support blocks that the girders rest on while in the closed position. The live load shoes can be located forward of the trunnions, holding the main girder up, or behind the trunnions resisting the upward movement of the counterweight (Figure 65). The former type is the most common type, and is the type used for the Sunrise Bridge. Cracking and wear are rarely seen on the live load shoe, but mainly the operational problems such as full contact are of concern. If misaligned or improperly balanced, the bridge may not fully sit on the live load shoe. In that case, the dead load

and traffic load are transferred to the gears and shafts, which cause damage on mechanical assemblies. Small gaps also lead to the girders pounding on the live load shoes, which results in further misalignment, additional stresses, fatigue damage and excessive wear.



Figure 65. Live load shoe (LLS)

5.5.2 *Span Locks*

Span locks on double-leaf bascule spans are used to connect the tip ends of two cantilevered bascule leaves together. In this way, both leaves are forced to deflect equally and prevent a discontinuity in the deck as traffic crosses the span. Most span locks consist of a rectangular lock bar supported by a pair of guides on one leaf that engages a single receiver on the opposite leaf. During operation, the lock bar slides across bronze shoes mounted in the rectangular guide and receiver housings. The coupling has to be loose enough to allow it to happen but at the same time the gap between the bar and the receiver has to be small enough to ensure the adequate connection. This is achieved by placing metallic sheets (or shims) to adjust this space according to the needs. The

housings are usually mounted to the side of the bascule girders or in the webs of the floor beams (Figure 66). Lock bars are typically driven or retracted directly using a linear actuator that can be electric, hydraulic or mechanical (Figure 67). Span locks are one of the members that fail the most. Most of the time, the shims are lost or destroyed due to deterioration, or incorrect operation, in other occasions the bar itself or the actuator mechanism fail, preventing the appropriate functioning. The alignment and the stresses on the locking bar should be monitored to ensure the locks are in order.



Figure 66. Span Lock Compartment

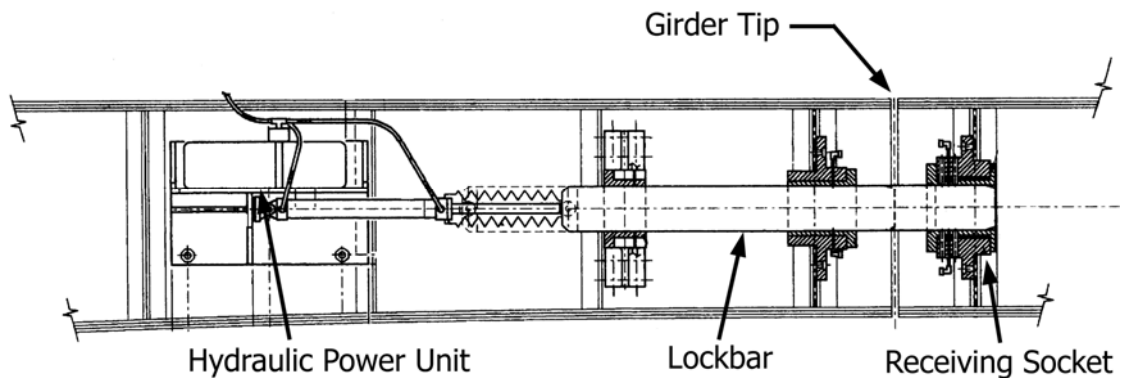


Figure 67. Typical Span Lock

Strain gages at the tip of the girders can indicate continuity between two leaves as a result of span lock connectivity. It may be possible to monitor lock bar also. Stresses on the locking bar will indicate whether the lock is on or off and also inform span lock failure. This component is planned to reduce span lock failures due to overloading or the bridge operator overriding the opening action while the lock is in place, assuming a limit switch failure. Further on-site investigation need to be carried out for gage installation, running cables and access requirements.

5.6. Damage Scenarios

Based on the collaboration with FDOT engineers, girder not fully seated on the LLS (Case 1), and slightly increasing the gap between the SL bar and the receiver (Case 2) conditions were recreated at the bridge. Both conditions were induced progressively, i.e., first the some of the LLS shims were removed and the bridge was monitored during normal traffic operation (Case 1). Then shims of the SL housing were retired and vehicles were allowed to cross the bridge while the system was monitoring the structural responses (Case 2).

One of the main goals of any structural monitoring system is to detect the damage or malfunction at early stages in such a way that can be promptly corrected. For this reason, it was decided to just slightly alter the structural condition. Some of the shims used to ensure the appropriate contact between the LLS and the support pads were retired to create a gap of approximately only 1/8" up to 3/16" on South West LLS (Figure 68). This was performed by the FDOT contractors under the research team supervision (Figure 69).



Figure 68. Induced Damage in LLS



Figure 69. FDOT Contractor Removing Some of the Shims

For case of the Span Lock, some of the shims were also removed to create a gap of approximately only 1/8" up to 3/16" on South West Span Lock (Figure 70).



Figure 70. FDOT Contractors Removing Some of the Shims from the SL

Receiver

5.7. Extraction of the Unit Influence Line for Damage Conditions

The bridge was monitored continuously before, during and after the induction of the previously discussed damage scenarios. Traffic information regarding detection and tracking was obtained by the images and the computer vision analysis performed. Classification provided the information corresponding to weight and separation of each axis. Initially, bridge raw response is captured in time domain and filtered as explained in previous chapters. Figure 71 shows results from this process applied the strain gage ES3-SG1.

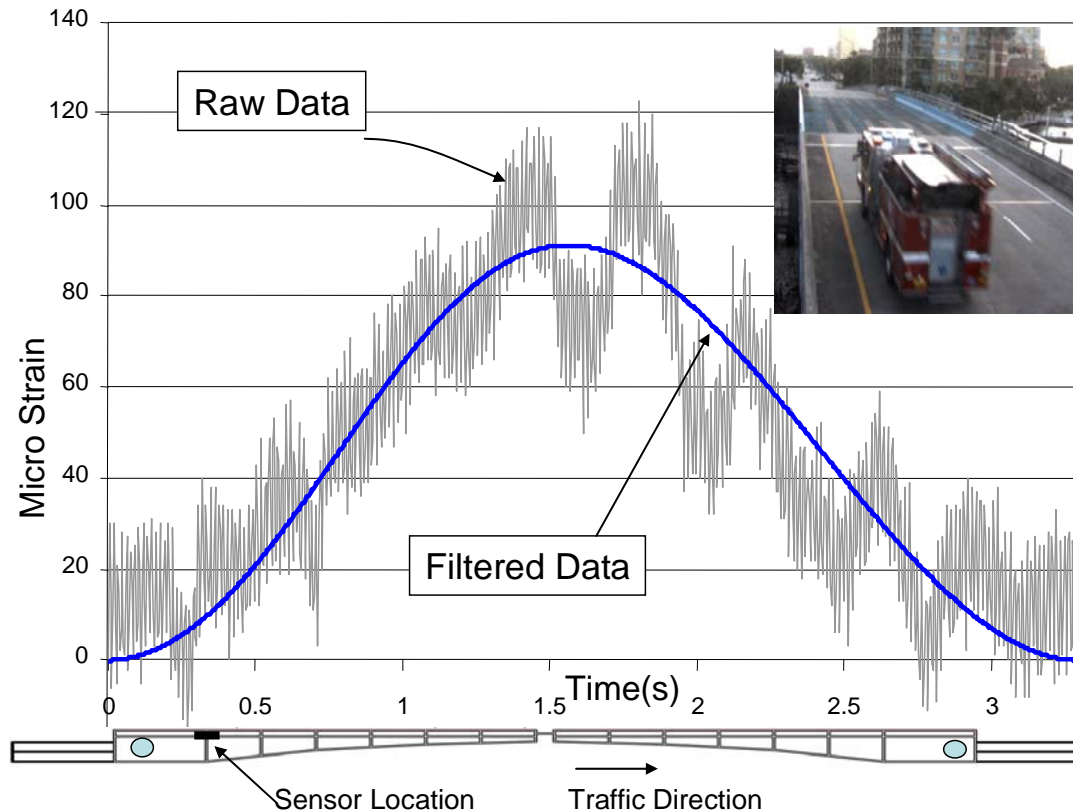


Figure 71. Raw (Dynamic) and Filtered (Static) Response for ES3-SG1 under Fire Truck

Once the data is filtered, correlation with the position is obtained by using the tracking computer vision algorithm. Responses are now presented as a function of the front axis as shown in Figure 72 for different type of vehicles.

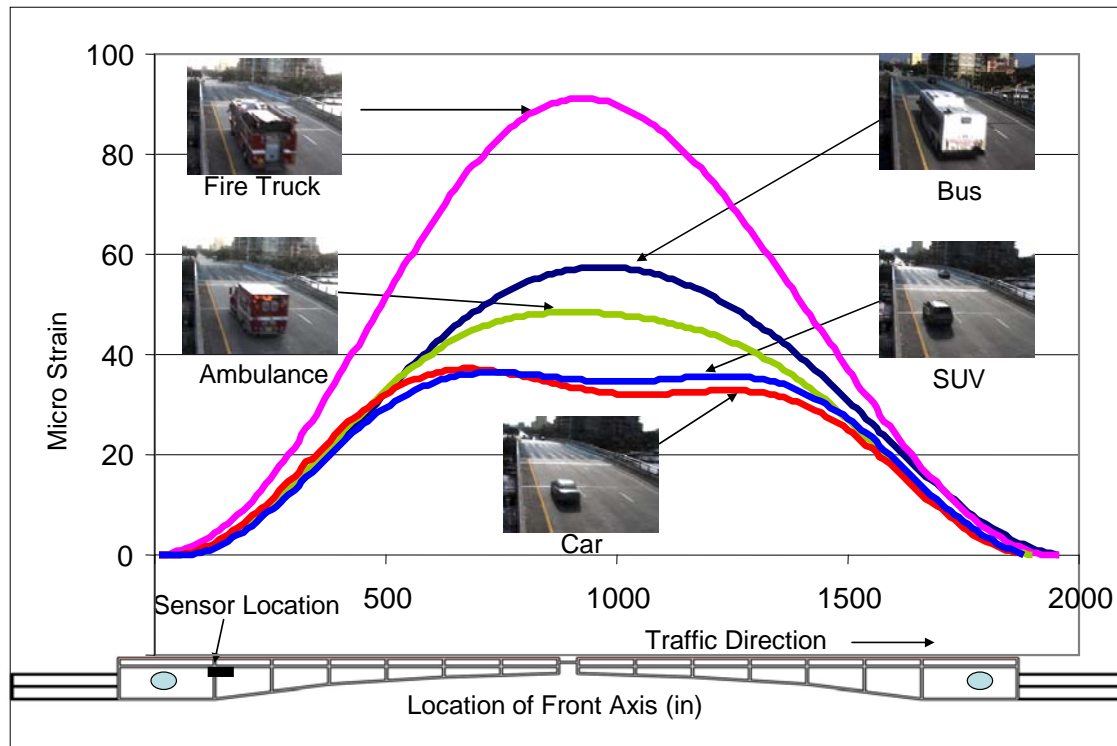


Figure 72. Responses vs. Location of the Front Axis (ES3-SG1)

After response correlation with distance is obtained, UILs are determined for each one of the sensors and for every vehicle. Figure 73 shows the extracted UILs for the Fire Truck and the RTA bus for the indicated location (ES3-SG2). As previously explained in Section 5.4.2, the actual loads transmitted by the bus axis to the bridge vary depending on the passenger occupancy. Two UILs are presented for the bus, one considering it to be empty and the other one assuming it is fully loaded. For the Fire Truck case, the exact axis loads are known from its specifications. It can be seen that the UIL corresponding to

the empty RTA bus assumption correlates very good with the one extracted from the Fire Truck for the same sensor.

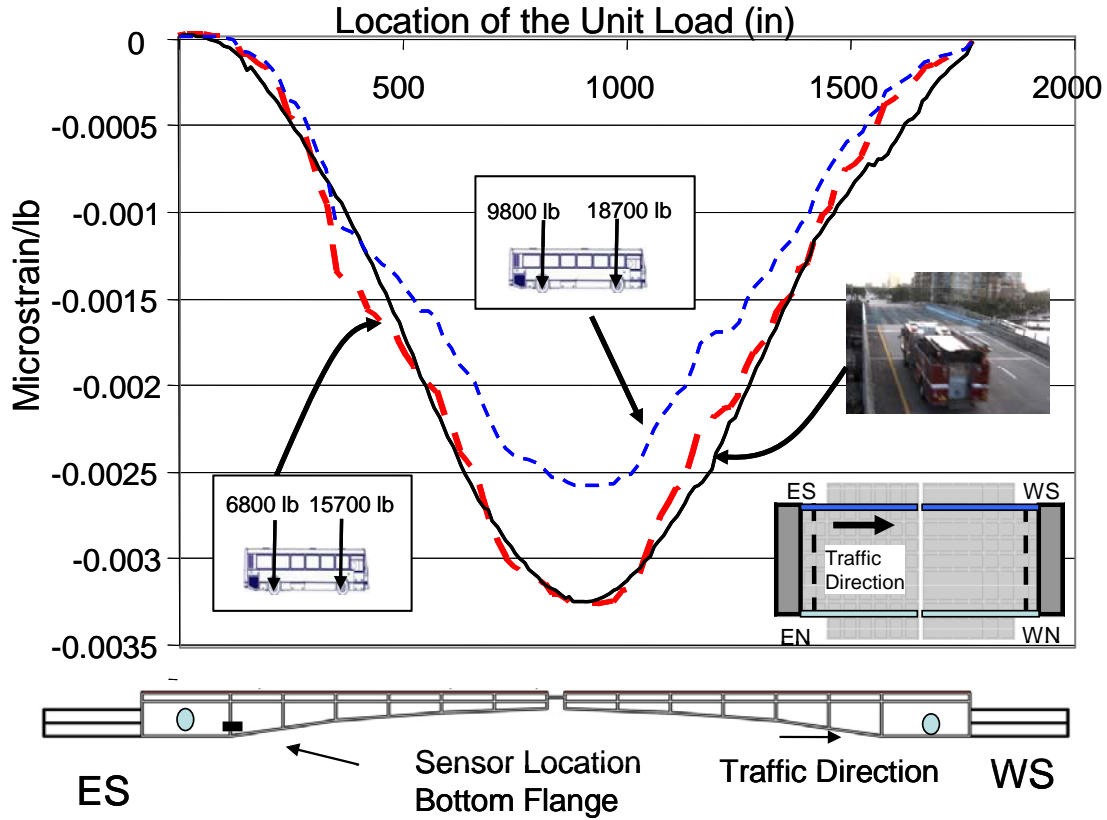


Figure 73. Unit Influence Lines for Fire Truck and RTA Passenger Bus

Figures 74 to 77 show examples of the UILs extracted from several strain gages. Three curves are presented in each figure: One for the bridge before damage was induced (Baseline), another for the case of the damaged Live Load Shoe (Case 1), and the last one for the case when shims were removed from the LLS as well as Span Lock (Case 2). It should also be mentioned that these UILs are obtained from averaging the results from three different data sets.

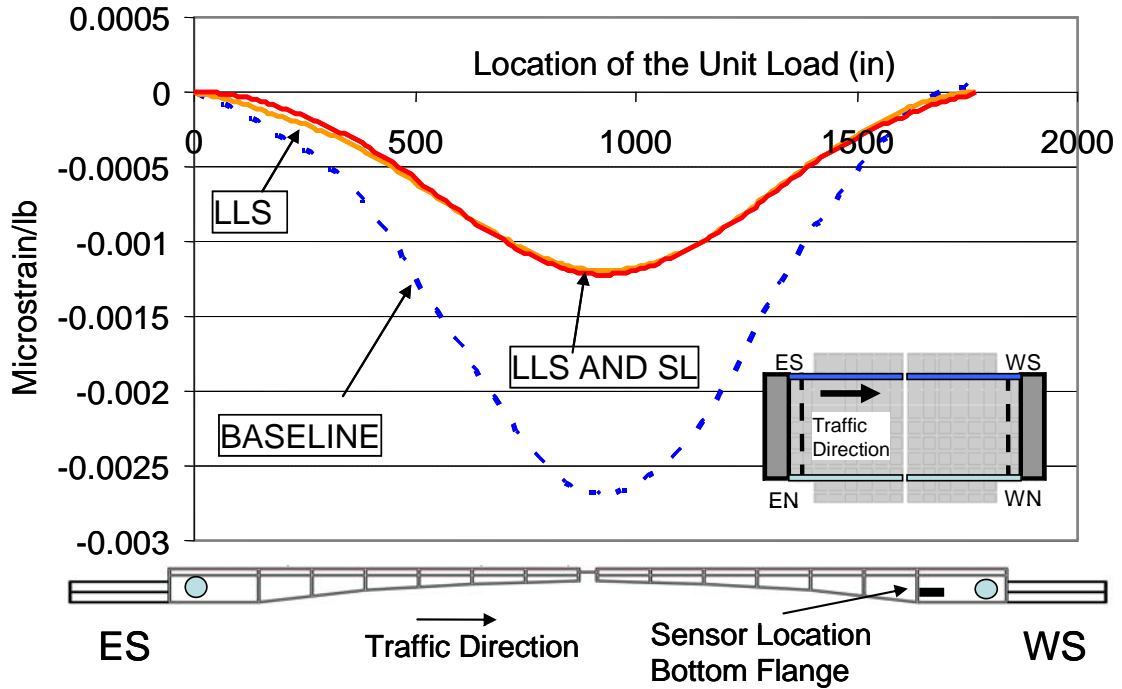


Figure 74. UILs for WS3-DSG2 (before and after damage)

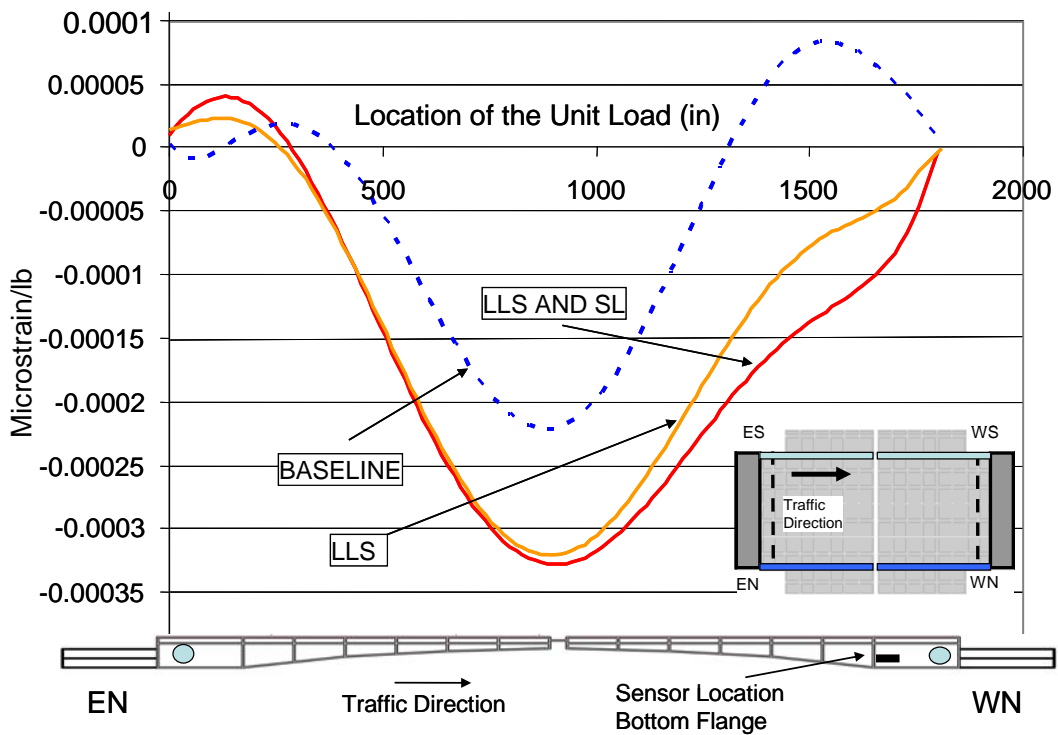


Figure 75. UILs for WN3-DSG2 (before and after damage)

Figure 74 shows the sensor located at the bottom flange of the main girder in the vicinity of the West South LLS, where the alteration was induced. It is shown that creates a clear change between the baseline UIL and UILs of Case 1 and Case 2. However, the change is not as obvious between the Case 1 and Case 2. The damage induced in the LLS is masking the effect of the span lock because it is significantly closer to the sensor WS3-DSG2. Also, the UIL for the damaged cases show smaller values than the baseline. This is probably due to the fact that by creating a small gap between the LLS and the support, the West South girder is not resting appropriately on this point causing the occurrence of a stress redistribution within the different structural components of the bridge. An inspection of the Figure 75 reflects that in this location, the effect of damage cases is more differentiable since the two plots for Case 1 and Case 2 can be identified independently. Also, it can be noticed that the UILs corresponding to damage cases show greater values than those of the baseline due to the stress redistribution.

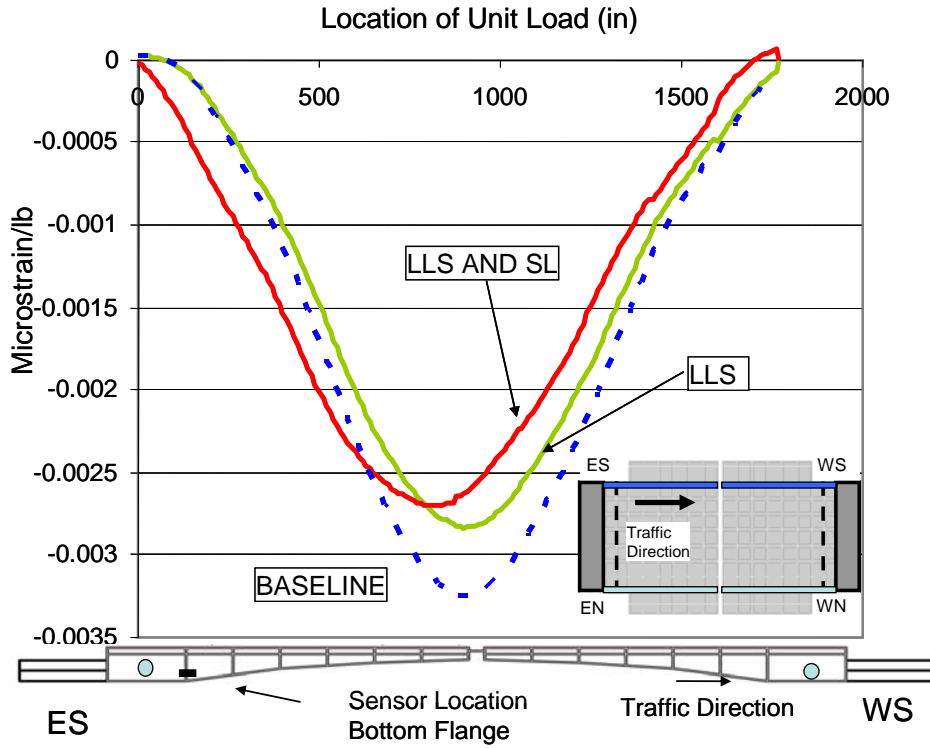


Figure 76. UILs for ES3-DSG2 (before and after damage)

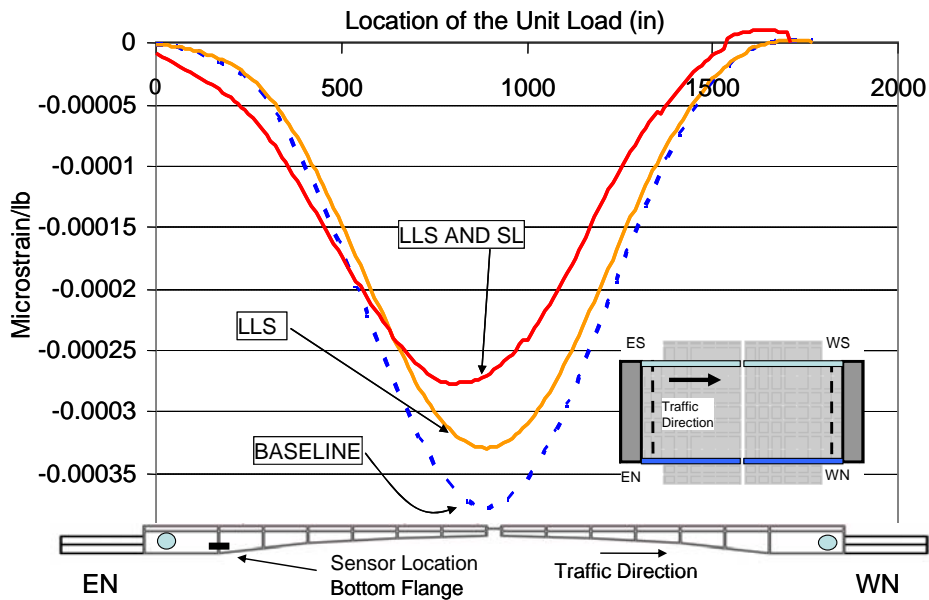


Figure 77. UILs for EN3-DSG2 (before and after damage)

In Figures 76 and 77 the difference between the baseline UIL with the Case 1 and Case 2 is clearly identifiable. It can be also noticed that the strain gage ES3-DSG2 experience a greater strain than the EN3-DSG2 because the damage scenarios were created on the South girder and the vehicles inducing the load for the UILs crawl over the South lane.

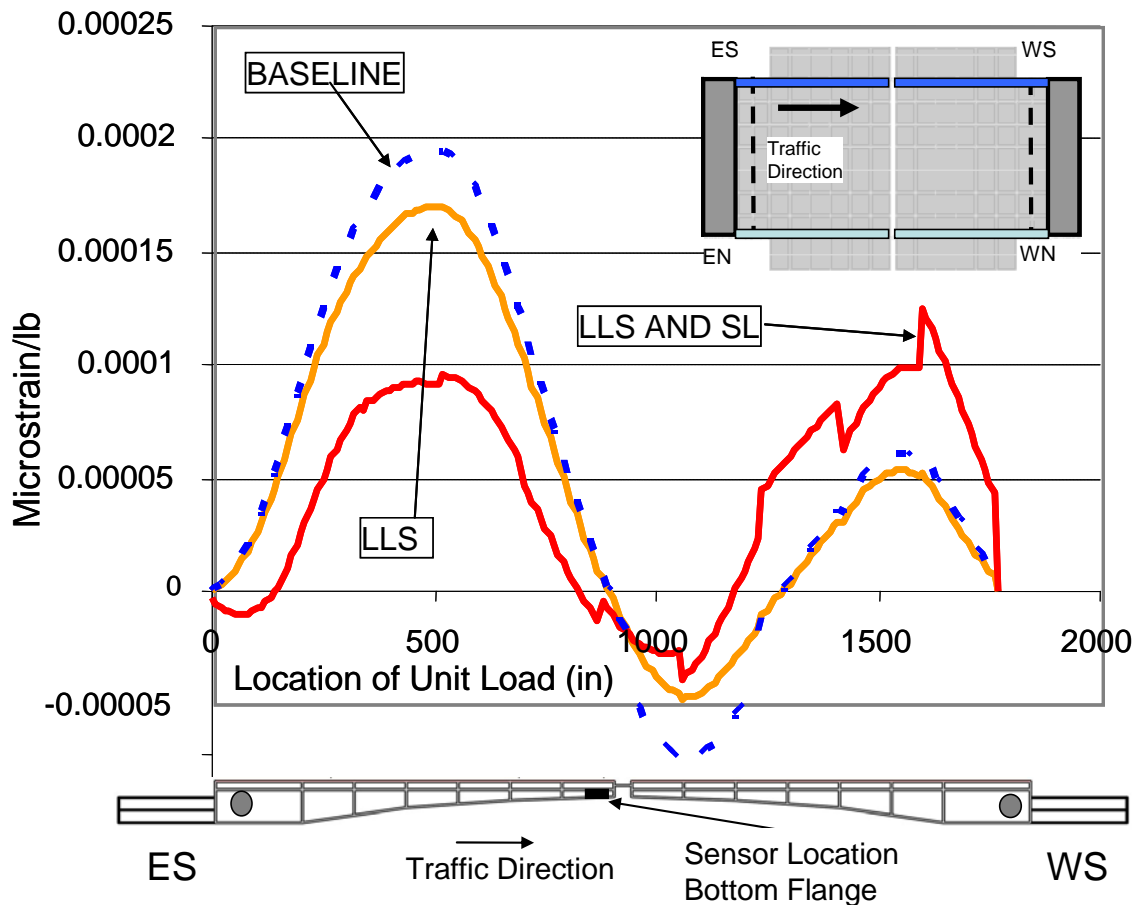


Figure 78. UILs for ES1-DSG1 (before and after damage)

Figure 78 illustrates the effects of both damage cases on the sensor ES1-DSG1, which is located close to the South span lock (where the gap between the bar and the receiver was created). It is observable that the different effects are captured by the sensor as reflected in the corresponding UILs. Also, the UIL for the case when span lock continuity was

altered shows a small bouncing effect due to the impacts produced by spanlock bar over the receiver when traffic crossed over the South lane.

5.8. Damage Identification

In the previous section, UILs are extracted and examples are presented with figures (Figures 74-78). The slight modifications on the boundary conditions of the LLS and SL caused significant changes in the UILs that are easily observable. Also, it was shown that the sensors are affected differently by a particular damage case with respect to their location. In the following, the demonstration of the new index \bar{N}_d is presented for the same damage scenarios. Figures 79 and 80 show the plots of \bar{N}_d obtained for all sensors for the two cases studied. Type and location of the damage is shown in each figure along with the sensor locations. As in Chapter 4, the bar diagram shown on the top of the bridge and its instrumentation figure corresponds to \bar{N}_d for each sensor.

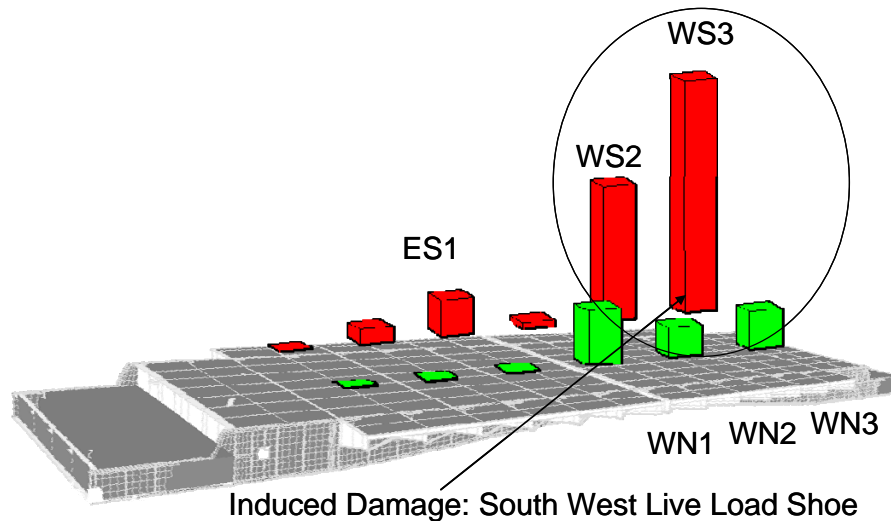


Figure 79. Damage Index for Case 1 with 1/8"-3/16" Gap created between LLS and Support.

As can be seen from

Figure 79 (damage was induced by creating a gap between the LLS and the support), the \bar{N}_d bar corresponding at this location (WS3) indicates a great separation from the baseline corresponding to the undamaged case (Case 0). Also a big change can be identified for the position WS2 which is relatively close to the LLS. The location ES1 shows a variation as well, indicating that the response at the Span Lock is changing due to the modification induced at the LLS. The North girder, presents some identifiable variations for WN3, WN2 and WN1 positions.

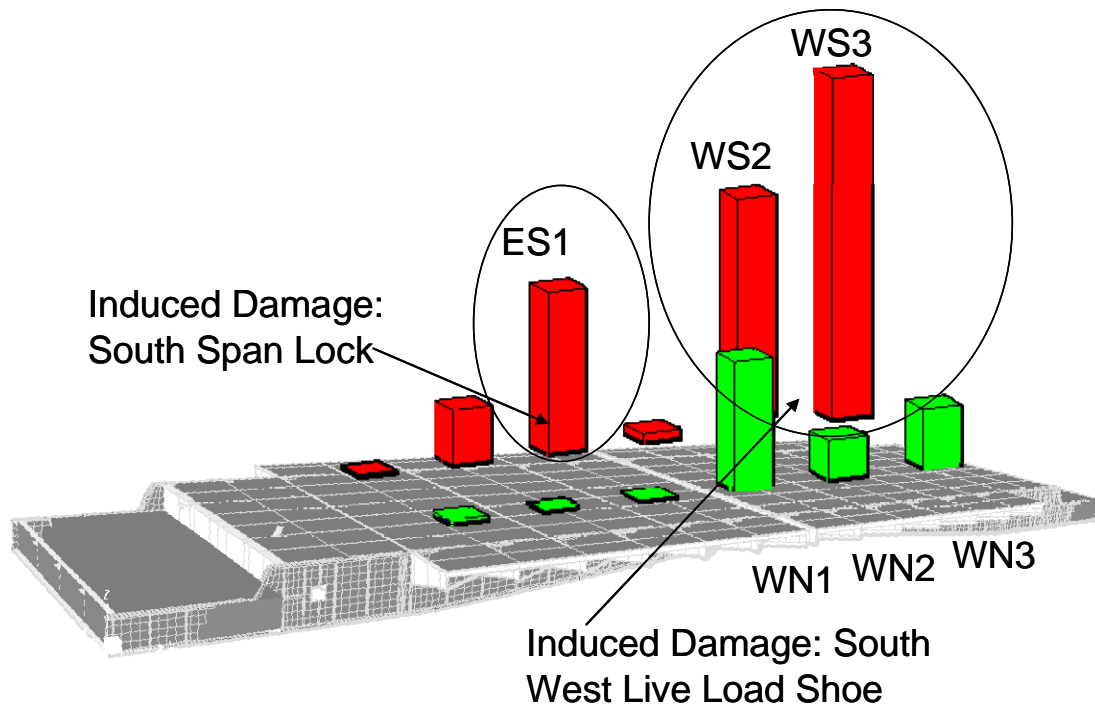


Figure 80. Damage Index for Case 2 with Gap Created between LLS and Support plus
Some Shims Removed from SL Receiver

Figure 80, represents the plot for \bar{N}_d when shims are removed from LLS and SL as well. Here, the \bar{N}_d bar corresponding to the LLS remains practically the same. This corroborates with the information presented in Figure 74. However, the \bar{N}_d at the span lock location (ES1) shows a significant increase as well as for the location WN1 (North Span Lock). The approximate location of the damage is signaled and also the relative magnitude of the change, proving the viability of the method.

5.9. *Summary*

This chapter introduces a real life monitoring project conducted at a movable bridge in Ft. Lauderdale, Florida. Description of the bridge as well as the monitoring system is presented. The bridge was monitored under regular traffic load to extract the UIL feature vectors explained in Chapter 4. This UIL vectors obtained directly from operational traffic video and sensor data are used for damage detection and bridge load rating. One of the novel aspects of the study is that a load test can be conducted with the traffic on the bridge, without any lane closure or special vehicles as well as any Weigh-in-motion device. Any heavy vehicle crossing the bridge can be employed for load testing as they are detected using the cameras, can be tracked over the bridge while synchronized sensor data collection provides the bridge response at the measurement locations. The classification of the vehicle gives information in terms of axle spacing and empty and fully loaded weight of the vehicle, which are used to obtain upper and lower bound normalized UIL responses. These UILs can be employed to determine the load rating

under commonly used American Association of State Highway Transportation Officials (AASHTO) HL93 truck as well as any other given vehicle. Load Rating results for the HL93 truck are presented along with the corresponding Finite Element Model (FEM) simulations, which are conducted for verification purposes.

In addition, slight structural alterations that represent the most common maintenance problems are induced on the bridge with the collaboration of the FDOT. The bridge is monitored under regular traffic load and also after inducing the damage. Two damage cases are considered. The first one consists on creating a gap (1/8"-3/16") on the West South Live Load Shoe. The second case adds up an extra alteration to the first case by removing some of the shims from the South Span Lock receiver to create a gap of the same size approximately.

The UILs are extracted as discussed in the previous chapters for the undamaged and damaged condition of the bridge. The results are presented in a comparative fashion. The new index \bar{N}_d is calculated and plotted showing the validity of the method by pinpointing the approximate damaged location.

6. CHAPTER SIX: SUMMARY, CONCLUSIONS AND RECOMMENDATIONS

The main objective of this dissertation is to investigate the development and integration of novel methods and techniques using sensor networks, computer vision, modeling for damage indices and statistical approaches for Structural Health Monitoring (SHM) of bridges. The dissertation can be summarized in five parts: 1) review of some of the methods and procedures involving the analysis of images, currently used for damage detection methods on structures as well as the presentation of a proposed SHM framework for bridges, 2) the explanation of some of the computer vision tools used within this study as well as some common issues and practical solutions for SHM of bridges, 3) demonstration of technologies and methods on a laboratory, and presentation of procedures for the extraction of Unit Influence Line (UIL) obtained by means of correlating video images with synchronized traditional sensor data, 4) explanation and demonstration of a new index (N_d) for damage identification that makes use of the UILs as feature vectors for damage identification with the application of statistical techniques, and 5) implementation and validation of the methods on a real life structure.

6.1. Structural Health Monitoring Applications and Needs

Methods and procedures currently used for damage detection on structures are presented. Visual inspections, benefits and shortcomings are discussed as well. It is presented that there is a need for practical and conceptual methods and techniques for inspection and assessment of Civil Infrastructure Systems (CIS). Structural Health Monitoring (SHM) is expected to close the gap between the current needs and the use of

available technologies. A review of various research studies dedicated to the use of video images for SHM and damage detection is also presented. This review shows that the implementation of computer vision based methods presents limited results for condition assessment of structures with conceptual damage indices. As a result, an SHM framework that also incorporates computer vision components is presented and discussed. This framework for bridges takes advantage of synchronized video streams and traditional sensor data, which is discussed in more detail and its feasibility is demonstrated.

6.2. Implementation of Computer Vision for Structural Health Monitoring

Computer vision is a major research area with advanced methods for various applications such as medical imaging, activity recognition, personal identification. Here, the specific application to civil infrastructure systems with emphasis on bridge monitoring is discussed. Some of the computer vision techniques considered for the application on SHM of bridges may have some shortcomings and issues due to the nature of the problem. Some simplified solutions are possible to overcome these challenges. The techniques known as background subtraction, tracking, and classification are explained and demonstrated on a real life structure. In the case of background subtraction, theoretical solutions about how to handle changing of illumination by adjusting the threshold, for SHM of bridges, are suggested. A simplified classification of the vehicles, based on size and wheel base distance is evaluated. Further parameters as shape and traffic distribution are suggested to be incorporated into the classification algorithm. Traditional computer vision techniques for tracking and conversion of image-to-world coordinate system are summarized along with a simplification used within this research

in the laboratory as well as in real life structures.

6.3. Computation of Unit Influence Line Using Video Stream and Sensor Data

Laboratory demonstrations of technologies and methods are very important since validation in a controlled environment is needed before the real life implementations. As a result, an experimental laboratory setup, the UCF 4-span bridge, was designed and built for this research. Although the structure is not a scaled down bridge model, its responses are representative of typical response values for most small to medium span bridges. This setup is a four span bridge-type structure consisting of two approach (end) spans and two main spans with a steel deck supported by two girders. Supports were designed in such a way that they could be easily changed to roller, pin or fixed boundary conditions. It is designed in such a way that girder and deck can be connected together by using bolts at different locations to modify the stiffness of the system and to simulate damage. Radio controlled vehicles can crawl over the deck with different loading conditions. Wheel axis distance and speed are also variable to simulate real traffic data. A video camera is used to identify and track the vehicle, a set of strategically located sensors collects the synchronized data to be correlated with the video stream in real-time.

The structure response is monitored and tracked under various load conditions by using a conceptual damage index called Unit Influence Line (UIL). The UIL is a normalized index extracted from the response of a structure due to moving loads. It is an inverse analysis to obtain the response due to a unit load. Benefits and uncertainties of this index are discussed. A demonstration of this method is presented where two different types of vehicles with different loads and wheel bases are driven over the UCF 4-span

bridge while computer vision techniques are utilized to detect, classify and track the vehicles (input loads) as traditional sensors measure the structural response (output). Synchronization of the video images of the vehicles and the sensor data is achieved allowing obtaining the structure response with respect to the vehicles location. Finally, UIL are extracted and compared for different types of vehicles, loads and speeds. The results of the UIL line obtained from computer vision based analysis show very good correlation with results from static tests as well as finite element analysis.

6.4. Data Analysis for Damage Detection

The use of UILs as a feature vectors for damage detection is proposed and presented. An outlier detection algorithm based on Mahalanobis distance between the UILs feature vectors is used to identify change between feature vector sets for damage detection. Also, it is shown that handling of large data sets by statistical analysis of these feature vectors can be done efficiently. To demonstrate the effectiveness and efficiency of damage detection, six of the most common damage conditions on real bridges are simulated and induced to the UCF 4-span bridge. Two vehicles carrying different loads are used for this experiment. Each vehicle runs over the bridge 15 times for a total of 60 passes. This is done to simulate real traffic and to obtain a valid statistical sample. Vehicles are detected, tracked and classified while synchronized data are collected and correlated. UILs are extracted for each case.

A new index, \bar{N}_d , is also formulated by calculating normalized distance based on the inliers and outliers from continuous monitoring data. This index is shown with simple plots and by rapid inspection, damage can be identified and localized. The methodology

discussed in this part is able to sense and detect changes on the experimental test set-up. Even small and localized damage cases like four missing bolts (Case 4) are successfully detected. It should be noted that the sensor spatial resolution is also important to capture the behavior. For the demonstration of the method, strain and rotation data are presented. It is observed that tiltmeters show a clear indication of structural variations for all the studied cases. Due to its global nature, UILs for rotation proved to be more affected than strains even when loading and damage are not very close to the tiltmeters. However, the use of tiltmeters for damage localization could lead to misinterpretation if they are not evaluated in combination with additional information provided by the analysis of data from other sensors such as strain gages. On the other hand, it is shown that the bar plot for the \bar{N}_d s generated from UILs extracted from strain data provides a more localized response which leads to an easier identification of the damage.

6.5. Field Demonstration on a Movable Bridge

One of the main goals of this study is the field demonstration and validation of the technologies and methods that have been developed and implemented in the laboratory. The field demonstration is carried out on a movable bridge located in Fort Lauderdale, Florida. On this bridge, the Structures and Systems Research Group of the University of Central Florida is conducting a SHM project which is sponsored by the Florida Department of Transportation (FDOT) and Federal Highway Administration (FHWA). Especially the support and coordination of the FDOT have been a very important non-technical aspect of the project.

The technologies and methods are demonstrated by using the video stream and

sensor data from the traffic for bridge load rating as well as for damage detection, which are critical for decision-making.

First, a new approach for obtaining the field monitoring based load rating of bridges is discussed and results are presented along with the corresponding Finite Element Model (FEM) simulations, conducted for verification purposes. For this, operational traffic is utilized as follows. By using the video cameras, a Riverside Transit Agency (RTA) passenger bus is detected and tracked over the bridge, while synchronized sensor data collection provides the bridge response at the measurement locations. The information regarding weight per axle in full and empty occupancy conditions, as well as the wheelbase distance (axle spacing) is known. With this information, normalized UIL responses are extracted, defining an upper and a lower bound. The two UILs are used to predict the response of the bridge under the commonly used AASHTO HL93 truck. Load rating results for the HL93 truck is presented with the FEM simulations showing a very good correlation. One of the novel aspects of the study is that a load test can be conducted with the operational traffic on the bridge, without any lane closure or special loading vehicles as well as any Weigh-in-motion device.

The movable bridge is also utilized to prove the damage detection potential of the new methods and the index previously tested on the laboratory set-up. For this reason, slight structural alterations that represent the most common maintenance problems are induced on the bridge with the collaboration of the FDOT. Two damage cases are considered: The first one consists of creating a gap (1/8"-3/16") on the West South Live Load Shoe. The second case simulates a progression of the damage by including the elimination of some of the shims from the South Span Lock receiver to create also a gap,

of the same size approximately. The bridge is monitored under regular traffic load before and after the creation of the damage scenarios. Video and sensor data are collected before inducing any damage to the structure and UILs are extracted. This data is considered as the baseline. It is important to indicate that in the case of existing real life structures establishing a baseline can be a challenging task. This bridge has been in operation since 1989 and is expected to have certain deterioration and damage with respect to its brand new condition. In this study, the baseline is considered as the condition of the bridge before inducing the predetermined damages.

Modifications are induced as explained before and data is collected. The UILs corresponding to Baseline, Case 1, and Case 2 are extracted and analyzed for several sensors. Results show a clear variation between the UILs before and after damage. Also, the internal load distribution can be observed by means of the SHM system when there is a change or damage on the structure. In this study, it is seen that alterations cause a distinct change in UILs not only in the vicinity of damage but also at other measurement locations due to internal load redistribution.

Finally, the new index, \bar{N}_d , is also tested and presented with bar charts. For Case 1 (induced damage in the Live Load Shoe (LLS)), the bar corresponding to damage location indicates a great separation from the baseline with respect to the undamaged case (Baseline). The location corresponding to the South Span Lock (SL), shows a variation as well, pointing out that this area is also changing due to the modification induced at the LLS. For Case 2, the \bar{N}_d bar corresponding to the LLS remains practically the same, showing that damage exists in this area. In addition, the \bar{N}_d at the South SL location

shows a significant increase as well as for the North SL. Based on the results of the field application, it is shown that the proposed method is very promising for damage detection implementation in the context of SHM.

One immediate step for the future research is the verification of the proposed methodology with different laboratory and real life structures. Also, the effect of multiple vehicles driving simultaneously over various lanes of the bridge should be studied.

Vehicle classification algorithm has to be improved by including extra features such as incorporation of statistical studies on the traffic distribution analysis of the bridge location. The use of neural networks can also be considered and studied for classification purposes.

Special hardware that also incorporates the various algorithms should be explored. This will increase the computational speed which will allow the system to work in real-time. In addition, the system setup and operation will be more efficient.

After improving the method and making sure that it can be used for a variety of structures under different loading and environmental conditions, the methodology can be implemented to a wireless sensor network, avoiding the complicated and expensive task of cabling.

LIST OF REFERENCES

1. Liu, S.C. and M. Tomizuka. *Strategic Research for Sensors and Smart Structures Technology*. in *Proceedings of the International Conference on Structural Health Monitoring and Intelligent Infrastructure*. 2003. Tokyo, Japan.
2. Zaurin, R. and F.N. Catbas. *Computer Vision Oriented Framework for Structural Health Monitoring of Bridges*. in *IMAC XXV. Society for Experimental Mechanics*. 2007. Orlando, Florida.
3. Aktan, A.E., et al., *Issues in Infrastructure Health Monitoring for Management*. Journal of Engineering Mechanics, ASCE, 2000. 126(7): p. 711-724.
4. Farrar, C.R. and W. Keith, *An Introduction to Structural Health Monitoring*. Philosophical Transactions of the Royal Society, 2007. 365: p. 303-315.
5. Catbas, F.N., D.L. Brown, and A.E. Aktan, *Parameter Estimation for Multiple-Input Multiple-Output Modal Analysis of Large Structures*. ASCE Journal of Engineering Mechanics, 2004. 130(8): p. 921-930.
6. Phares, B.M., et al., *Health Monitoring of Bridge Structures and Components Using Smart Structure Technology. Volume 1*, in *Center for Transportation*. 2005, Report No. 0092-04-14 prepared for Wisconsin Highway Research. Center for Transportation Research and Education. Iowa State University.
7. Aktan, A.E., et al. *Monitoring and Managing the Health of Infrastructure Systems*. in *Proc 2001 SPIE Conference on Health Monitoring of Highway Transportation Infrastructure*. 2001. Irvine, CA.
8. Aktan, A.E., et al. *Integrated Field, Theoretical and Laboratory Research for Solving Large System Identification Problems*. in *Advances in Structural Dynamics*. 2000. Hong Kong.
9. Doebling, S.W., et al., *Damage Identification and Health Monitoring of Structural and Mechanical Systems from Changes in Their Vibration Characteristics: A Literature Review*. 2006, Los Alamos National Laboratory.
10. Sohn, H., et al., *A Review of Structural Health Monitoring Literature: 1996-2001*. 2003, Los Alamos National Laboratory Report.
11. Catbas, F.N. and A.E. Aktan, *Condition and Damage Assessment: Issues and Some Promising Indices*. Journal of Structural Engineering, ASCE, 2002. **128**(8): p. 1026-1036.
12. Ciloglu, S.K., et al. *Exploration of Structural Identification Tool and Barriers on a Laboratory Model*. in *Proceedings of SPIE, Smart Materials and Structures*. 2004.
13. Catbas, F.N., et al. *Challenges in Structural Health Monitoring*. in *Proceedings of the 4th International Workshop on Structural Control*. 2004. Columbia University, New York.
14. Burkett, J.L., *Benchmark Studies for Structural Health Monitoring using*

- Analytical and Experimental Models*, in *Department of Civil and Environmental Engineering*. 2005, University of Central Florida: Orlando, FL.
15. Caicedo, J.M., et al. *Phase I of the Benchmark Problem for Bridge Health Monitoring: Numerical Data*. in *18th Engineering Mechanics Division Conference*. 2007: ASCE.
 16. Catbas, F.N., J.M. Caicedo, and S.J. Dyke. "Benchmark Problem on Health Monitoring of Highway Bridges". 2005.
 17. Caicedo, J.M., et al. *Benchmark Problem for Bridge Health Monitoring: Definition Paper*. in *4th World Conference on Structural Control and Monitoring*. 2006. San Diego, California.
 18. Gul, M., *Investigation of Damage Detection Methodologies for Structural Health Monitoring*, in *Civil, Construction and Environmental Engineering*. 2009, University of Central Florida: Orlando.
 19. Dyke, S.J., et al. *An Experimental Benchmark Problem in Structural Health Monitoring*. in *Proceedings of the 3rd International Workshop on Structural Health Monitoring*. 2001. Stanford, CA.
 20. Caicedo, J.M., et al., *Phase II Benchmark Control Problem for Seismic Response of Cable-Stayed Bridges*. *Journal of Structural Control: Special Issue on the Cable-Stayed Bridge Seismic Benchmark Control Problem*, 2003. 10(3-4): p. pp. 137-168.
 21. Dyke, S.J., et al., *Phase I Benchmark Control Problem for Seismic Response of Cable-Stayed Bridges*. *ASCE Journal of Structural Engineering*, 2003. 129(7): p. pp. 857-872.
 22. Wahbeh, A.M., J.P. Caffrey, and S.F. Masri, *A vision-based approach for the direct measurement of displacements in vibrating systems*. *Smart Materials and Structures*, 2003. 12(5): p. 785-794.
 23. Lee, J. and M. Shinozuka, "Real-Time Displacement Measurement of a Flexible Bridge Using Digital Image Processing Techniques" *Experimental Mechanics*, 2006(46): p. 05-114
 24. Lin, L., et al. "Application of digital photogrammetric technique for deformation measuring in structural experiment". in *Monitoring and Intelligent Infrastructure*. 2003. Vancouver, Canada.
 25. Hanji, T., K. Tateishi, and K. Kitagawa. "3-D Shape Measurement of Corroded Surface by Using Stereography". in *Structural Health Monitoring and Intelligent Infrastructure*. 2003. Vancouver, Canada.
 26. Yoshida, J., et al., "Construction of a Measurement System for the Dynamic Behaviors of Membrane by Using Image Processing". *Textile and Inflatable structures*. , 2003.
 27. Kanda, K. and Y. Miyamoto. "Seismic Damage Monitoring with Optical Motion Tracking". in *Structural Health Monitoring and Intelligent Infrastructure*. 2003.

28. Basharat, A., F.N. Catbas, and M. Shah. *A Framework for Intelligent Sensor Network with Video Camera for Structural Health Monitoring of Bridges*. in *Pervasive Computing and Communications Workshops. Third IEEE Conference*. 2005.
29. Javed O, Z., A. Rasheed Z, and M. Shah. *KNIGHT:A Real Time Surveillance System for Multiple Overlapping and Non-overlapping Cameras*. in *ONDCP International Technology Symposium*. 2003.
30. Elgamal, A., et al. *Health Monitoring Framework for Bridges and Civil Infrastructure*. in *4th International Workshop on Structural Health Monitoring*. 2003. Stanford University, Stanford, CA.
31. Achler, O. and M. Trivedi. *Camera Based Vehicle Detection, Tracking, and Wheel Baseline Estimation Approach*. in *7th International IEEE Conference on Intelligent Transportation Systems (ITSC 2004)*. 2004. Washington, DC.
32. Chang, R., G. Tarak, and M. Trivedi. *Computer Vision for Multi-Sensory Structural Health Monitoring System*. in *Proceedings of the 4th International Workshop on Structural Health Monitoring*. 2003. Stanford, CA.
33. Fraser, M., *Development and Implementation of an Integrated Framework for Structural Health Monitoring. Doctoral Dissertation*, in *Department of Structural Engineering*. 2006, University of California at San Diego: La Jolla, CA.
34. Fraser, M. and A. Elgamal. *Video and Motion Structural Monitoring Framework*. in *4th China-Japan-US Symposium on Structural Control and Monitoring*. 2006.
35. Zhang, G., R. Avery, and Y. Wang. *A Video-based Vehicle Detection and Classification System for Real-time Traffic Data Collection Using Uncalibrated Video Cameras* in *87th TRB Annual Meeting*. 2007. Washington, DC.
36. Malinovskiy, Y., Y.-J. Wu, and Y. Wang. *Video-Based Vehicle Detection and Tracking Using Spatio-Temporal Maps*. in *88th TRB Meeting 2009*. Washington, DC.
37. Zaurin, R. and F.N. Catbas. *Demonstration of a Computer Vision and Sensor Fusion Structural Health Monitoring Framework on UCF 4-Span Bridge*. in *International Modal Analysis Conference- Technologies for Civil Structures*. 2008. Orlando, Florida.
38. Zaurin, R. and F.N. Catbas. *Benchmark Studies for Structural Health Monitoring using Computer Vision* in *The Fourth International Conference on Bridge Maintenance, Safety, and Management*. 2008. Seoul, Korea: IABMAS'08.
39. Zaurin, R. and F.N. Catbas, *Computer Vision and Sensor Fusion Structural Health Monitoring Framework, with Emphasis in Unit Influence Line Analysis, for Condition Assessment.UCF 4-Span Bridge*, in *ociety for Experimental Mechanics. IMAC XXVII*. 2009: Orlando, Florida.
40. Catbas, N., et al., *Long Term Monitoring Demonstration on a Movable Bridge*. 2009, FDOT.
41. Haritaoglu, L., D. Harwood, and L. Davis. *W4: Who? When? Where? What? a*

- Real-time System for Detecting and Tracking People.* in *Proc. the third IEEE International Conference on Automatic Face and Gesture Recognition.* 1998. Los Alamitos, California.: IEEE Computer Society Press.
42. Zaurin, R. and F.N. Catbas. *Issues in Using Video Images for Structural Health Monitoring.* in *SMSST07.* 2007. China.
 43. Kass, M., A. Witkin, and D. Terzopoulos. *Snakes:Active contourmodels.* in *Proc. First Int. Conf Computer Vision.* 1987.
 44. Paragios, N. and R. Deriche, *Geodesic active contours and level sets for the detection and tracking of moving objects.* IEEE Transactions on Pattern Analysis and Machine Intelligence, 2000.
 45. Lowe, D.G., *SIFT.* 2004, The University of British Columbia: USA.
 46. Aktan, A.E., et al., *Structural Identification: Analytical Aspects.* Journal of Structural Engineering, 1998. 124(7): p. 817-829.
 47. Turer, A., A. Levi, and A.E. Aktan, *Instrumentation, proof-testing and monitoring of three reinforced concrete deck-on-steel girder bridges prior to, during, and after superload.* 1998, Cincinnati Infrastructure Institute: Cincinnati, OH.
 48. Turer, A. and A.E. Aktan. *Issues in Super-Load Crossing of Three Steel-Stringer Bridges in Toledo, Ohio.* in *Transportation Research Record, TRR No. 1688, pp. 87-96.* 1999. Washington, DC: National Academy Press.
 49. Koglin, T.L., *Movable Bridge Engineering.* 2003: John Wiley and Sons.
 50. Wallner, M. and M. Pircher, *Kinematics of Movable Bridges.* ASCE Journal of Bridge Engineering, 2007: p. 147-153.
 51. Catbas, F.N., et al., *Integrative Information System Design for Florida Department of Transportation. A Framework for Structural Health Monitoring of Movable Bridges.* 2007, FDOT.
 52. FHWA Report, *Bridge Inspector's Reference Manual,* in *US Department of Transportation.* 2002, Publication No. FHWA NHI 03-001: US Department of Transportation.
 53. Aktan, A.E., et al. *Monitoring and Managing the Health of Infrastructure Systems.* in *Proceedings of the 2001 SPIE Conference on Health Monitoring of Highway Transportation Infrastructure.* 2001. Irvine, CA.
 54. Catbas, F.N., et al. *Fleet Monitoring of Large Populations: Aged Concrete T-Beam Bridges in Pennsylvania.* in *Proceedings of SPIE, Health Monitoring of Civil Infrastructure Systems.* 2001.
 55. Lichtenstein, A.G., *Manual for Bridge Rating Through Load Testing,* N. Research Results Digest, Editor. 1998, National Cooperative Highway Research Program: Washington, D.C.
 56. AASHTO, *Manual for Condition Evaluation and Load and Resistance Factor Rating (LRFR) of Highway Bridges.* 2003.